



UIT

THE ARCTIC
UNIVERSITY
OF NORWAY

Faculty of Science and Technology – Department of Geosciences

Connection between chemical zonation and crystallographic preferred orientation as an indicator for the fabric development in eclogites

Example from the Saxothuringian eclogites, Bohemian massif, Czech Republic

Ane Kongsro Finstad

Master thesis in Geology – GEO-3900

May 2017



Abstract

The presence of eclogites is one of the strongest evidences for high pressure metamorphism, and for the presence of a paleo subduction zone. Deformation of eclogites can yield important information about the kinematics of subduction zones. The main mechanism for fabric development in eclogites is still a matter of debate among various research groups and has split the field in two. Most previous studies suggest that dislocation creep is the main deformation mechanism, but some studies suggest grain boundary diffusion as the main mechanism for the elongation of the high-pressure minerals and fabric evolution.

Eclogites from the Saxothuringian domain in the Czech part of the Erzgebirge in the Bohemian Massif exhibit a strong lineation fabric. Omphacite, zoisite and elongated garnet contribute most to this fabric. SEM, BSE, EDS and EBSD analysis of the eclogites show an asymmetric, prograde zonation in omphacite and garnet, which is related to the elongation direction, parallel to lineation. Zoisite is expected to act as a rigid particle without any intracrystalline deformation, yet it occurs as elongated particles in the lineation direction. Quartz is located as elongated aggregates in pressure shadows of garnet parallel to lineation and does not show any signs of intra crystalline deformation.

The asymmetric prograde chemical zonation of omphacite and garnet indicates growth and elongation of garnet and omphacite during prograde and peak metamorphic conditions. The correlation of the zonation patterns in omphacite and garnet, as well as weak CPO in garnet suggest that the elongated shape of the minerals and the fabric in the eclogites are a result of dissolution and grain growth by grain boundary diffusion. As well as rotation and oriented dependent growth of omphacite in the [001] direction causing a strong CPO and elongation in the lineation direction.

Acknowledgements

I can't believe my 5 years here at UiT – the Arctic University of Norway is over! I'm finishing my years here feeling sad, as well as extremely proud and happy. I have met the best people I have ever had the chance to know here in Tromsø, and made lifelong friends.

The process of producing a master thesis have been fun, frustrating, sometimes felt impossible, but mostly very interesting, and I have probably learned more than in my previous 4 years. I could not have done this alone. First of all I have to thank my supervisors Holger Stünitz, Jiri Konopasek and Renee Heilbronner for always being available for questions in the busy life of a professor. To the lab-ladies Trine Merete Dahl and Karina Monsen thank you for always creating a good atmosphere in the lab, and helping with the thin section production. I also want to give a special thanks to Kai Naufeld for helping me interpret and process the data, for many helpful discussions and proofreading my thesis more than once. I really appreciate all the time you have spent on this project.

During the frustrating times my mom, dad and brothers have kept me going by endless support and words of wisdom, thank you! To my office mate Kristine Hafne, Renate Paulsen next door, Julie Berg down the hall, and all my other friend here in Tromsø and back home, thank you for all the support and for bearing with me during this process. To Rune Einrem, thank you for always taking care of me, motivating and helping me during the ups and downs of this intense period. I could not have done this without you!

So, this is it! Thank you everyone for making this the best years of my life.

Ane Kongsro Finstad

Tromsø 14/05/2017

Table of Content

Abbreviations	1
1.0 Introduction	3
Aim of the thesis	3
2.0 Background	5
2.1 Geological setting.....	5
2.2 Eclogite petrology	8
2.3 Deformation mechanisms.....	8
2.3.1 Brittle fracturing.....	8
2.3.2 Diffusion creep.....	9
2.3.3 Intra crystalline deformation	10
2.3.4 Recrystallization.....	11
2.3.5 Deformation twinning and kinking	12
2.3.6 Recovery.....	12
2.3.7 Grain boundary area reduction (GBAR), grain growth and post-tectonic recrystallization	13
2.4 Deformation and microstructures in eclogite minerals	14
2.4.1 Omphacite deformation at eclogite facies conditions	14
2.4.2 Garnet deformation at eclogite facies conditions.....	16
2.4.3 Accessory minerals	18
3.0 Methods.....	21
3.1 Fieldwork	21
3.2 Preparation of thin sections	23
3.3 Microscopy.....	23
3.4 Scanning electron microscopy (SEM) imaging and analysis.....	23
3.4.1 BSE and EDS imaging	24
3.4.2 EBSD-mapping	25
3.4.3 Pole figures.....	26
3.5 Production of grain boundary and phase maps	27
3.6 Modal composition.....	28
3.7 Grain size analysis.....	28
3.8 PAROR & SURFOR analysis	29
3.8.1 PAROR.....	30
3.8.2 SURFOR	30
4.0 Results	31

4.1 Grain boundary and phase maps	31
4.2 Mineralogy and volume fraction	34
4.3 Thin section description	35
4.4 Description of phases	36
4.4.1 Omphacite	38
4.4.2 Garnet	44
4.4.3 Zoisite.....	51
4.4.4 Hornblende	54
4.4.5 Quartz.....	56
4.5 Grain size analysis.....	57
5.0 Discussion	59
5.1 Metamorphic history and zonation.....	59
5.2 Deformation structures and zonation pattern	61
5.3 Deformation mechanisms and fabric development.....	63
6.0 Conclusions	69
7.0 References	71
8.0 Appendix	75

Abbreviations

2D – two dimensional
3D – three dimensional
BLG – bulging
BSE – backscatter electron
CPO – crystallographic preferred orientation
EBSD – electron backscatter diffraction
EDS – energy dispersive x-ray spectroscopy
Equ corr r – equivalent corrected radius
GBAR – grain boundary area reduction
GBM – grain boundary migration
Grt – garnet
Hbl – hornblende
HP – high pressure
HT – high temperature
kbar – kilobar
LPO – lattice preferred orientation
Ma – million years
mbar – millibar
Mud – multiples of uniform density
NE – north east
nm – nanometer
ODF – orientation distribution function
Omp – omphacite
PAROR – particle orientation
Pg – paragonite
P-T – pressure and temperature
px – pixel
Qtz – quartz
Rt – rutile
SPO – shape preferred orientation
SW – south west
SURFOR – surface orientation

SGR – subgrain rotation

TEM – transmission electron microscope

UHP – ultra high pressure

VPSC – visco plastic self-consistent

wt% – weight percentage

Zo – zoisite

ϵ – strain

μm – micrometer

1.0 Introduction

Eclogites from the Saxothuringian domain in the Czech part of the Erzgebirge in the Bohemian Massif are the result of a Devonian-Carboniferous oceanic subduction of the Saxothuringian oceanic crust (Jeřábek et al., 2016). Peak metamorphic conditions for the formation of these eclogites have been interpreted to be 600-650 °C and 25-26 kbar by Klapova et al. (1998) and Collett et al. (2017). Samples from Meluzina and Na skalách outcrops were studied using scanning electron microscopy (SEM), electron backscatter diffraction (EBSD) and energy dispersive x-ray spectroscopy (EDS). Image analysis software has been used for grain size and shape/particle orientation analysis.

The fabric development in eclogites has been interpreted by previous studies to be a result of dislocation creep on dominant slip systems; $[001] (100)$, $[001] \{110\}$ or $\frac{1}{2} \langle 110 \rangle \{110\}$ (Godard and van Roermund, 1995; Rehman et al., 2016). The activation of these dominant slip systems produces a typical L- or S-type fabric, or an intermediate fabric between the two endmember symmetries. Helmstaedt et al. (1972) introduced that a L-type fabric normally is produced in a constrictional regime, while S-type fabric normally is a result of flattening. On the other hand, some other authors suggest that the fabric development during eclogite-facies deformation can be a result of grain boundary diffusion mechanisms, during which the orientation-dependent dissolution and growth causes elongation of minerals and production of CPO (Wheeler, 1992; Bons and den Brok, 2000; Mauler et al., 2001; Storey and Prior, 2005).

Geological history and different deformation mechanisms will be presented, as well as dominant deformation mechanisms and related microstructures for eclogite facies minerals. All methods used for preparation and analysis of the samples and interpretation of the results will be presented. The results will then be discussed and compared to previous work and the thesis will summarize the main findings by presenting conclusions.

Aim of the thesis

The aim of the thesis is to study chemical zonation, zonation patterns and microstructures to discuss grain boundary diffusion creep as a mechanism for fabric and CPO development in eclogite facies minerals by using image analysis tools, SEM, BSE, EDS and EBSD orientation data.

2.0 Background

In this chapter, the geological setting and tectonic evolution of the study area will be presented. Following this deformation mechanisms and structures will be presented in a general term as well as dominating deformation mechanisms and related structures for eclogite facies minerals.

2.1 Geological setting

The Bohemian Massif is a result of the closure of the Saxothuringian Ocean during Devonian oceanic subduction and subsequent early Carboniferous continent-continent collision (Jeřábek et al., 2016). The Saxothuringian oceanic crust was subducted beneath the eastern plate that today represent the Teplá-Barrandian domain, Moldanubian domain and Brunia domain (Schulmann et al., 2009). The Bohemian Massif is divided into several domains and allochthones, this thesis will focus on an area of the southeastern Saxothuringian domain (in green colors in Fig. 2.1.1) in the western Bohemian Massif, Czech Republic. The Saxothuringian domain, represents the lower plate collisional system, and it contains relics of the subduction zone. Teplá-Barrandian domain represented the fore-arc and the Moldanubian domain represented the back-arc region. The different domains of the Bohemian massif and their most prominent rock units are illustrated in Fig. 2.1.1.

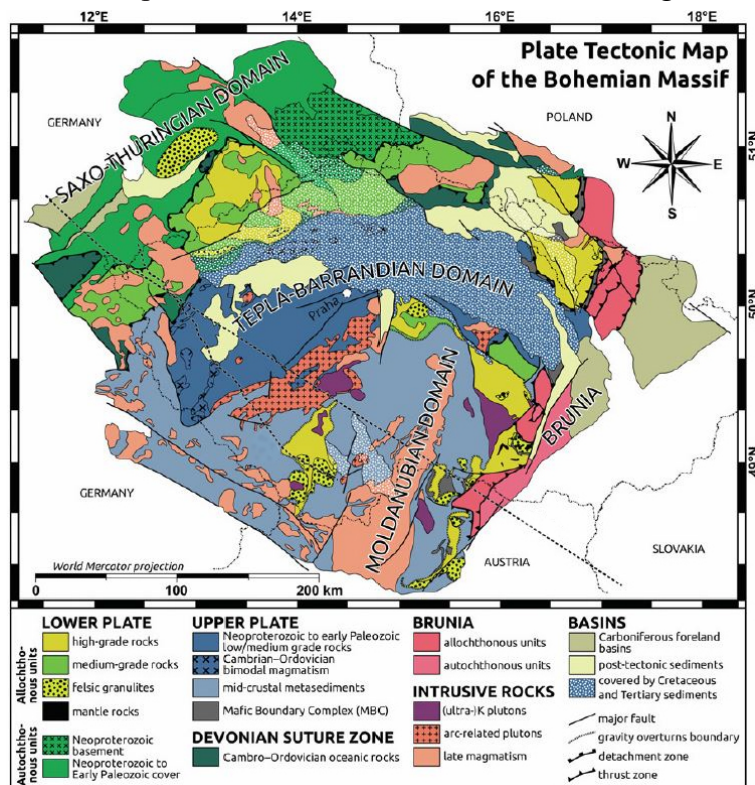


Fig. 2.1.1: geological and tectonic map of the Bohemian Massif modified from Schulmann et al. (2014).

The Saxothuringian domain is divided into upper-Proterozoic basement rocks consisting of grey and red granitic gneisses, schists, metagreywackes, micaschists and metaconglomerates, as well as overlying lower-Paleozoic metasedimentary rocks (quartzite, quartz metaconglomerate and dolomitic marble) (Lorenz, 1979; Hoth et al., 1983; Lorenz and Hoth, 1990; Klapova et al., 1998). Above the basement in the highest structural position, orthogneisses and some metapelites, marbles and magnetite skarns are present (Lorenz and Hoth, 1967; Lorenz and Hoth, 1990). The uppermost allocthonous unit contain boudins of eclogites, which are studied in this thesis (Klapova et al., 1998). The Saxothuringian eclogites vary in cooling ages from 360-333 Ma, with the youngest in the north and oldest in the south. P-T conditions show a decrease of pressure and temperature from the SW to NE (Schmädicke et al., 1995).

Between the Saxothuringian and the Teplá-Barrandian domain, the Teplá suture (the subduction channel) worked as an exhumation channel for the HP rocks during the subduction (Klapova et al., 1998; Schulmann et al., 2009; Schulmann et al., 2014). The exhumed, subduction-related rocks show similar peak metamorphic and cooling ages. This indicates a very fast exhumation of the rocks within the subduction channel, where the HP rocks were brought very quickly back to the surface (Schmädicke et al., 1995; Konopásek and Schulmann, 2005). The peak metamorphic conditions during the formation of the Erzgebirge eclogites have been determined by Collett et al. (2017) at 615 °C and 26 kbar. The metamorphic conditions for the Meluzina eclogites, which were sampled for this study, have been interpreted to be 600-650 °C and 25-26 kbar by Klapova et al. (1998).

The eclogites in the central Erzgebirge Mountains have been divided by Schmädicke et al. (1995) and Klapova et al. (1998) into three main types based on differences in mineral assemblage and grain size, called type 1-3:

Type 1 is the most frequent of the three in the area. Compared to type 2 and 3 it is finer grained, darker in color and often banded with more omphacite-rich layers and more garnet-rich layers. Type 1 has a mineral assemblage of:

omphacite + garnet + rutile + quartz + amphibole
± paragonite ± phengite ± zoisite.

Type 2 is less frequent than type 1. It is lighter in color, coarser grained, and contains lenses or discontinuous bands of zoisite. Presence of talc and kyanite and the higher amount of zoisite differs this eclogite from type 1. The typical mineral assemblage for type 2 eclogite is:

omphacite + garnet + zoisite + rutile

± paragonite ± phengite ± kyanite ± talc ± amphibole ± quartz.

A gradual transition in mineral assemblage between type 1 and type 2 can occur.

Type 3 differs from type 1 and 2 by having a coarser grain size, it is missing the banded structure, and shows different distribution of omphacite and garnet. These less common eclogites from the Erzgebirge Mountains have a typical mineral assemblage of:

omphacite + garnet + amphibole + quartz + rutile + white mica

± primary carbonate.

The study area is located around the Meluzina and Na skalách outcrops in the central Erzgebirge Mountains. The metamorphic age for the Meluzina eclogites was calculated by Hurych and Brueckner (1995) by Sm-Nd method to be 333 ± 2 Ma. Meluzina eclogites exhibit a strong mineral lineation and foliation, developed by two syn-eclogitic deformation events. Post-eclogitic deformation events have affected some of the eclogite bodies. Folding of the area rotated some of the eclogite boudins and in a later deformation event, shear zones developed and caused intensive retrogression. Well preserved eclogite mineral assemblage is still present in areas not affected by the shear zones and the related retrogression (Klapova et al., 1998). These eclogites with preserved syn-eclogitic deformation fabric and mineral assemblage are important for the understanding of kinematics during deformation and fabric development in HP rocks, and these will be further discussed in this thesis.

2.2 Eclogite petrology

Eclogite is a high pressure (HP) or ultra-high pressure (UHP) rock, mostly produced by subduction of a mafic (basaltic) oceanic crust or continental crust e.g. (Rehman et al., 2016). Research on eclogites is an important part of understanding mechanisms and deformation parameters in a convergent plate margin. These rocks can offer information on pressure and temperature (P-T) conditions and strain rates during formation and are important markers for reconstructing earlier orogenic belts and subduction zones e.g. (Godard and van Roermund, 1995).

2.3 Deformation mechanisms

In HP regimes, mostly at deeper crustal levels, most minerals deform by different ductile flow processes. Different minerals react and deform in different ways during various factors such as grain size, mineralogy, external fluids, preferred orientation, porosity and permeability and external factors as temperature, fluid and lithostatic pressure, differential stress and strain rate. Some ductile deformation mechanisms will be explained in this chapter and the most prominent and relevant deformation structures in stable eclogite facies minerals will be enlightened (Passchier and Trouw, 1998). Deformation induced microstructures for different phases can help determine deformation processes and accommodate the study of deformation regimes and its kinematics.

2.3.1 Brittle fracturing

Brittle deformation by development of cracks, joints or faults can change grain shapes. This is common in low temperature (LT) or high strain rate regimes. Most micro-cracks in minerals develop in a certain crystallographic direction, for example in the cleavage direction of micas (Wong and Biegel, 1985). Fractures normally heal and close by a secondary phase, often the same as the host crystal of the cracked grain. Larger micro-cracks that show evidence for propagation or displacement can obtain information about the normal stress that have worked on the rock (Passchier and Trouw, 1998).

2.3.2 Diffusion creep

Diffusion creep deforms grains by migration of vacancies through the crystal lattice (grain-scale diffusive mass transfer) and transfers material from areas exposed to high normal stress to low normal stress areas of the grain. Diffusion creep mostly occurs at high temperatures, with respect to the melting temperature of the minerals in the deforming rock, and diffusion creep mechanisms may take over or accompany dynamic recrystallization by dislocation creep mechanisms. Diffusion creep also favors smaller grain sizes since the diffusion path is shorter. In conclusion grain size is one of the main parameters if a crystal deforms by dislocation creep or diffusion creep. The main types of diffusion creep are: Coble creep, Nabarro-Herring creep and pressure solution (if a fluid is present). During Coble creep the vacancies diffuse through the crystal using the crystal lattice, while diffusion along a grain boundary is called Nabarro-Herring creep. Grain boundary sliding is a process where crystals, especially fine grained crystals, slide past each other. To avoid voids between the sliding crystals diffusion creep processes fill these voids with transferred material. These two accommodating processes are referred to as granular flow (Knipe, 1989; Passchier and Trouw, 1998).

Pressure solution deformation can change grain shapes in rocks that contain an intergranular fluid (Passchier and Trouw, 1998). Pressure solution is the equivalent deformation mechanism to Coble creep in dry rocks, and is an important deformation mechanism in the crust and upper mantle (Wheeler, 1992). The solubility of minerals is higher where the crystal lattice is under higher stress, so when stress is applied to the rock material in the grains will dissolve around areas with high differential stress and precipitate at areas around the grain with lower differential stress. This process can change the shape of grains and fabrics can be formed without internal deformation of the grain, by precipitation at a high angle to the highest stress direction and elongation of the grain perpendicular to the shortening direction. The dissolved material may also migrate and deposit in strain shadows of more rigid minerals or in veins (Passchier and Trouw, 1998).

Grain boundary diffusion can occur in most deformation regimes, but some parameters favor this deformation mechanism. Around smaller grains the diffusion distance for the material in the fluid is shorter, so the dissolution and precipitation become a more competitive process in smaller grains. At lower temperatures, pressure solution processes are often more dominant than dislocation creep, since the activation energy for diffusion is lower than dislocation creep.

As well as at high stresses dislocation creep tends to be a more dominant deformation mechanism than pressure solution (Wheeler, 1992).

Crystallographic preferred orientation (CPO) is often used as an indicator for dislocation creep deformation mechanisms. However Bons and den Brok (2000) have experimentally modelled that CPO in anisotropic minerals can form by dissolution precipitation creep and rigid rotation of the crystal. This is due to crystallographic orientation dependent dissolution and precipitation around the grains, and preferred precipitation and dissolution in respect to the highest and lowest normal stress.

2.3.3 Intra crystalline deformation

At elevated temperatures rocks deform by movement of defects within the crystal lattice. Different types of lattice defects can occur. Point defects are a missing or extra atoms or molecules in the crystal lattice, called vacancies and interstitials. There are several types of dislocations effecting the crystal lattice. A missing or extra part of a lattice plane is called an edge dislocation, a displaced or twisted lattice plane caused by a screw dislocation are some members of several more types of dislocations. Dislocation creep is an accommodating process between dislocation glide and recovery (see chapter 2.3.6). Deformation by dislocation creep occurs when dislocations glide in specific crystallographic planes and in a specific direction. The direction of the glide and the amount of displacement of a dislocation is called the Burgers vector. By transmission electron microscope (TEM) studies the Burgers vector of the moving dislocation can be determined, this is called the slip system. Slip systems are presented using Miller indices of the plane and slip direction e.g. (001) [010] for a specific (plane) and [direction] and e.g. {001} <010> for a family of equivalent {planes} and <directions>. Deformation by dislocation creep depends mainly on temperature, and some on differential stress, strain rate and water content. Different slip planes in different minerals can be activated based on the orientation of the grain and the magnitude of the stress. Since dislocations move in a specific slip system in a mineral during a deformation event, a CPO can develop. This CPO is commonly taken as a good indication for deformation by dislocation creep (Passchier and Trouw, 1998).

2.3.4 Recrystallization

Recrystallization is a process during deformation (dynamic recrystallization) where new dislocation free grains are formed from a recovered or deformed grain that contains dislocations (Rollett et al., 2004). Recrystallization and formation of new grains and grain structure can lead to preferred orientation, misorientation and can change the shape and size of original grains or replace them completely (Guillope and Poirier, 1979). There are three different mechanisms depending on temperature and flow stress for dynamic recrystallization, corresponding to regime 1-3 of dislocation creep by Hirth and Tullis (1992). These are bulging (BLG), subgrain rotation (SGR) and grain boundary migration (GBM), in order from low to high temperature and high to low strain rate (Passchier and Trouw, 1998).

Recrystallization by BLG is a mechanism where grains with a low dislocation density bulge into grains with a high dislocation density. New small, recrystallized grains are formed by the formation of subgrain boundaries that eventually can evolve into grain boundaries by rotation of the new grain (Passchier and Trouw, 1998).

SGR recrystallization occurs when dislocations are added to a subgrain boundary by dislocation climb in the crystal lattice, normally at a higher temperature and lower flow stress than recrystallization by BLG. This will cause misorientation and rotation of the subgrain with respect to the host grain, and to other new recrystallized grains. Subgrains mostly occur as sheets between relics of the older host grains, or old grains get entirely consumed by new recrystallized grains (Passchier and Trouw, 1998).

GBM recrystallization occur at higher temperatures than recrystallization by BLG and SRG. Grain boundaries become mobile and sweep through grains and remove dislocations and new dislocation free grains form. Recrystallization in this regime occurs by a mix of grain boundary migration and subgrain rotation. This forms new dislocation free grains and subgrain boundaries eventually evolve into grain boundaries and recrystallized grains forms. This mechanism often lead to interlobate grain shapes with few internal deformation structures like subgrains and undulose extinction (Hirth and Tullis, 1992; Passchier and Trouw, 1998).

2.3.5 Deformation twinning and kinking

Twinning and kinking are described as an accommodating deformation mechanism at lower temperatures and mostly occur in certain minerals e.g. plagioclase, quartz, micas, jadeite and more. Deformation twinning in minerals is mostly restricted to develop in a specific crystallographic direction and plane. A crystallographic plane in the crystal is displaced and sheared causing a change in orientation in relation of the rest of the crystal (Christian and Mahajan, 1995). Kinking develops in the same way but is not restricted to a specific direction and plane in the crystal. It is more dominant in crystals with a single slip system like micas, but can also occur in other minerals e.g. feldspars, amphiboles, pyroxenes, quartz and kyanite. Deformation twins separate from growth twins by often have a tapered shape (thicker in the area with high strain and reduces towards the low strain area of the crystal) shown in Fig. 2.3.1 b and more concentrated at high strain parts of the crystal, while growth twins commonly are straight and may have steps (Fig. 2.3.1 a) (Passchier and Trouw, 1998).

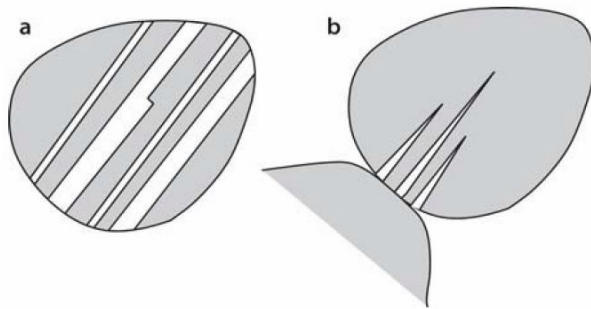


Fig. 2.3.1: a) straight growth twins with step, b) tapered deformation twins at a high stress site of a crystal (Passchier and Trouw, 1998).

2.3.6 Recovery

Recovery are mechanisms that reduce the dislocation density in a crystal. Longer length and higher amount of dislocation per volume of a crystal will cause a higher amount of internal strain energy. Recovery of the crystal can rearrange dislocations by straightening and shorten dislocation, as well as arrange dislocations into networks. This will lower the internal strain energy in the crystal. During recovery dislocations are often consternated in a planar zone, rather than distributed in the whole crystal, and decrease the dislocation density in these dislocation free areas. These bands of dislocations are called a deformation band. Deformation bands can evolve into a subgrain boundary that have a slightly different orientation than the host grain and other subgrains in the crystal (Gerald et al., 1983). A crystal containing subgrains

will show different extinction in the crystal, while dislocations distributed in the entire crystal often will show undulose extinction. Recovery mechanism in crystals can operate after the stress causing the deformation has stopped (Passchier and Trouw, 1998).

2.3.7 Grain boundary area reduction (GBAR), grain growth and post-tectonic recrystallization

Grain boundaries can be seen as planar defects in the crystal, and store internal free energy as well as other defects in the crystal lattice do. GBAR is a process that lower the internal free energy of a crystal by decreasing the total surface area of grain boundaries, by straightening the boundaries and causing growth of more polygonal shaped crystals. GBAR is a much less effective process than recrystallization by SGB or GBM to decreases the internal energy in the crystal, so GBAR is a more prominent mechanism after the deformation has stopped. The strength of the GBAR depends on temperature, presence of other phases and fluids surrounding the grain, mineral chemistry and CPO. The most important factor for a grain to grow and the area of grain boundaries to reduce is that the grain can grow without obstacles (e.g. different phases surrounding the grain). This effect will cause monomineralic aggregates and layers to be more accepting to GBAR, and show coarser and more polygonal shaped grains in monomineralic areas and smaller grains in polymineralic areas (Passchier and Trouw, 1998).

When the deformation of the rock stops crystals may still contain dislocations, subgrain boundaries and unstable grain boundaries, which leads to a higher internal free energy. If the temperature during deformation was high or if water was present in the system along grain boundaries, recrystallization, recovery and GBAR processes can continue to work in the rock to lower the internal energy of the crystals after the deformation have stopped. This process is known as static recrystallization and will replace unstable minerals, cause GBAR and remove dislocation tangles. It changes the grain and subgrain boundaries and can destroy the shape preferred orientation (SPO) but will not affect the CPO (Passchier and Trouw, 1998).

2.4 Deformation and microstructures in eclogite minerals

Main minerals in the studied eclogites and the dominant deformation mechanism working in eclogite facies minerals will be presented in this chapter. Omphacite and garnet deformation and related microstructures at eclogite facies will be the main focus. Eclogite fabric is typically interpreted to be a result of dislocation creep, and the production of a strong CPO in omphacite and other eclogite facies minerals (Bascou et al., 2001; Zhang et al., 2006; Rehman et al., 2016). However some previous studies also suggest that the eclogite fabric may be connected with grain boundary diffusion creep and pressure solution as a CPO forming mechanism (Wheeler, 1992; Bons and den Brok, 2000; Storey and Prior, 2005). If the fabric is mainly produced by dislocation or diffusion creep presently divides the field into two groups with different interpretations for the main mechanism for fabric development.

2.4.1 Omphacite deformation at eclogite facies conditions

Omphacite, the major component in eclogites, is a HP and Na-rich clinopyroxene variant, with a composition between diopside ($\text{MgCaSi}_2\text{O}_6$) and jadeite ($\text{NaAlSi}_2\text{O}_6$) (Zhang et al., 2006). Plastic deformation in minerals is an important deformation process in deformed rocks, and is often recorded by development of CPO in different minerals (Rehman et al., 2016). The formation of CPO in omphacites is interpreted to be a result of dislocation creep deformation, and main types of omphacite CPO fabric have been determined (Helmstaedt et al., 1972; Godard and van Roermund, 1995; Rehman et al., 2016) to be:

1. S-type (foliation)
2. L-type (lineation)
3. Annealed fabrics
4. Composite fabrics
5. Misoriented fabrics

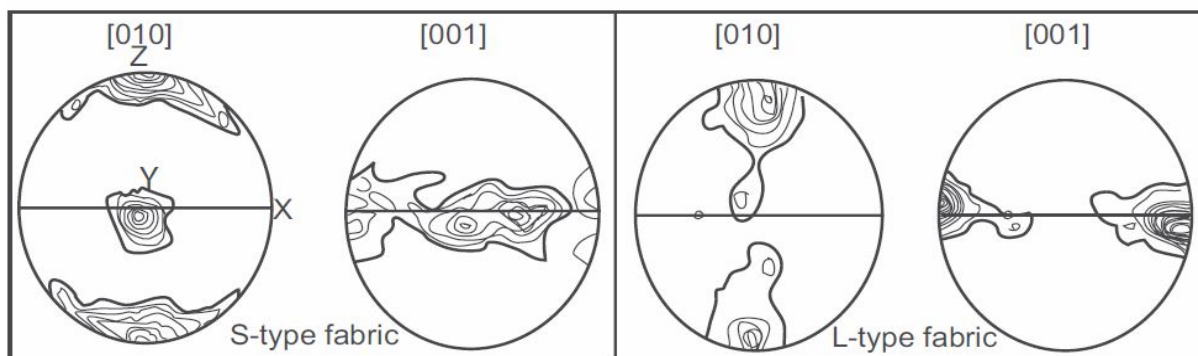


Fig. 2.4.1: typical S- and L-type fabric in omphacite (Rehman et al., 2016). X=lineation, Y=foliation and Z=perpendicular to foliation.

S-type fabric is considered to be a flattening fabric and L-type a constrictional fabric. The S-type fabric may indicate recrystallization of omphacite grains during flattening and development of a foliation, while L-type is believed to originate from recrystallization during constrictional conditions and develop a lineation of the omphacite. Both flattening and constrictional regimes can occur during the same deformation event, and an intermediate between L- and S-type fabrics can develop, called L-S-fabric. As illustrated in Fig. 2.4.1 S-type fabric has a strong [010] axes perpendicular to the foliation (Z) and [001] axes forms a girdle perpendicular to [010] and parallel to lineation (X). While the L-type fabric show a girdle of [010] axes perpendicular to lineation (X) and [001] axes form a strong girdle parallel to lineation (X) (Helmstaedt et al., 1972; Rehman et al., 2016).

Dominant dislocation slip systems to produce the dominant L- and S-fabrics in omphacite, have been determined by several studies using TEM and viscoplastic self-consistent (VPSC) - modeling. The dominant slip systems identified in omphacite are [001] (100), [001] {110} and $\frac{1}{2}$ <110> {110} (Godard and van Roermund, 1995; Rehman et al., 2016).

Dislocation creep as the main deformation mechanism controlling the CPO has been discussed by several studies (Bascou et al., 2001; Zhang et al., 2006; Rehman et al., 2016), but diffusion creep or pressure solution as a mechanism for omphacite CPO has also been discussed as a possible mechanism (Wheeler, 1992; Bons and den Brok, 2000; Mauler et al., 2001). Anisotropic growth (growth rate not equal in all directions), and dissolution precipitation can also be a mechanism for development of CPO in omphacites (Bons and den Brok, 2000). This will cause the crystals to grow in the elongation direction and dissolve in the shortening direction in the rock (Wintsch and Yi, 2002). The C-axis of omphacite is the longest axis, and the growth rate parallel to the C-axis is higher than perpendicular to the C-axis or other directions. As seen in Fig. 2.4.2 the precipitation rate parallel to the C-axis and highest normal stress perpendicular to the C-axis (orientation A), is more efficient than for orientation B with the C-axis parallel to the highest normal stress. This effect will produce a grain shape fabric between the L- and S-type fabrics, and may account for development of CPO in eclogites by dissolution of material in unfavorable grain orientation and growth in the elongation direction (Mauler et al., 2001) .

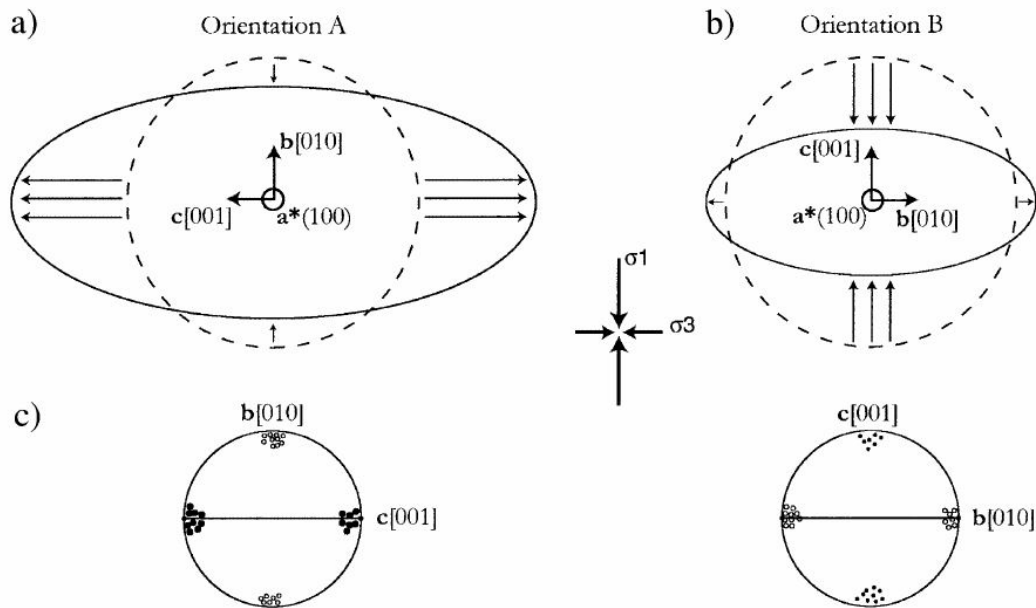


Fig. 2.4.2: illustration of the effect of grain shape and CPO of omphacite due to antistrophic dissolution and precipitation of omphacite (Mauler et al., 2001).

Most eclogites exhumed to the surface have gone through some retrogression of the mineral assemblage. Symplectites of plagioclase and diopside between omphacite grains are a well-known product of the retrograde P-T path of eclogites (Vogel, 1967; Engels, 1972). The symplectites may occur as lamellas of plagioclase and clinopyroxene or as a globular structure of the two phases (Joanny et al., 1991).

2.4.2 Garnet deformation at eclogite facies conditions

Garnet is the main mineral in eclogite beside omphacite. The generic formula for garnet is: $X_3^{2+} Y_2^{3+} Si_3 O_{12}$ where $X=Ca, Fe^{2+}, Mn$ or Mg and $Y=Al, Cr$ or Fe^{3+} . The main members of the garnet group are:

Pyrope: $Mg_3Al_2Si_3O_{12}$

Almandine: $Fe_3^{2+}Al_2Si_3O_{12}$

Grossular: $Ca_3Al_2Si_3O_{12}$

Spessartine: $Mn_3Al_2Si_3O_{12}$

Andradite: $Ca_3Fe_2^{3+}Si_3O_{12}$

Uvarovite: $Ca_3Cr_2Si_3O_{12}$

Garnet is an important mineral in many metamorphic rocks and the understanding of garnet deformation is important for understanding the kinematics of the crust, mantle, subduction processes and is used for many geothermobarometers (Storey and Prior, 2005). Garnet is especially important for understanding of ultra-high pressure rock deformation as in eclogites (Mainprice et al., 2004). In eclogites the cubic structure of garnet makes it a much more rigid mineral than omphacite and other minerals. Omphacite often accommodates the deformation while garnet acts as rigid particles in the rock (Rehman et al., 2016).

By using EBSD, TEM and VPSC modeling microstructures in garnet can be studied, where other microscope techniques do not work for isotropic minerals such as garnet. Deformation by dislocation creep may occur in garnet at high temperatures, and the brittle-ductile transition in garnet occur at around 600-800 °C (Mainprice et al., 2004). CPO, dislocation and diffusion creep related microstructures in garnet has been discussed by several studies (Mainprice et al., 2004; Storey and Prior, 2005) and dominant slip systems and deformation structures have been determined. By simulations and comparison with natural deformed garnets the dominant slip system in garnet has been interpreted to be the $1/2 \langle 111 \rangle \{110\}$ slip (Mainprice et al., 2004; Storey and Prior, 2005). The cubic crystal structure of garnet comes with a large number of slip systems that can be activated during deformation. Either way CPO patterns in garnets are rarely strong. One explanation discussed by several authors is that garnet is mainly associated with other mechanically weaker minerals, and these will accommodate most of the strain and deformation while garnet grain acts as rigid particles (strain partitioning) (Mainprice et al., 2004; Rehman et al., 2016). It has been interpreted by Mainprice et al. (2004) that formation of a strong CPO pattern in garnets high temperatures and strain are required, as found in the mantle transition zone and lower continental crust. Also rocks with a higher fraction of garnet should lower the partition of strain to weaker minerals, and garnets may develop a stronger CPO.

Even if CPO patterns of garnets normally are weak and random, other deformation mechanism except dislocation creep can deform garnets. Garnet growth and production of chemical zonation requires diffusion processes. Grain boundary diffusion (coble creep or pressure solution) can deform garnet by change in grain shapes without effecting the internal structures of the garnet. Dislocation creep mechanisms such as subgrain rotation and recrystallization can produce more fine grained garnet. This can later accommodate grain-size sensitive flow (diffusion creep) processes (Storey and Prior, 2005).

The chemical composition of garnet is very sensitive to changes in temperature and pressure, and variations in the P-T conditions of metamorphic rocks can form chemical zonation in garnets and other minerals. These chemical changes and zonation patterns can be used for constraining the P-T conditions of the rock. Some zonation patterns and chemical composition of garnet have been determined to be typical for prograde metamorphism. The increase of XMg (Mg/Mg+Fe) pyrope content from core to rim is one of these typical prograde chemical zonation patterns (Konrad-Schmolke et al., 2006).

Fibrous rims (kelyphites) composed of amphibole and plagioclase, are a known product of retrogression in eclogites, and have been observed surrounding garnet grains (Klapova et al., 1998; Štípská and Powell, 2005).

2.4.3 Accessory minerals

The main focus in this thesis is to study deformation structures in garnet and omphacite, however accessory minerals such as quartz, zoisite, rutile, hornblende and paragonite are also often present in eclogite and will receive some attention in this study.

Quartz (SiO₂) is present in almost all eclogites in minor proportions but there are not many previous studies on quartz deformation and fabric development at eclogite facies. Mauler et al. (2001) studied lattice preferred orientation (LPO) fabrics in quartz in eclogites and did not find any preferred orientation or hardly any signs of intracrystalline deformation. The quartz grains had straight grain boundaries and a large grain size. Recovery or post-tectonic recrystallization by GBAR during retrogression in quartz may be the reason for the absent signs of intracrystalline deformation, the shape of the grains and may have erased a pre-existing SPO (Mauler et al., 2001). A study on microfabrics in eclogites from Keppler et al. (2016) stated that quartz in these samples are mostly found in pressure shadows of the garnets and more garnet and quartz rich layers forms.

Zoisite, (Ca₂Al₃(Si₂O₇)(SiO₄)O(OH)), mostly occurs as rigid minerals during deformation without intra crystalline plastic deformation. Solution mass transfer and diffusion creep along the grain boundaries may cause elongation and CPO of the grains by grain boundary diffusion dissolution and precipitation at grain areas with high and low stress (Stünitz, 1993). Collett et

al. (2017) suggest that zoisite is the product of hydration and/or cooling during an early stage of exhumation of eclogites.

Amphiboles, in this case hornblende ($\text{Ca}_2(\text{Mg,Fe,Al})_5(\text{Al,Si})_8\text{O}_{22}(\text{OH})_2$), in eclogites is reported to be mainly a product of retrograde metamorphism to lower P-T conditions and replacement of stable eclogite facies minerals. Hornblende can replace omphacite as crystals or form retrograde symplectite rims around garnet and omphacite in eclogites (Engels, 1972; Zhang et al., 2003). In some cases hornblende grains can show a similar CPO fabric as omphacite. When replacing the omphacite hornblende inherits the pre-existing CPO of the omphacite. This process is called homoaxial (Engels, 1972) or homotactic growth (Rehman et al., 2016). Growth of hornblende grains and symplectites during exhumation may also rely on influx of some hydrous fluid to the system, and not only decreasing P-T conditions (Massonne, 2012).

Rutile (TiO_2) is almost always present in eclogites in minor proportions. Rutile is tetragonal and often forms elongated prismatic crystals. It has been observed to have C-axis laying in the foliation plane and/or oriented parallel to the lineation and probably deforms by dislocation and diffusion creep mechanisms as other phases present in the rock (Mauler et al., 2001). Paragonite, Na-rich muscovite, can be present in eclogites in minor or larger amounts and often aligns along the foliation in rocks, as mica minerals normally do (Collett et al., 2017).

3.0 Methods

Different methods for data collection were performed during this thesis: fieldwork, production of thin sections, different methods of imaging and digitalization of the thin section images, image analysis and statistical analysis. These methods will be presented in this chapter.

3.1 Fieldwork

The fieldwork took place in the Northern Bohemian Massif Area, around the Meluzina and Na skalách Mountains (see Fig. 3.1.1) in the Czech part of the Erzgebirge. The goal of the fieldwork was to collect several rock samples and structural data from different localities in the eclogite bodies in the area. Lineation, foliation and sample number were marked on each sample that was collected in situ and the strike and dip/plunge were measured (see Table 3.1.1). The coordinates of the sample localities was noted. The samples, which were primarily used for the study, M1 and M7, are marked with bold text and have all the structural data available:

Table 3.1.1: table showing samples, coordinates, name of outcrop, foliation and lineation.

Sample	Coordinate	Outcrop	Foliation (strike & dip)	Lineation (strike & plunge)
M1	N 50°23,434' E 013°00,391'	Meluzina	184/53°	247/25°
M2	N 50°23,442' E 013°00,411'	Meluzina	Loose block	Loose Block
M3A	N 50°23,435' E 013°00,490'	Meluzina	170/28°	Not visible in field
M3B	N 50°23,435' E 013°00,490'	Meluzina	Loose block	Loose block
M4	N 50°23,399' E 013°00,581'	Meluzina	Not visible in field	Not visible in field
M5	N 50°23,396' E 013°00,599'	Meluzina	205/45°	250/35°
M6	N 50°23,392' E 013°00,625'	Meluzina	Not visible in field	Not visible in field
M7	N 50°23,112' E 012°59,704'	Na skalách	268/54°	245/50°
M8		Na skalách	240/50°	223/48°

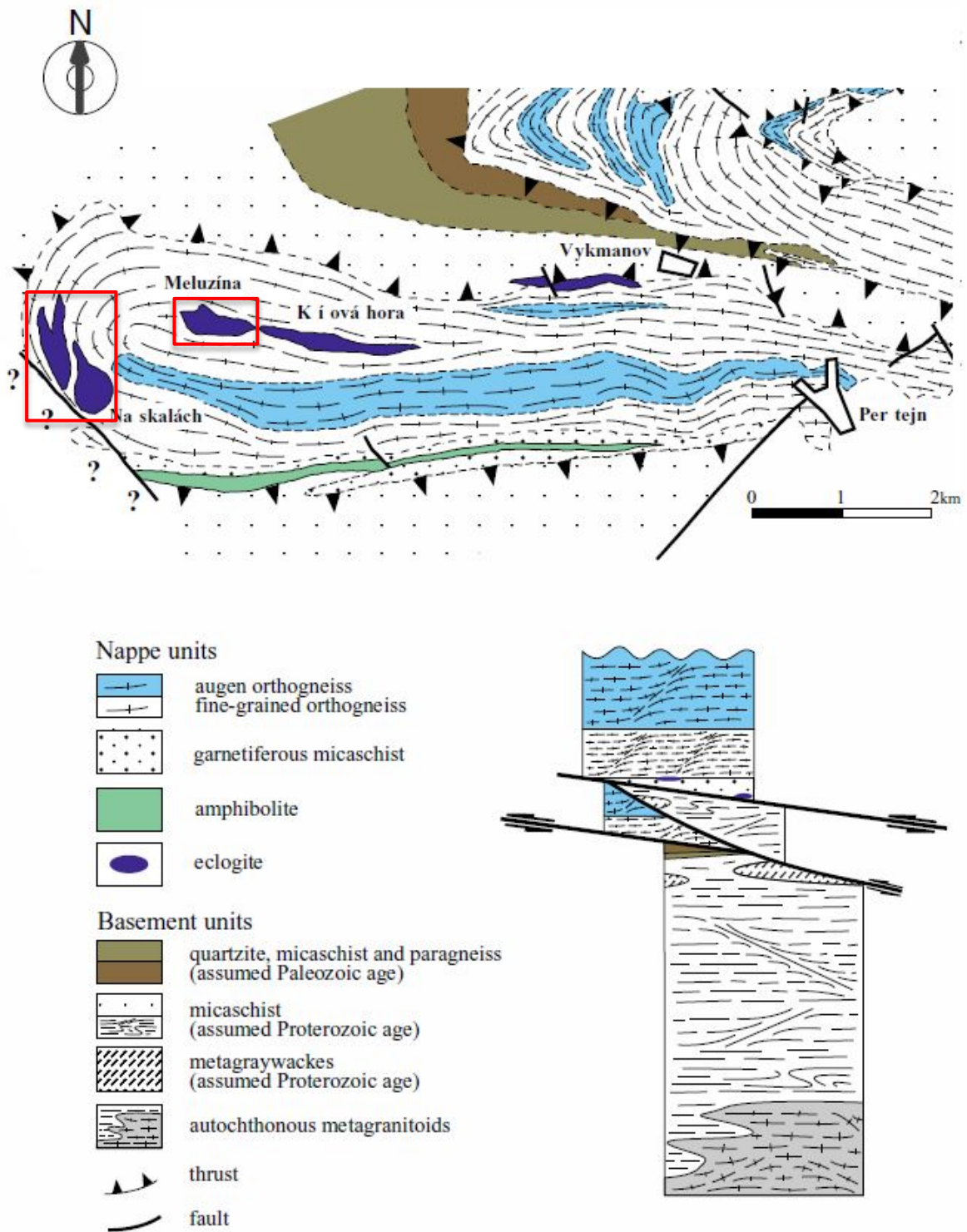


Fig. 3.1.1: geological map of the Saxothuringian domain in the Erzgebirge Mountains in the Bohemian Massif presented by (Klapova et al., 1998), with modifications showing the sampled eclogite bodies (Na skalách and Meluzina) with red squares.

3.2 Preparation of thin sections

The rock samples were first cut in two pieces parallel to the lineation and perpendicular to the foliation using a tile saw. The samples were further cut into 1 cm thick slices by cutting it parallel to the first cut. The slices were studied to find a preferred area for the thin section. Thin section areas had to be as unaffected as possible by retrogression as well as chemical and physical weathering. One thin section per sample was produced. Selected thin section areas were marked and cut into 1 cm (thick) x 2 cm (wide) x 3 cm (long) rectangles. Additional thin sections cut perpendicular to lineation and foliation were produced for selected samples to get a three dimensional (3D) view of the particles. The further preparation of the thin sections were done by the laboratory staff at Institute for Geosciences at University of Tromsø.

3.3 Microscopy

Polarization microscope Leica Laborlux 11 Pol S was used for observation of the thin sections, mineral identification and to gain a rough structural overview. After light microscope studies, two samples were chosen for further work: M1 and M7. The microscope was also used for mineral identification during the production of phase maps, and for identification of grain boundaries for the redrawing of phase and grain boundaries.

3.4 Scanning electron microscopy (SEM) imaging and analysis

Regions of interest on each section were imaged in the SEM. Element maps of some areas were produced by energy dispersive x-ray spectroscopy (EDS) for phase recognition. The thin sections M1-L and M7-L are the ones cut parallel to lineation and perpendicular to foliation, while M1-P and M7-P are cut perpendicular to lineation and foliation. Before producing images of the thin sections in the SEM a carbon coating was applied to avoid electron charging. This was done in a carbon evaporator, which coated the section with a thin (≈ 20 nm) carbon layer from a carbon thread. A Zeiss MERLIN VP compact SEM located at the Department of Medicine and Health at University of Tromsø was used for all imaging.

3.4.1 BSE and EDS imaging

The greyscale of the back scatter electron (BSE) images is related to the average atomic number of the elements in the minerals present in the sample. The lower the atomic number of the elements, the darker the greyscale on the BSE-image. This is due to the number and intensity of backscattered electrons, and the energy absorbed by the BSE detector (Schwartz et al., 2009). The section was placed in the chamber of the SEM, and pumped down to a vacuum of at least 1×10^{-5} mbar. The same magnification and working distance (the distance between the pole piece of the electron gun and the focused sample) was used for all BSE images produced for the redrawing of phase and grain boundary maps, 300x magnification and 8.5 mm working distance. The acceleration voltage (EHT) level applied was constant at 20.00 kV and a BSE detector was used for all images. The settings used are shown in Fig. 3.4.2.

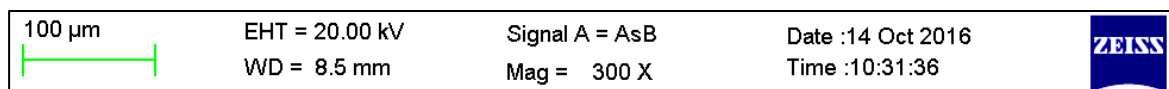


Fig. 3.4.1: setting used for BSE imaging.

The contrast, brightness and focus was adjusted to achieve the clearest image of grain boundaries, zonation and phases. The images were taken one by one to cover the area of interest for each thin section by using a joystick that moved the stage the sample was placed on.

Around 100 BSE images were taken with a working distance of 8.5 mm and 300x magnification for each thin section. Adobe Photoshop CS6 was used to stitch the separate images together and produce one map for each area of interest. This was done by inserting all the images to a blank canvas with no compression of the original image size (1024 x 768 pixels) to keep the high resolution and to not compress the size of the image.

Element maps of selected areas from the BSE images was produced using the EDS detector and AZTEC software by Oxford instruments for post-processing. The EDS produces elements maps in AZTEC software where different elements are given different colors. The density of each color/element in different phases help to determine the mineral. The EDS detector was also used for point and linescan analysis to help identify different phases in the sample, and to study chemical zonation in single crystals.

3.4.2 EBSD-mapping

EBSD is an additional technique in the SEM to obtain crystallographic orientation of grains and identification of phases. The electron beam hits the tilted sample and the diffracted electrons backscattered by the lattice planes form a Kikuchi pattern on a phosphorus screen, as illustrated in Fig. 3.4.2. A camera placed behind the phosphorus screen captures the pattern. The angles between the lines in the Kikuchi pattern and the pattern itself can identify the phase and the crystal orientation of the grain. The sample needs to be tilted about 70° to obtain high intensity Kikuchi patterns. The identification of phases are done automatically by a software, in this case AZTEC from Oxford instruments that recognizes the pattern and angles of the Kikuchi pattern from a database (Schwartz et al., 2009).

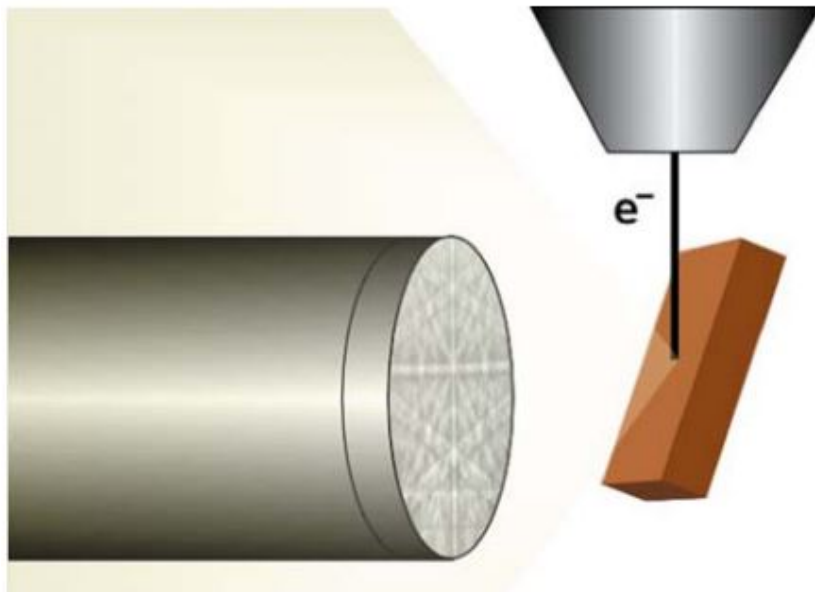


Fig. 3.4.2: illustration from (Schwartz et al., 2009) with the pole piece with the detector, the tilted sample and the phosphorus screen with a Kikuchi pattern.

The sample was placed with a 70° tilt oriented parallel to the lineation. The area to be mapped was marked and phases present in the sample was chosen from a database. The Kikuchi pattern recognition software was checked to make sure it identified the right phase. The settings used for the EBSD are found in Table 3.4.1.

Table 3.4.1: settings used for EBSD analysis.

<i>Sample</i>	<i>M7-L (large map)</i>	<i>M7-P (single window)</i>	<i>M7-L (single window)</i>	<i>M1-L (large map)</i>	<i>M1-L (single window)</i>
<i>Coating</i>	Carbon	Carbon	Carbon	Carbon	Carbon
<i>Direction</i>	Parallel to X	Parallel to X	Parallel to X	Parallel to X	Parallel to X
<i>SEM</i>	Zeiss Merlin compact VP	Zeiss Merlin compact VP	Zeiss Merlin compact VP	Zeiss Merlin compact VP	Zeiss Merlin compact VP
<i>Tilt (deg)</i>	70°	70°	70°	70°	70°
<i>Acc. Volt (kV)</i>	20 kV	20 kV	20 kV	30 kV	30 kV
<i>Working distance</i>	23.9 mm	18.3 mm	22.9 mm	23.8 mm	23,8 mm
<i>EBSD</i>	Oxford instruments	Oxford instruments	Oxford instruments	Oxford instruments	Oxford instruments
<i>Step (µm)</i>	3 µm	0.7 µm	0.7 µm	6 µm	2.5 µm

3.4.3 Pole figures

Pole figures was plotted and contoured using HKL Channel 5 by Oxford instruments. Equal area projection and lower hemisphere pole figures were constructed for all phases. Relevant crystallographic planes was chosen for each phase. The horizontal line in the pole figures is the lineation direction and is marked with X and foliation with Y, Z is perpendicular to X and Y. An estimation for amount of grains per phase in the EBSD maps, and hence number of grains used for the construction of pole figures were estimated from the grain boundary and phase maps for the samples.

3.5 Production of grain boundary and phase maps

For redrawing of grain boundaries and image analysis of the particles ImageJ, an image analysis software for image processing and analysis in Java and connected toolboxes was applied. The stitched images from sections M1-L, M1-P, M7-L and M7-P were used. The redrawing of grain boundaries was done by using a “paintbrush tool” with a 2 pixel wide brush. Each grain boundary was identified and drawn for all phases. A light microscope was used to separate cracks from grain boundaries and to help separate clustered grains. When the drawing of all boundaries was complete, the “thresholding tool” was used to extract only the black boundaries. Since some holes, cracks and noise are always present in a BSE image, post processing was done to remove this by using the “skeletonize tool” to first reduce all lines to a width of 1 pixel, then the “prune tool” to erase all non-closed lines, e.g. boundaries cut by the edge of the image and holes/noise. Most analysis in ImageJ rely on 2 pixel wide grain boundaries, so the tool “thicken lines” was used to make the perfect grain boundary map. When the grain boundary map was complete, each of the 7 phases (omphacite, garnet, quartz, hornblende, zoisite, paragonite and rutile) was assigned its own greyscale, which varies from 0 (black)-255 (white) in ImageJ. The greyscale was chosen based the darkness/brightness the phases in the BSE image to avoid confusion. From darkest to lightest greyscale for each phase (in non-inverting LUT):

Table 3.5.1: the different greyscales used for each mineral phase in the imaging. 0-255 from darkest to lightest greyscale. Calibration bare for greyscale to the right.

Phase	Greyscale
Quartz (Qtz)	55
Paragonite (Pg)	83
Omphacite (Omp)	111
Hornblende (Hbl)	139
Zoisite (Zo)	167
Garnet (Grt)	195
Rutile (Rt)	223
Unidentified	250
Boundaries + edge	0

Each phase was colored by using a “flood fill tool” in ImageJ. Identification of each phase was obtained by the BSE images and by using a light microscope. Some of the smaller grains that

were difficult to identify, both in the BSE image and in the light microscope, were marked with an own shade of grey (250) and called unidentified. To make sure that 100% of the image was filled with a greyscale, the “thresholding tool” was used. A grain boundary map and a phase and grain boundary map were now produced. Color maps were also produced to better separate the phases.

Each grain boundary map and phase map was scaled using the scale bar on the BSE image. During stitching and pre-processing of the images, no resizing was done so all the images still had the same size. The scale is 1.1296 pixels/ μm .

3.6 Modal composition

The modal composition of the different samples can be analyzed by using the grain boundary and phase maps. This was done by thresholding the phases one by one and see how much of the image contains that specific greyscale. This method will only give the area fraction of each phase in the image, but this is a good estimation for the volume fraction of the phases. The most important factor for the volume fraction is the total area of the image and sufficient amount of pixels per phase, based on this the average area fraction mostly equals the volume fraction of the section (Heilbronner and Barrett, 2014).

3.7 Grain size analysis

For the grain size analysis the phases were separated, and bitmaps of all the phases in each image were made (see Fig. 3.7.1) using “threshold tool” and grey level slicing. By separating the phases separate grain size analysis can be done for each phase.

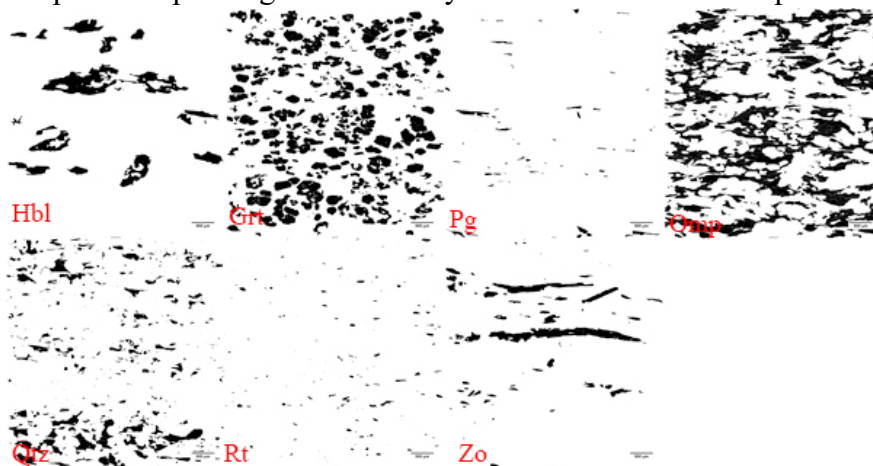


Fig. 3.7.1: example of bitmaps of phases in M1-L. Mineral abbreviations by Siivola and Schmid (2007). Parallel to lineation (\leftrightarrow).

Each phase was analyzed by using the “analyze particles-tool” in ImageJ on an unscaled image. The data were imported to Kaleidagraph, a graphing and analyzing software, to continue the analysis. From the analysis the area of each grain was derived, which is the number of pixels in one grain and the perimeter of the grains. From this the equivalent corrected radius (equ corr r) can be calculated. This is a circle with equal area as the grain, with correction for the 2 pixel wide line that separates the grains. This is calculated for every grain using this formula (Heilbronner and Barrett, 2014):

$$Equ\ corr\ r\ (pixel) = \sqrt{\frac{Area + Perimeter}{\pi}} \quad \text{Equation 3.7.1}$$

Since an unscaled image was used the radius had to be recalculated from pixels to μm . The pixel resolution is 1, 1296 px/ μm , so the equivalent corrected radius in μm was calculated using:

$$Equ\ corr\ r\ (\mu\text{m}) = equ\ corr\ r(px) * 1,1296 \quad \text{Equation 3.7.2}$$

The equivalent corrected radius for each phase was calculated. In the statistics from the equivalent corrected radius column, the mean and median grain size can be found. While the modal grain size is represented by the highest occurrence of a grain size in the sample. This was found by binning the equivalent corrected radius data and make a histogram where the highest column represents the mode. Which ‘average’ that best fit the real grainsize can be determined by looking at the skewness of the histogram of equ corr r (μm). If the histogram is positively skewed, the mean is larger than the median and the median is larger than mode (Heilbronner and Barrett, 2014). All grain size data is in two dimensions (2D).

3.8 PAROR & SURFOR analysis

PAROR and SURFOR are two different approaches to study mineral fabrics, and this method was used to analyze particle and shape fabric of omphacite and garnet. Digitalized XY coordinates for single phase bit maps were obtained by using the Jazy Macro “Jazy_XY_export_header” and the tool “XY-export-regdist-smooth” in ImageJ and a pixel distance resolution of 5 for each XY point was used.

3.8.1 PAROR

PAROR analysis of the particle fabric is based on 2D projections of the longest and shortest axis and the orientation of the longest axis of the particles (Panozzo, 1983). From the PAROR analysis, the preferred orientation of the particles and the axial ratio (shortest axis (b) divided by the longest axis (a) of the particle) can be obtained. The PAROR data will be presented as rose diagrams of the orientation distribution function (ODF) of the relative length of the longest axis of the particles. And projection curves of the relative length of projections divided by the longest projection of an axis. The minimum value of the projection curve is the axial ratio of the bulk fabric (Heilbronner and Barrett, 2014).

3.8.2 SURFOR

SURFOR analysis of particles in 2D are based on projection of outline segments of particles, and how the length of the projected outline is depending on the orientation of the particle. The SURFOR results are presented by a plot for the bulk characteristic shape of the particles, this is based on the total length of projected lines per orientation for the bulk surface fabric. As for the PAROR, rose diagrams of the distribution of the relative length of line segments per angle are presented. The axial ratio from the SURFOR analysis can be measured from the bulk characteristic shape of the particles, and shape preferred orientation (SPO) fabrics can be visualized (Heilbronner and Barrett, 2014).

4.0 Results

In this chapter all data collected using the different methods will be presented. Original greyscale grain boundary and phase maps that were produced using ImageJ will be presented in the appendix (Fig. 8.1-8.4). BSE images, EDS data, EBSD phase maps and pole figures for the main phases will be presented in separate chapters for each phase. Finally grain size data will be shown.

4.1 Grain boundary and phase maps

Grain boundary maps and phase maps were produced for M1-L, M1-P, M7-L and M7-P. These maps and the single phase bit maps obtained from the phase maps were used for grain size analysis, volume fraction and SURFOR and PAROR analysis. The number of grains per map is relevant for the amount of data points available for the analysis. The amount of grains per phase is shown in Table 4.1.1.

Table 4.1.1: number of grains for each phase, and total number of grains per image.

Phase	M1-L	M1-P	M7-L	M7-P
Quartz	567	76	480	84
Paragonite	71	45	7	0
Omphacite	1704	757	2540	658
Hornblende	25	18	22	5
Zoisite	86	54	630	165
Garnet	538	95	359	39
Rutile	169	50	380	41
Total	3160	1095	4418	992

Colored phase maps were produced for M1-L, M1-P, M7-L and M7-P to better separate the phases. Note that the color legend is different than the EBSD images, the colors in the phase map below were selected to best optimize the separation of the phases. The color phase and grain boundary maps are presented below in Fig.4.1.1-4.1.4.

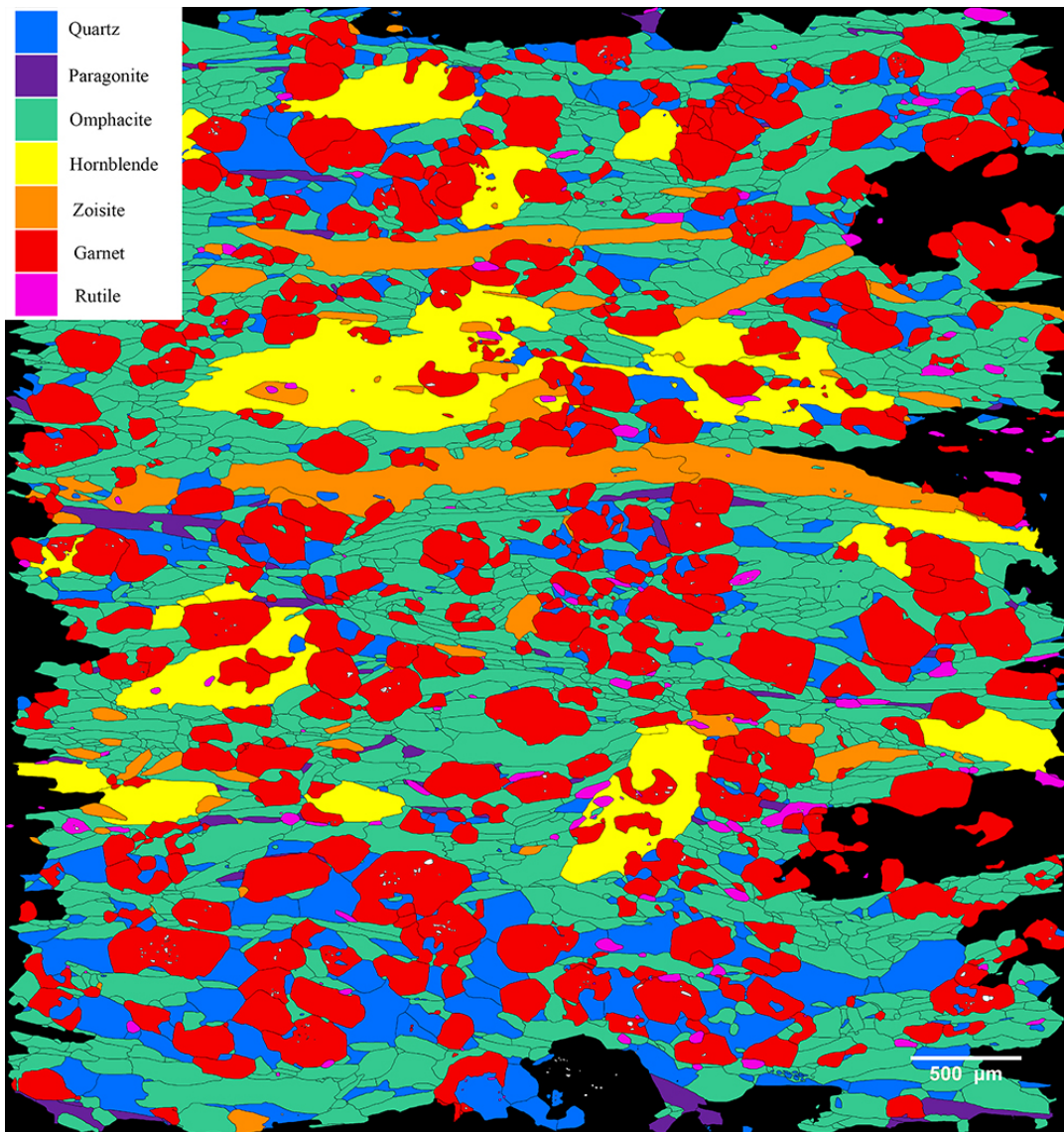


Fig. 4.1.1: redrawn grain boundary and phase map of M1-L, with scale and calibration bar. Parallel to lineation (↔)

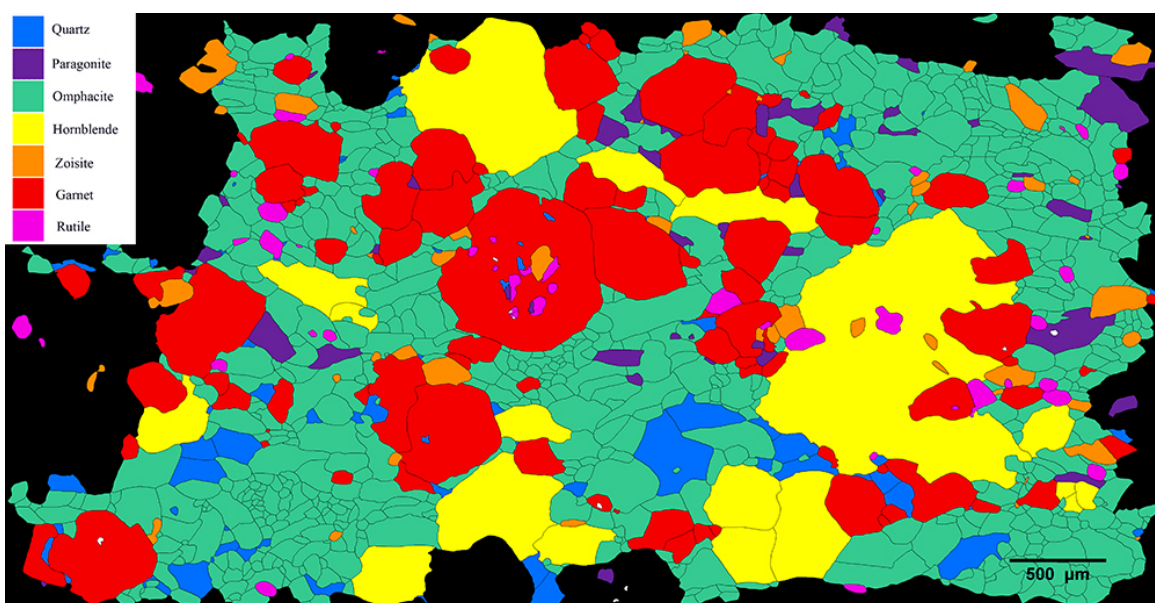


Fig 4.1.2: redrawn grain boundary and phase map of M1-P, with scale and calibration bar. Perpendicular to lineation.

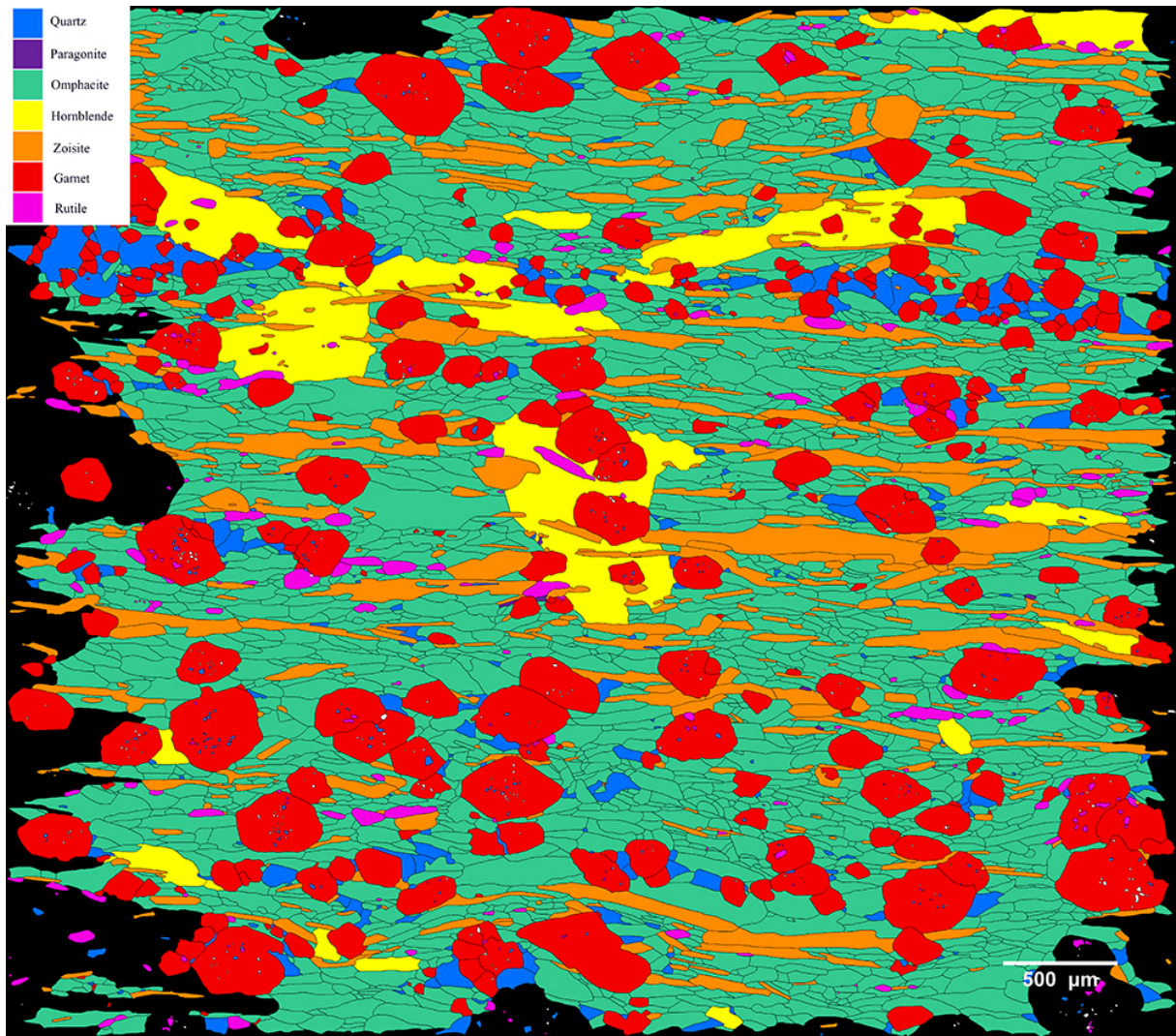


Fig. 4.1.3: redrawn grain boundary and phase map of M7-L, with scale and calibration bar. Parallel to lineation (\leftrightarrow).

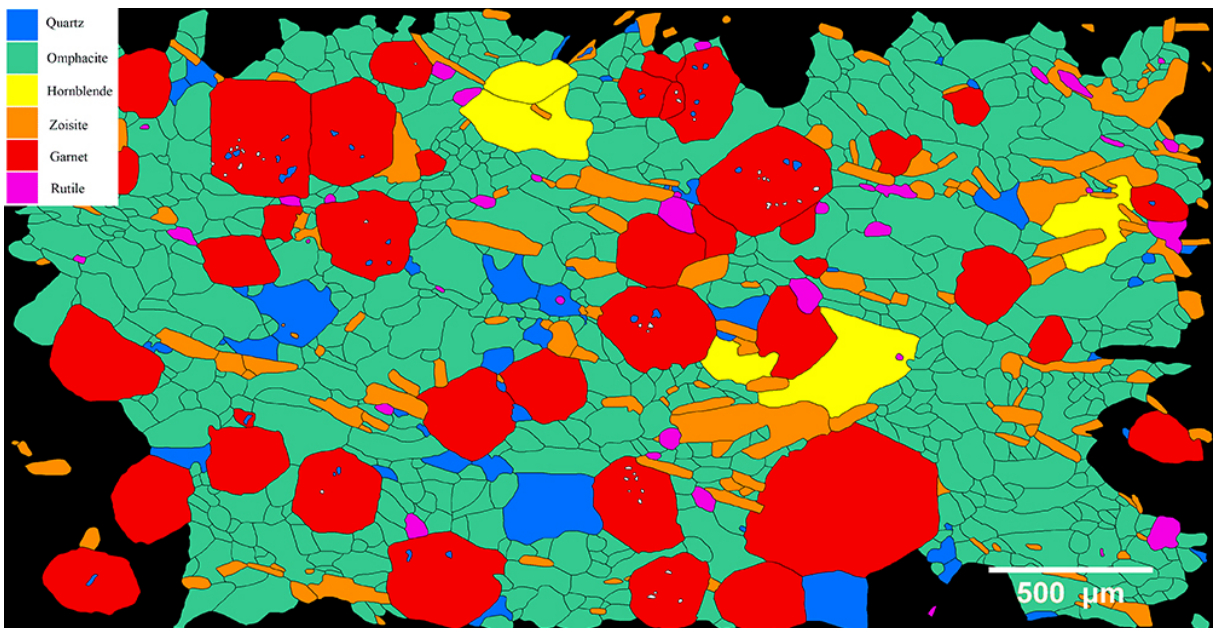


Fig. 4.1.4: redrawn grain boundary and phase map of M7-P, with scale and calibration bar. Perpendicular to lineation.

4.2 Mineralogy and volume fraction

The main phases identified by EBSD phase maps, EDS (element maps, point and line analysis), BSE and light microscopy were: Omphacite + garnet + quartz + hornblende + zoisite + rutile ± paragonite. The phases are presented in EBSD image (Fig. 4.2.1) from M7-P. Paragonite is absent from this sample.

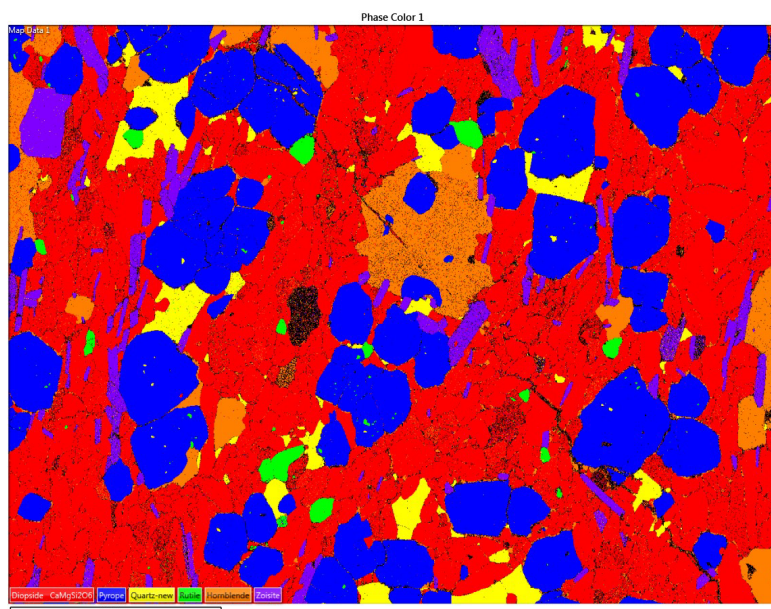


Fig. 4.2.1: EBSD phase map of M7-P, cut perpendicular to lineation. Red=omp, blue=grt, purple=zo, yellow=qtz, green=rut and orange=hbl.

The estimated volume fraction of each phase is presented in Table 4.2.2, together with the greyscale value, unidentified grains and boundaries + edge of the image. All phases, unidentified grains and boundaries/edges make 100%, indicating that all grains in the image have an assigned grey value.

Table 4.2.2: Phases present in the four samples, greyscale used for each phase and percentage of each phase in each individual sample.

Phase	Greyscale	M1-L %	M1-P %	M7-L %	M7-P %
Quartz	55	9,85	3,01	3,08	3,54
Paragonite	83	1,07	2,18	0,02	0,00
Omphacite	111	31,36	32,94	42,61	42,29
Hornblende	139	7,77	14,90	5,50	2,99
Zoisite	167	5,34	2,08	11,89	7,55
Garnet	195	26,75	19,47	19,03	22,55
Rutile	223	0,96	1,14	1,47	1,08
Unidentified	250	0,07	0,02	0,06	0,03
Boundaries + edge	0	16,83	24,26	16,34	19,97
Sum		100	100	100	100

4.3 Thin section description

Four thin sections from two samples were used in this study: M1-L (Fig. 4.3.1a), M1-P (Fig. 4.3.1b), M7-L (Fig. 4.3.1c) and M7-P (Fig. 4.3.1d). The thin sections were from outcrops about 1-2 km apart. They have some differences in modal composition but are structurally similar. In all samples omphacite and garnet are the major components in the eclogites, and the focus of this study. Elongated minerals such as omphacite, garnet and zoisite form most of the fabric observed in the rock with the long axis parallel to the lineation.

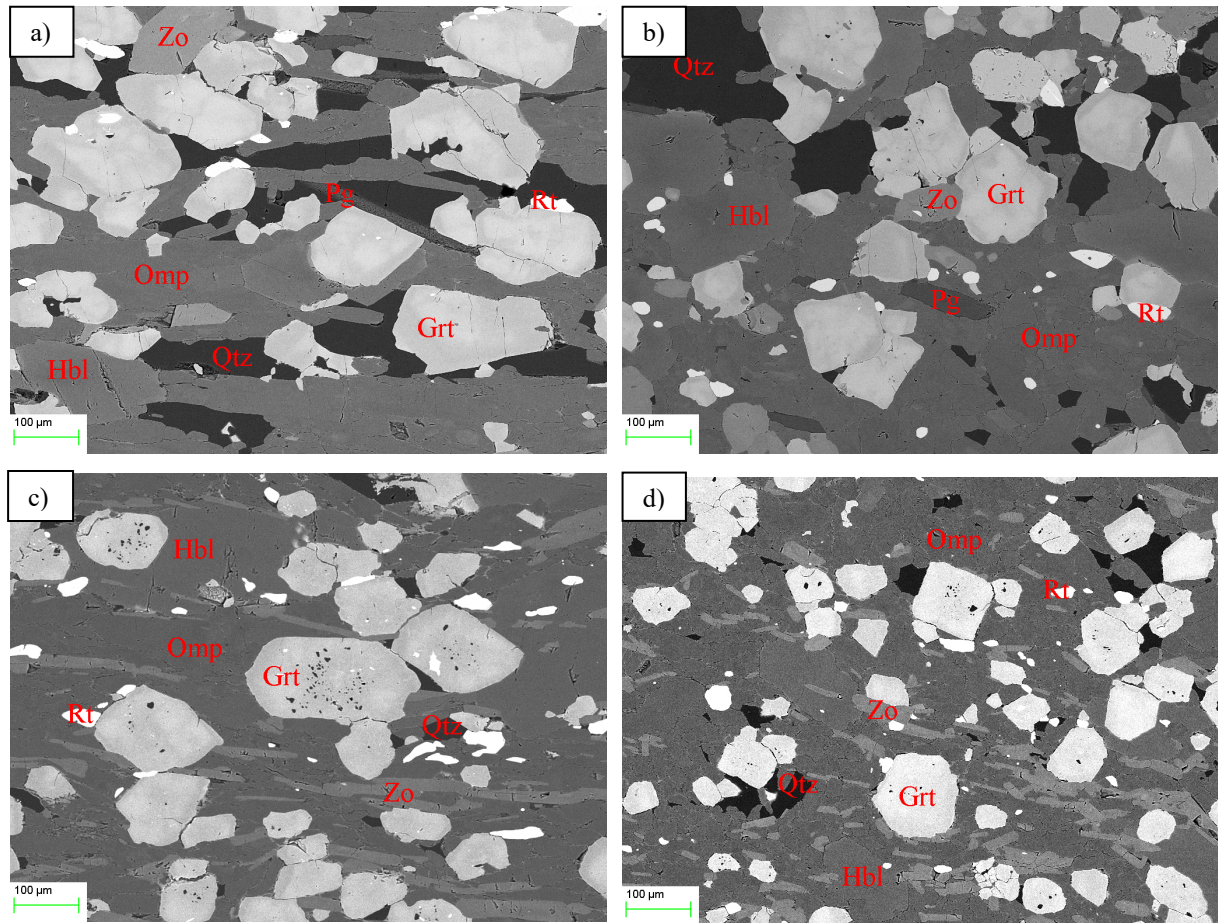


Fig. 4.3.1: from top left to bottom right M1-L, M1-P, M7-L and M7-P. BSE images of the different oriented samples. M7-L and M1-L parallel to lineation (\leftrightarrow) and M7-P and M1-P perpendicular to lineation. Phases and scale bare are presented on images.

Omphacite grains occur as elongated euhedral crystals, and are elongated in the lineation direction and have a modal grain size diameter between 50 and 100 µm. Omphacite is uniformly distributed in the entire rock, except for higher concentration of omphacite in layers with less garnet, and it is the main rock forming mineral in the eclogites. Garnets occur mostly as euhedral single porphyroblasts but also in clusters of several smaller garnets and a few hollow garnets filled with another phase. More garnet rich layers occur parallel to the foliation plane, besides these layers the garnet is uniformly distributed in the entire rock. The garnets have an

elongated shape with its long axis parallel to the lineation direction, and with a modal grain size diameter between 60 and 300 μm . Analysis in the EDS indicates a hornblende composition of the amphiboles. Hornblende grains are large, euhedral porphyroblasts with a modal grain size diameter ranging from 180 to 350 μm . Hornblende is randomly distributed and orientated, as well as overgrowing the original fabric in the eclogites. Zoisite occurs as elongated, prismatic particles, as well as aggregates of several elongated zoisite particles. Zoisite grains are elongated parallel to the lineation direction and exhibit tabular, shorter particles perpendicular to lineation. Modal grain size diameter is between 30-45 μm for the zoisite. Quartz is most frequently associated with garnet or zoisite and almost never as single crystals in the omphacite matrix. Quartz occurs mainly as aggregates of quartz grains with straight grain boundaries and a modal grain size diameter of 15-40 μm . More garnet rich layers were observed in the rock with alternating omphacite rich layers. Since quartz dominantly is associated with garnet, there is a higher abundance of quartz in these garnet rich layers. Paragonite is only present in small proportions in M1-L and M1-P, and occurs as elongated needles in the lineation direction, with a modal grain size diameter between 35 and 75 μm . Rutile is present in all samples in small proportions as euhedral single grain randomly distributed in the rock, but often found as inclusions in the garnet. Rutile has a slight elongated shape in the lineation direction and has a modal grain size diameter of 15-50 μm .

4.4 Description of phases

Omphacite ($\approx 32\text{-}43\%$) and garnet ($\approx 19\text{-}26\%$) make up $\approx 50\text{-}65\%$ of the samples. Zoisite ($\approx 2\text{-}11\%$), hornblende ($\approx 3\text{-}15\%$) and quartz ($\approx 3\text{-}10\%$) are the next most abundant phases, paragonite ($\approx 0\text{-}2\%$) content varies in the samples and rutile ($\approx 1\text{-}1.5\%$) was present in all samples in minor proportions, see table 4.2.2 for overview. In this section the main mineral facies will be described separately, with focus on omphacite and garnet. Chemical zonation of omphacite and garnet was studied using BSE images and EDS techniques such as point and linescans and chemical maps constructed in AZTEC. The zonation and the chemical differences are good indicators for P-T conditions during growth of the mineral. EBSD maps from M7-L single window and large map (see Fig. 4.4.1), M1-L large map (see Fig. 4.4.2), and M7-P single window (see Fig. 4.2.1) were used for construction of pole figures and for phase recognition.

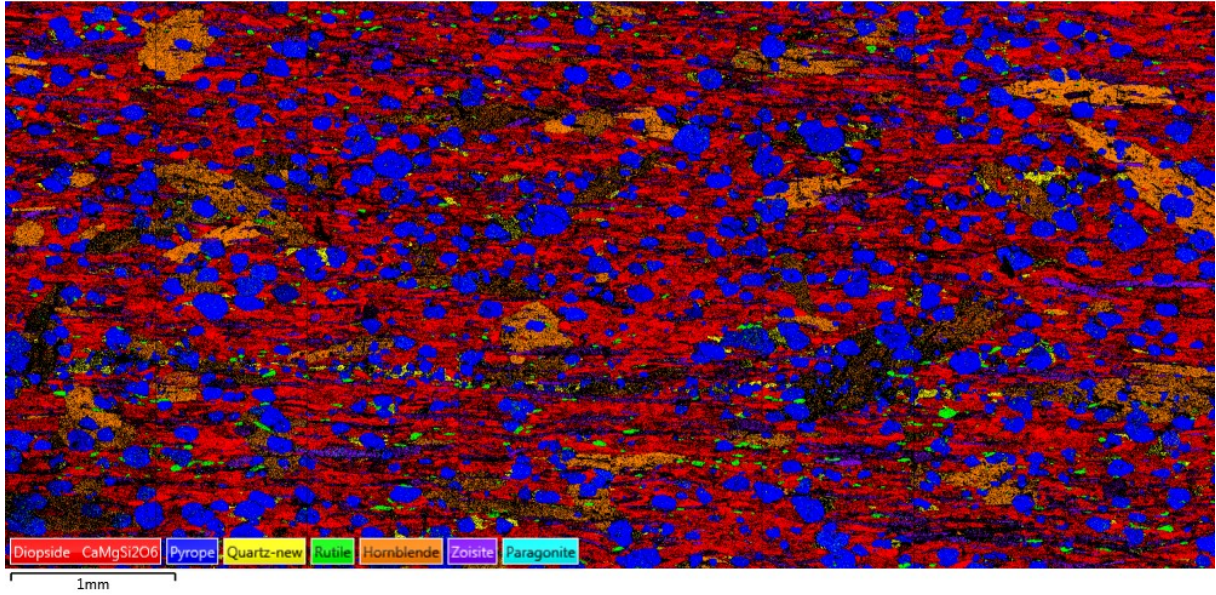


Fig. 4.4.1: EBSD map (large map) of M7-L parallel to lineation (\leftrightarrow)

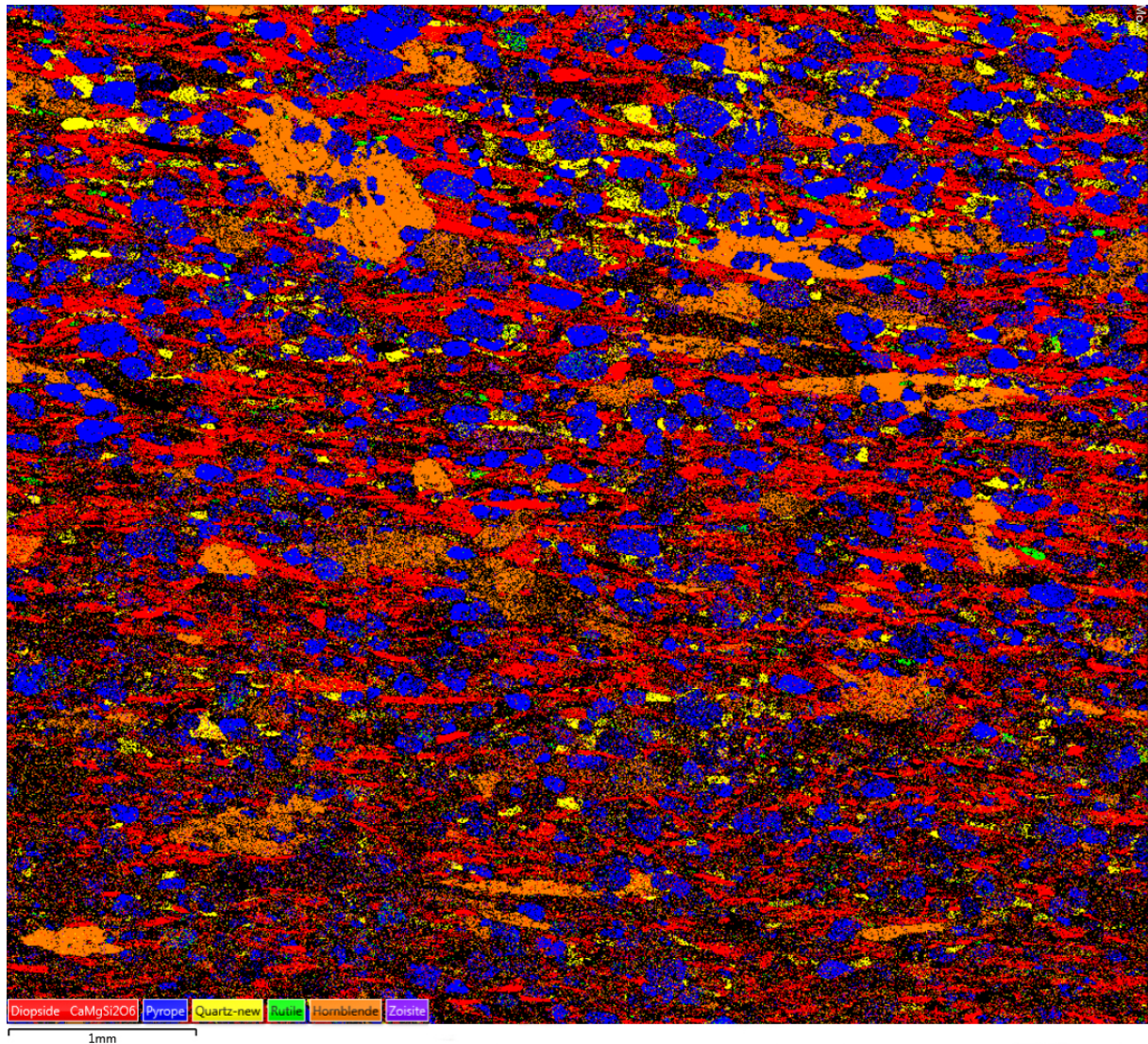


Fig. 4.4.2: EBSD map (large map) of M1-L parallel to lineation (\leftrightarrow).

4.4.1 Omphacite

In the BSE images chemical zonation are visible in some grains by lighter and darker areas indicating a difference in chemical composition (see Fig. 4.4.3).

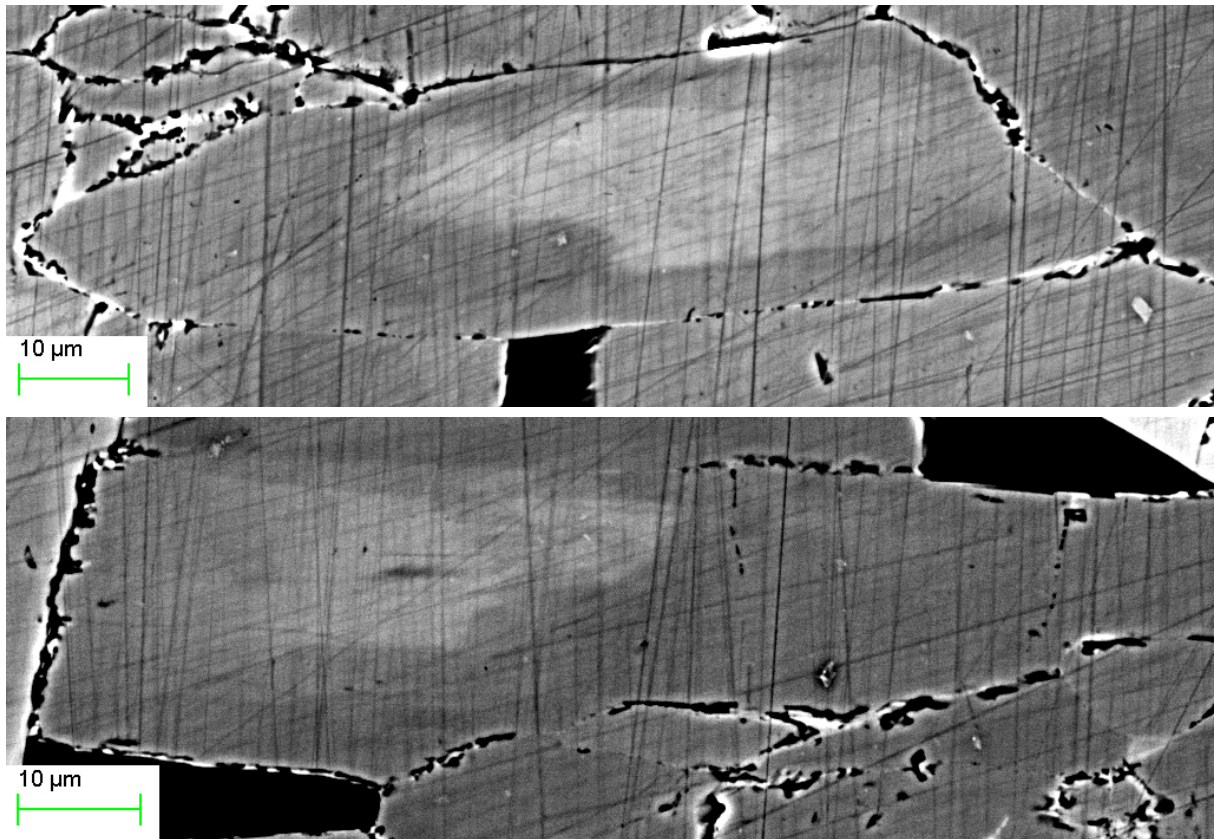


Fig. 4.4.3: asymmetric chemical zonation in single omphacite grains. The straight lines are scratches from the polishing. Parallel to lineation (\leftrightarrow).

The point and linescan EDS analysis show that the omphacite has a core with a higher diopside content compared to the rim. Towards the grain boundary the Na and Al content increases while the Mg and Ca content decreases, and the composition changes to a more jadeite component. The zonation show an asymmetric character with a wider rim in the lineation direction of the grains. The zonation is not as clear in the BSE images in all omphacite grains, compared to the garnet, due to a low difference in the atomic weight of the elements making up the zonation (Na, Mg, Al, Ca).

EDS linescans of single omphacite grains (see Fig. 4.4.4) confirms the trend with a core richer in Mg and Ca and a more diopside composition. Towards the rim the Ca and Mg content decreases while Na and Al increases, and the chemical composition changes to a more jadeite composition.

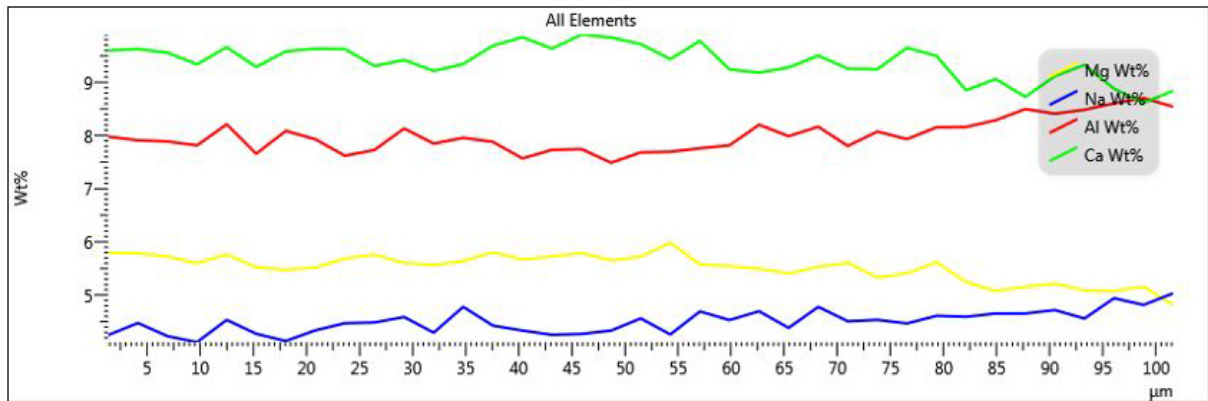
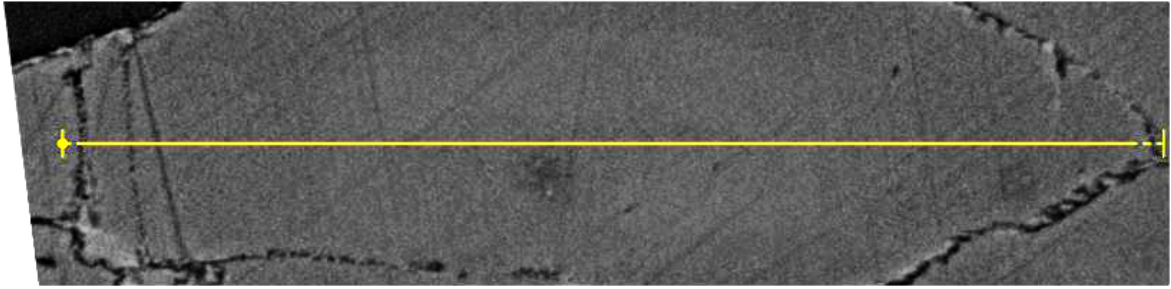


Fig. 4.4.4: EDS linescan of a single omphacite grain, Na (blue), Mg (yellow), Al (red) and Ca (green). Increase of Al and Na towards the rim and decrease of Ca and Mg, indicating chemical change from more diopside composition in the core and more jadeite composition towards the rim of the omphacite. Parallel to lineation (\leftrightarrow).

Electron Image 10

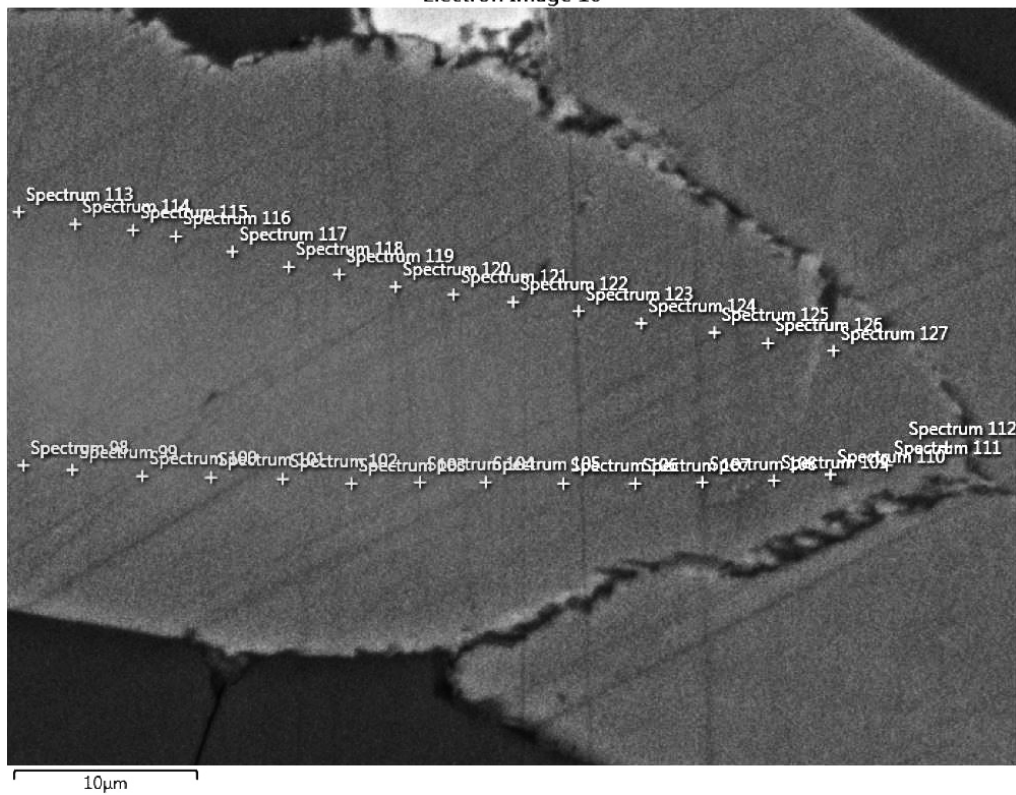


Fig. 4.4.5: EDS point analysis from core (left) to rim (right) in a single omphacite grain. Two lines of points, referred to as upper and lower line of points. Parallel to lineation (\leftrightarrow).

EDS point analysis (see Fig. 4.4.5) from core to rim in single omphacite grains show the same trend with increasing Na and Al values and decreasing Mg and Ca values from core to rim.

Table 4.4.1: spectrum for chemical point data analysis in a single omphacite grain.

Spectrum 98			Spectrum 102			Spectrum 107			Spectrum 111		
	Wt%	σ		Wt%	σ		Wt%	σ		Wt%	σ
O	43,9	0,1	O	44,6	0,1	O	44,4	0,1	O	44,2	0,1
Si	25,7	0,1	Si	26,0	0,1	Si	25,9	0,1	Si	25,8	0,1
Ca	10,6	0,0	Ca	10,4	0,0	Ca	10,0	0,0	Ca	9,7	0,0
Mg	5,5	0,0	Mg	5,6	0,0	Al	5,4	0,0	Al	5,6	0,0
Al	4,9	0,0	Al	5,1	0,0	Mg	5,3	0,0	Mg	5,1	0,0
Na	4,2	0,0	Na	4,5	0,0	Na	4,7	0,0	Na	4,8	0,0
Fe	3,3	0,0	Fe	3,3	0,0	Fe	3,2	0,0	Fe	3,1	0,0

Spectrum 98 and 102 have a higher content of Ca and Mg and a lower content of Na and Al and indicates a composition closer to diopside in the core. Spectrum 107 and 111 have increasing values of Na and Al compared to the core and hence a more jadeite composition in the rim (see Table 4.4.1).

At the grain boundary of omphacite a rim (1-5 μm) of finer grained diopside and plagioclase symplectite surround the grains, as shown in BSE images in Fig. 4.4.6 a. The chemical point analysis done in the SEM identified these facies to be diopside and plagioclase. Symplectites were also observed in cracks in the omphacite grains, shown in BSE image Fig. 4.4.6 b. The fabric of the symplectites are parallel to the lineation direction of the rock, and wider in the lineation direction. The symplectites between the omphacite grains had a more globular structure of the two phases in some areas.

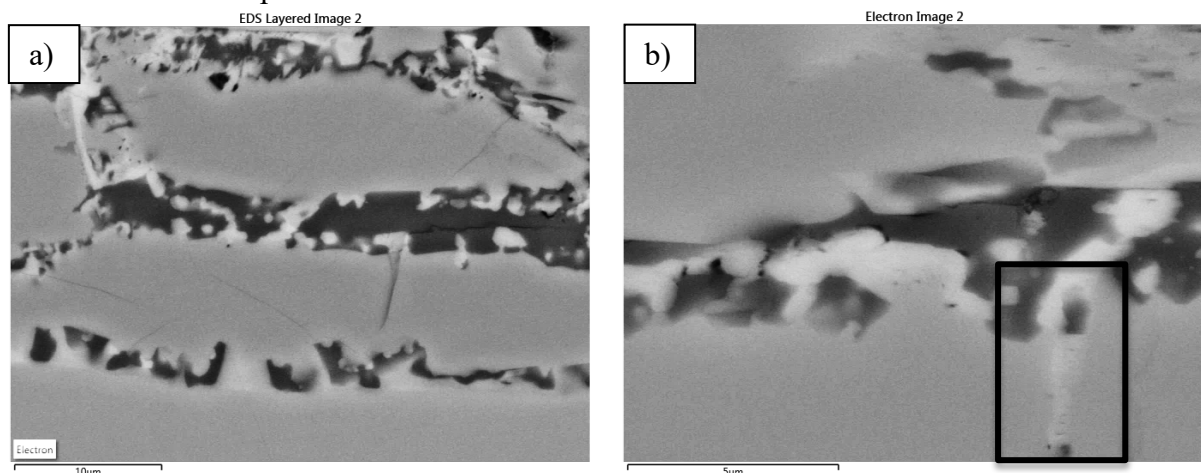


Fig. 4.4.6: BSE images of diopside and plagioclase symplectites, parallel to lineation (\leftrightarrow). a) Globular symplectites between omphacite grains. b) Symplectite fabric parallel to lineation in cracks (see black box).

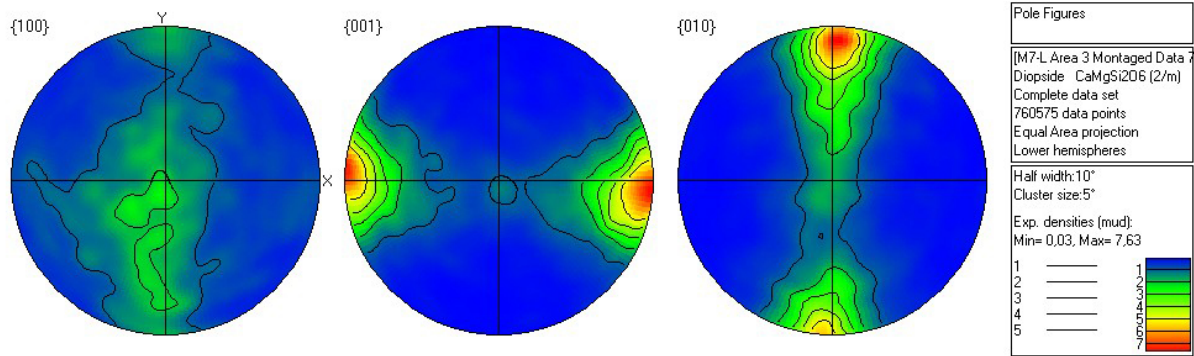


Fig. 4.4.7: omphacite pole figure from M7-L (large map), X=lineation, for ~ 9000 grains.

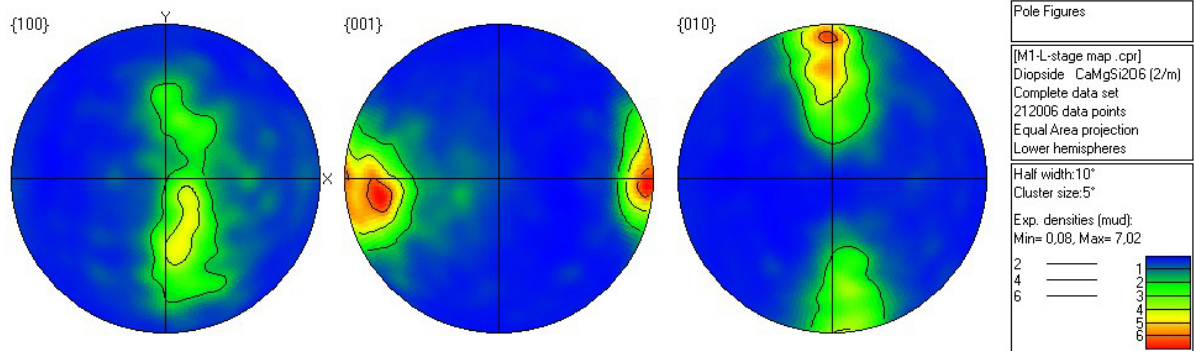


Fig. 4.4.8: omphacite pole figure from M1-L (large map), X=lineation, for ~ 5000 grains.

Omphacite pole figures for M7-L (Fig. 4.4.7) and M1-L (Fig. 4.4.8) show a strong alignment of {001} planes (the C-axis of omphacite) parallel to the lineation and {010} planes form a girdle perpendicular to lineation and parallel to foliation, but show some asymmetry. {100} planes show a weak maximum near the plane of foliation.

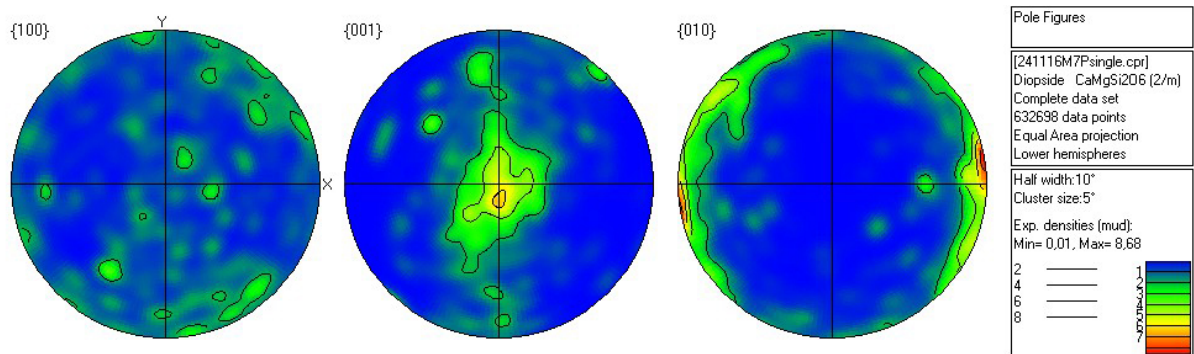


Fig. 4.4.9: pole figure for M7-P, X=lineation, for ~ 600 grains.

In M7-P (Fig. 4.4.9), cut perpendicular to lineation, the {100} planes show a random orientation. The {001} planes have a maximum perpendicular to lineation near the plane of foliation, and {010} planes show an alignment parallel to lineation.

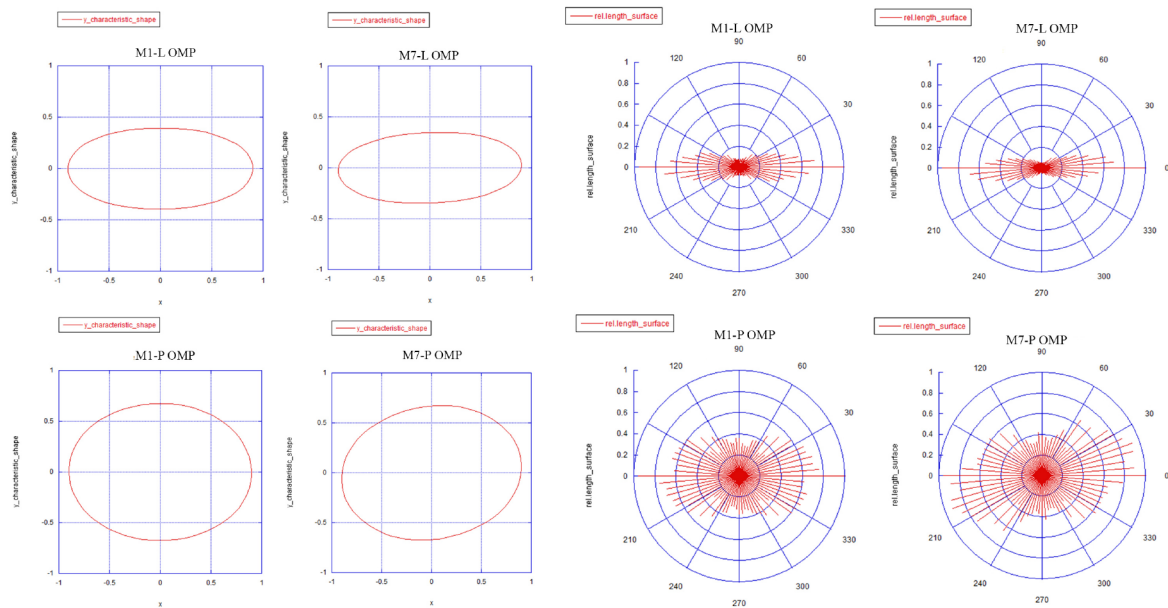


Fig 4.4.10: SURFOR plots for omphacite from M1-L (1704 grains), M7-L (2540 grains), M1-P (757 grains) and M7-P (658 grains). To the left plots for characteristic shape and to the right rose diagrams of orientation of the relative lengths of the line segment.

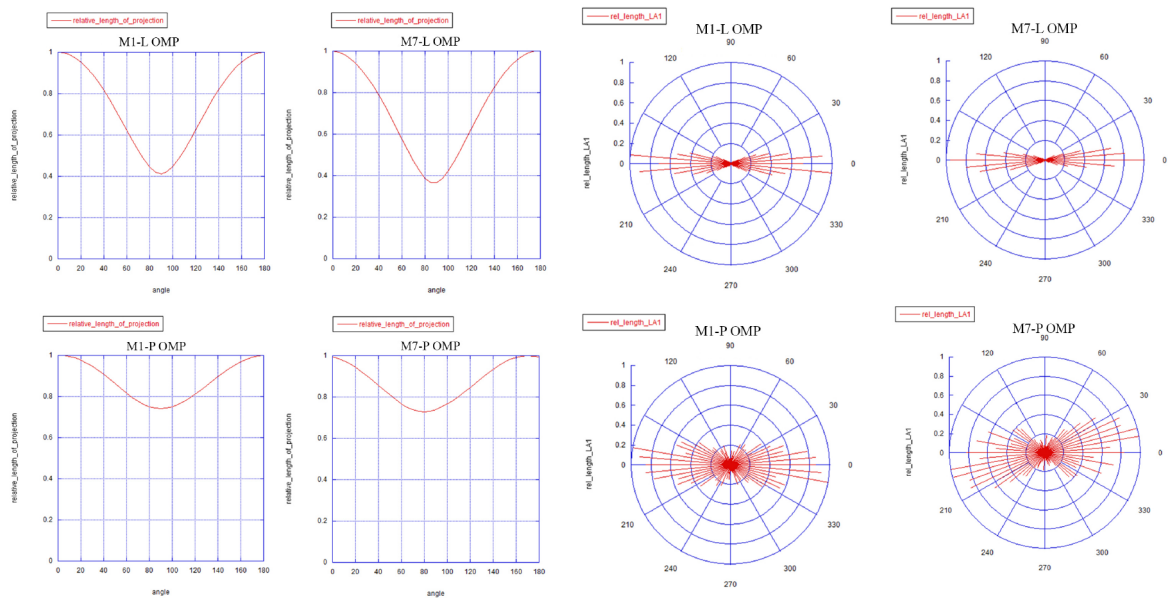


Fig 4.4.11: PAROR plots for omphacite (same input data as the SURFOR plots). To the left relative length of projections curve and to the right rose diagrams of long axis in particles.

The omphacite grains have a bulk axial ratio for the PAROR analysis of:

0.411 for M1-L

0.363 for M7-L

0.741 for M1-P

0.729 for M7-P

SURFOR analysis gave a bulk axial ratio of:

0.437 for M1-L

0.387 for M7-L

0.750 for M1-P

0.736 for M7-P

The lower value of the axial ratio for M1-L and M7-L shows that omphacite is elongated. The rose diagrams and plot for characteristic shape indicates that the omphacite particles are elongated with its longest axis parallel to the lineation, and have a strong SPO in the lineation direction of the eclogites. Perpendicular to lineation in samples M1-P and M7-P omphacite have a higher value for the axial ratio indicating a less elongated shape. The rose diagrams and plots for characteristic shape indicate that, especially for the SURFOR analysis, that omphacite exhibit a rounder shape perpendicular to lineation. PAROR rose diagrams show some SPO of the longest axis of the particles, but much weaker and more random than for M1-L and M7-L.

4.4.2 Garnet

Garnet mostly occurs as single crystals, but additionally as hollow garnets (see Fig. 4.4.12 a) and clusters (see Fig. 4.4.12 b). Based on the EDS analysis garnet have a composition varying between pyrope, almandine and grossular.

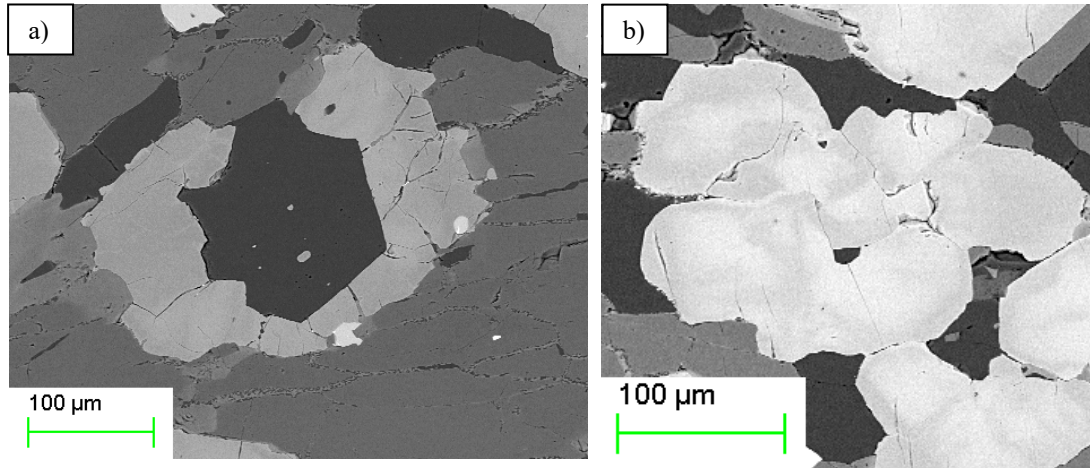


Fig. 4.4.12: hollow garnet filled with quartz (a) and garnet cluster (b), parallel to lineation (\leftrightarrow).

In the lineation direction garnets show an elongated shape (see Fig. 4.4.13a), while perpendicular to lineation they exhibit a rounder shape (see Fig. 4.4.13b). In BSE images a clear zonation in garnets are visible, with a lighter core and darker rim. As the omphacites, garnets also show an asymmetric zonation with a wider zonation in the lineation direction of the grains (see Fig. 4.4.13a elongated garnet). The zonation is seen as stronger in the BSE images in garnet compared to the omphacite, due to a higher difference in atomic weight of the present elements making up the zonation.

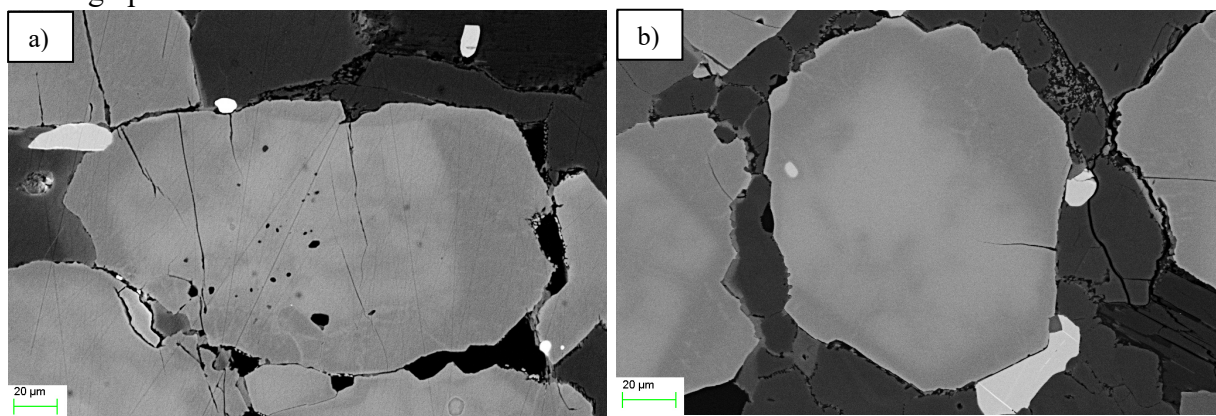


Fig. 4.4.13: to the left a BSE image of an elongated garnet from M1-L showing the asymmetric zonation stronger in the lineation direction (\leftrightarrow). To the right a garnet exhibiting a more round shape from M1-P, cut perpendicular to lineation.

In EDS linescans of single garnet grains (see Fig. 4.4.14), the Ca and Fe values increase towards the core, while the Mg increases towards the rims of the garnet. The core of the garnet represents a more grossular/almandine ($\text{Ca}_2\text{Al}_2\text{Si}_3\text{O}_{12}/\text{Fe}_3\text{Al}_2\text{Si}_3\text{O}_{12}$) composition, with higher amounts of Fe and Ca. Towards the rim the Mg increases and the Fe and Ca decreases, this indicates a more pyrope ($\text{Mg}_3\text{Al}_2\text{Si}_3\text{O}_{12}$) composition.

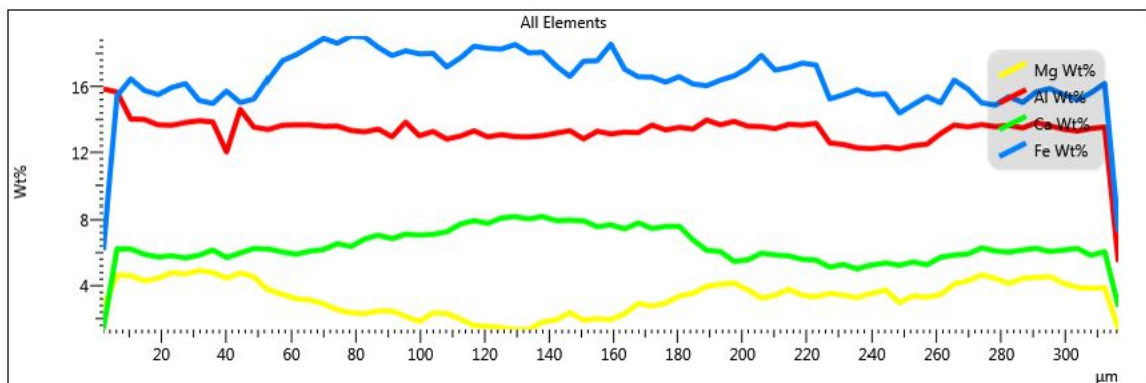
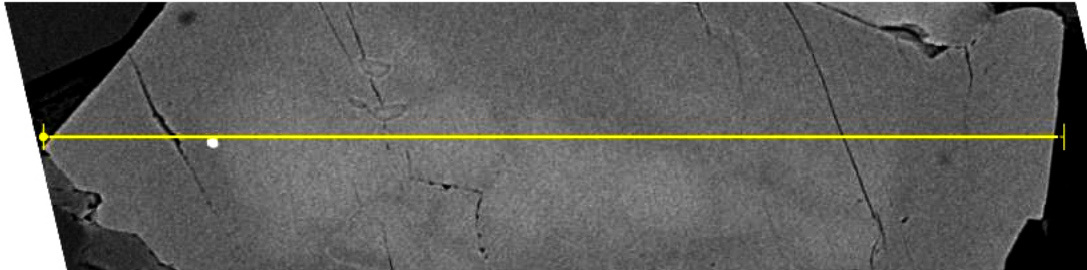


Fig. 4.4.14: linescan of a garnet showing chemical zonation, Mg(yellow), Al(red), Ca(green) and Fe(blue) in wt%. Fe and Ca decreases while Mg increases from core to rim, Al is consistent through the garnet grain. Parallel to lineation (\leftrightarrow).

In the garnet a thin rim at the grain boundary with a different composition is present (see Fig. 4.4.15). In the BSE images this outermost thin rim shows the same lighter grey as can be seen in the core of the garnet. Hence the rim has a higher Fe and Ca content, and a lower Mg content, similar to the chemical composition seen in the core. High magnification EDS point analysis of garnet from outer core, rim and outermost rim was done for single garnet grains (see Fig. 4.4.15).

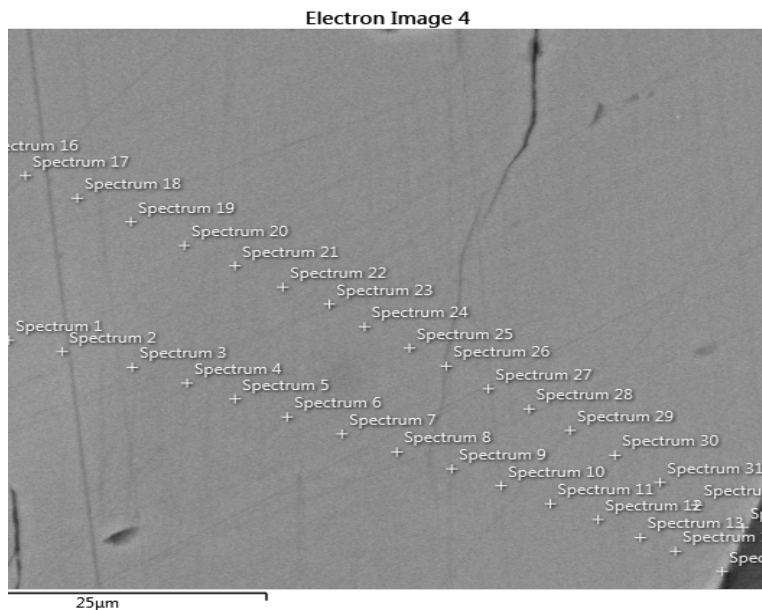


Fig. 4.4.15: point analysis from outer core in garnet, rim and outermost rim.

Table 4.4.2: point analysis from EDS data for upper and lower point line (see Fig. 4.4.15). The red lines separates the spectrums indicating core, rim and outermost core composition.

Spectrum 1	Spectrum 6	Spectrum 11	Spectrum 14	Spectrum 15
Wt% σ				
O 41,9 0,1	O 40,0 0,1	O 40,0 0,1	O 40,2 0,1	O 40,5 0,1
Fe 20,3 0,1	Si 18,5 0,0	Si 18,8 0,1	Si 18,7 0,1	Si 19,8 0,1
Si 18,3 0,0	Fe 17,1 0,1	Fe 17,9 0,1	Fe 18,2 0,1	Fe 18,3 0,1
Al 11,8 0,0	Al 11,9 0,0	Al 12,0 0,0	Al 11,9 0,0	Al 11,0 0,0
Ca 6,5 0,0	Ca 6,6 0,0	Ca 6,4 0,0	Ca 6,5 0,0	Ca 6,4 0,0
Mg 3,3 0,0	Mg 4,7 0,0	Mg 4,5 0,0	Mg 4,1 0,0	Mg 3,5 0,0
Mn 0,3 0,0		Mn 0,4 0,0	Mn 0,4 0,0	Mn 0,5 0,0
		Ta 0,0 0,0	Ta 0,0 0,0	Ta 0,0 0,0

Spectrum 16	Spectrum 21	Spectrum 27	Spectrum 32	Spectrum 33
Wt% σ				
O 40,0 0,1	O 40,4 0,1	O 40,3 0,1	O 40,3 0,1	O 40,5 0,1
Si 18,8 0,1	Si 18,8 0,0	Si 18,9 0,1	Si 18,6 0,0	Si 19,0 0,1
Fe 18,6 0,1	Fe 17,3 0,1	Fe 17,2 0,1	Fe 17,9 0,1	Fe 18,3 0,1
Al 11,8 0,0	Al 12,0 0,0	Al 12,0 0,0	Al 11,9 0,0	Al 11,6 0,0
Ca 6,8 0,0	Ca 6,8 0,0	Ca 6,3 0,0	Ca 6,6 0,0	Ca 6,3 0,0
Mg 4,1 0,0	Mg 4,7 0,0	Mg 4,9 0,0	Mg 4,2 0,0	Mg 3,9 0,0
Ta 0,0 0,0		Mn 0,4 0,0	Mn 0,4 0,0	Mn 0,4 0,0
		Ta 0,0 0,0	Ta 0,0 0,0	Ta 0,0 0,0

CORE		RIM		OUTER RIM
------	--	-----	--	-----------

Spectrums 1, 6, 11, 14 and 15 are from the upper point line and spectrum 16, 21, 27, 32 and 33 are from the lower line of points (see Fig. 4.4.15) and shows chemical variations from outer core in the garnet (spectrum 1 and 16) to rim (spectrum 6, 11, 14, 21, 27 and 32) and outermost rim (spectrum 15 and 33). Fe is highest in the core (spectrum 1 and 16) and outer rim (spectrum 15 and 33), and shows decreasing values in the rim (spectrum 6, 11, 14, 21, 27 and 32). Mg is increasing from the core to the rim, and decreases from the rim to the outermost thin rim. The

composition changes from a more almandine composition near the core, to a more pyrope composition in the rim and back to a more almandine composition in the outermost thin rim. Values shown in table 4.4.2.

Some garnet grains show a retrograde, fibrous rim composed of plagioclase and amphibole (see Fig. 4.4.16). As in the symplectites around the omphacite grains the fibrous rim is oriented in the lineation direction of the eclogites.

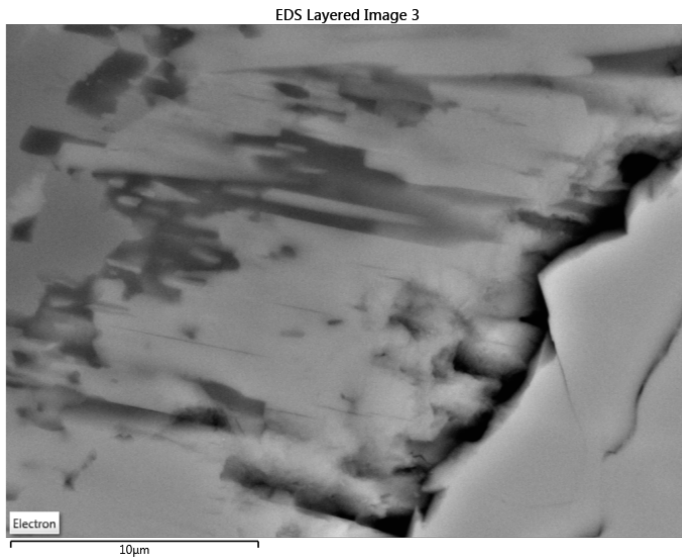


Fig. 4.4.16: fibrous rim, in semi-parallel to the lineation direction (\leftrightarrow) of plagioclase and amphibole at the edge of a garnet.

Garnet pole figures for M7-L (Fig. 4.4.17), M1-L (Fig. 4.4.18) and M7-P (Fig 4.4.19) show a low maximum multiple of uniform distribution (mud) intensity. There some weak maxima especially in the pole figures for $\{100\}$ planes that may indicate a weak cross girdle pattern, and may show a weak CPO.

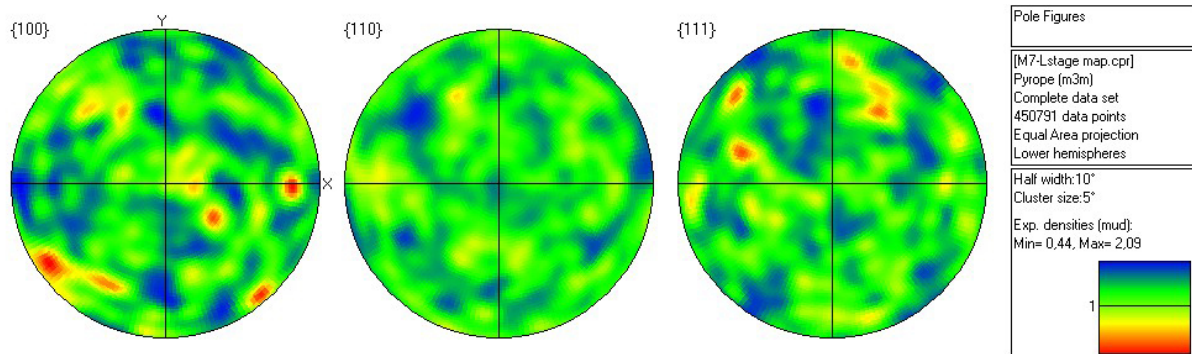


Fig. 4.4.17: garnet pole figure of M7-L (large map), X=lineation, for ~ 1500 grains.

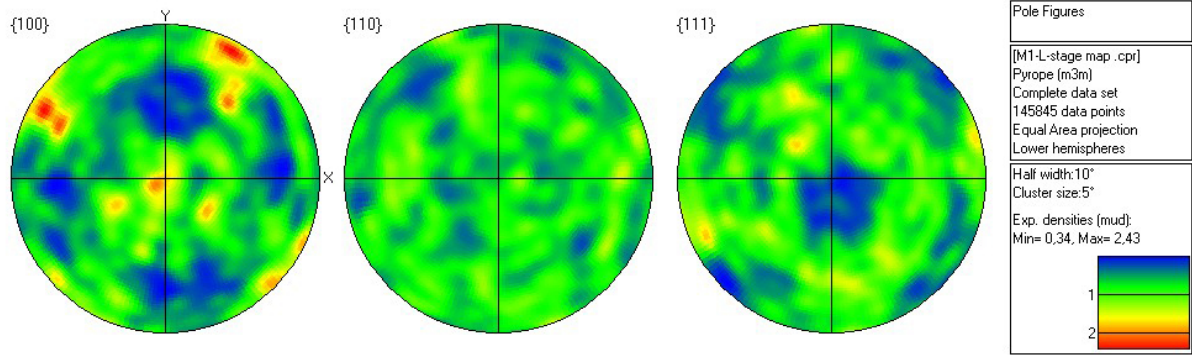


Fig. 4.4.18: garnet pole figure of M1-L (large map), X=lineation, for ~ 1600 grains.

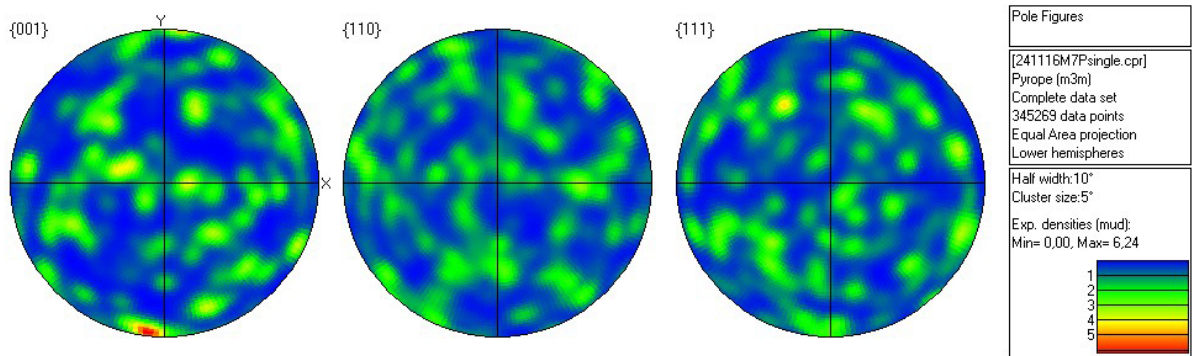


Fig 4.4.19: garnet pole figure of M7-P, X=lineation, for ~ 40 grains.

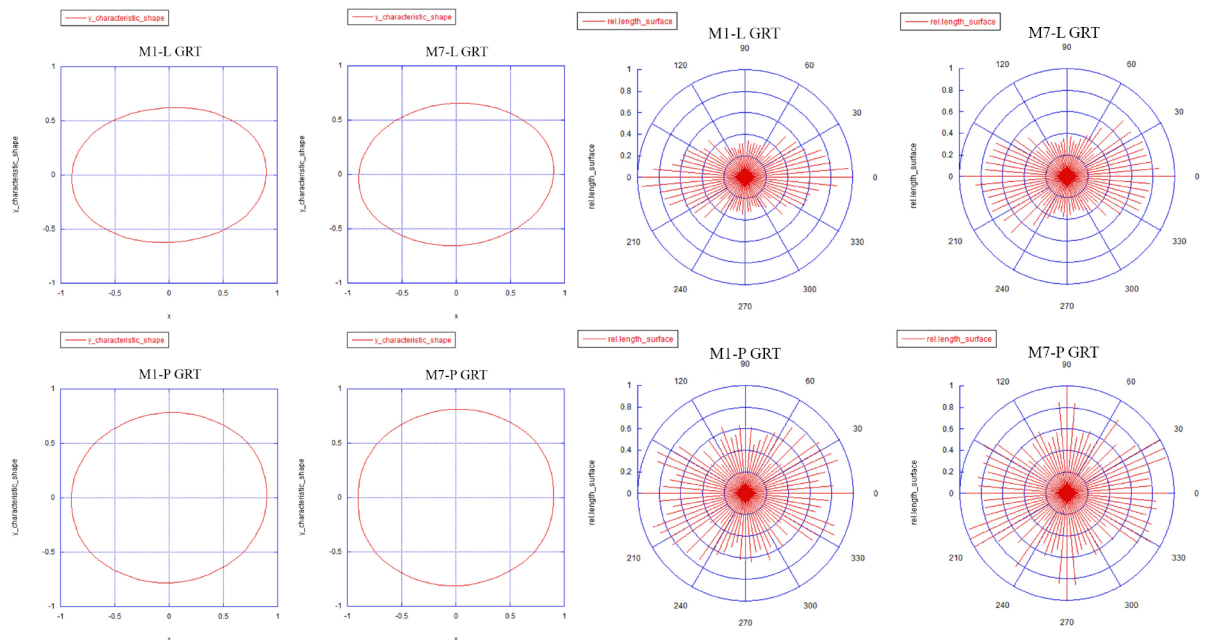


Fig. 4.4.20: SURFOR analysis of garnet for M1-L (538 grains), M7-L (359 grains), M1-P (95 grains) and M7-P (39 grains). To the left plots for characteristic shape and to the right rose diagrams of the orientation of relative length of the line segments.

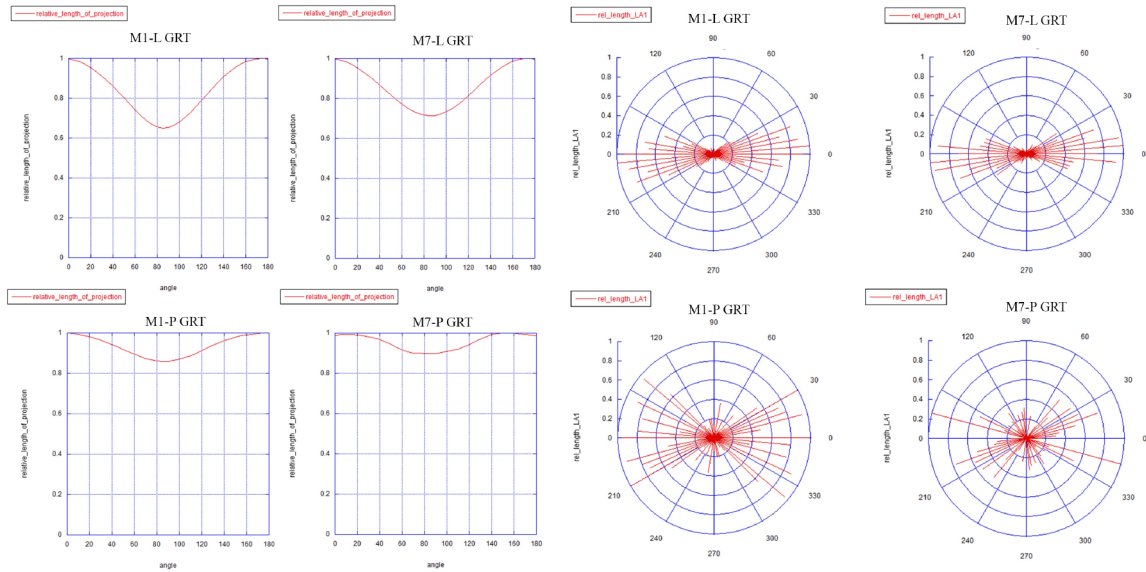


Fig. 4.4.21: PAROR analysis of garnet (same input file as the SURFOR analysis). To the left projection curve of the relative length and to the right rose diagram of the relative longest axis in the particles.

SURFOR (see Fig. 4.4.20) and PAROR (see Fig. 4.4.21) analysis for the garnet show that the garnets are elongated in the lineation direction and have a rounder shape perpendicular to lineation. The bulk axial ratio for the garnet particles for the PAROR analysis are:

- 0.651 for M1-L
- 0.713 for M7-L
- 0.858 for M1-P
- 0.896 for M7-P

The bulk axial ratio for the SURFOR analysis are:

- 0.688 for M1-L
- 0.725 for M7-L
- 0.866 for M1-P
- 0.894 for M7-P

The main findings indicate that the axial ratio and characteristic shape of garnet particles show that the garnets are elongated in the lineation direction and have a SPO with the longest axis of the particles parallel to lineation. Perpendicular to lineation garnet exhibits a more round shape and no clear SPO.

EBSD orientation measurements were done on a single garnet grain, constructing one pole figure for the left rim, the garnet core and the right rim. This was done by point analysis for the different garnet regions and construction of pole figures using AZTEC (point EBSD data cannot be constructed in Channel 5 software). The CPO for the three pole figures look identical even though they originate from different sites on the garnet crystal.

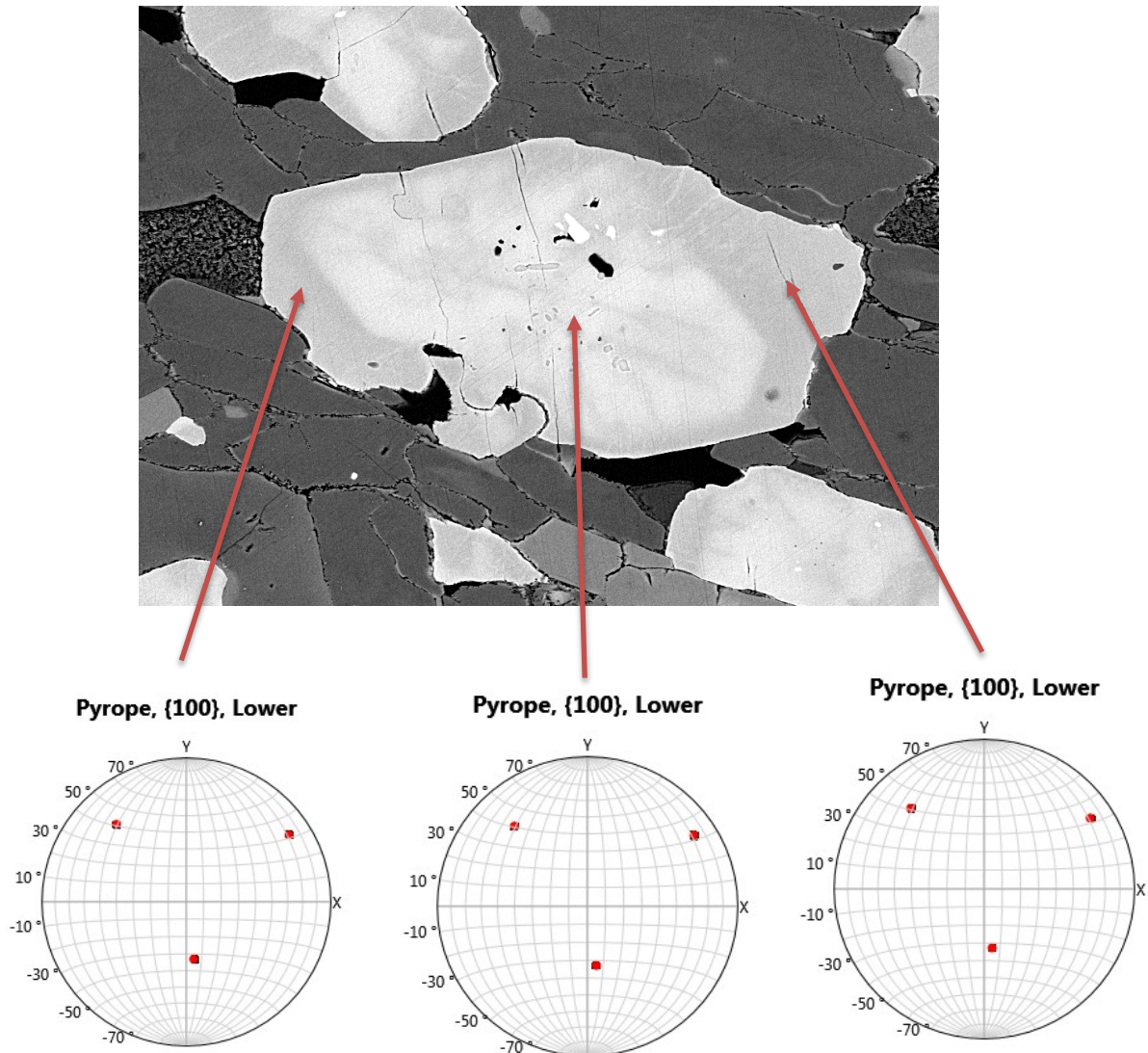


Fig.4.4.22: zonation in garnet from M7-L. Lower hemisphere pole figures from a single garnet grain reflecting different areas within the garnet (left rim, core and right rim), parallel to lineation (\leftrightarrow).

The pole figures for the different areas in the garnet exhibits exactly the same CPO, indicating that the CPO of the garnet is independent from the chemical zonation.

4.4.3 Zoisite

Fig. 4.4.23 shows an aggregate of elongated zoisite needles parallel to the lineation direction, and some smaller, single zoisite grains in the omphacite matrix.

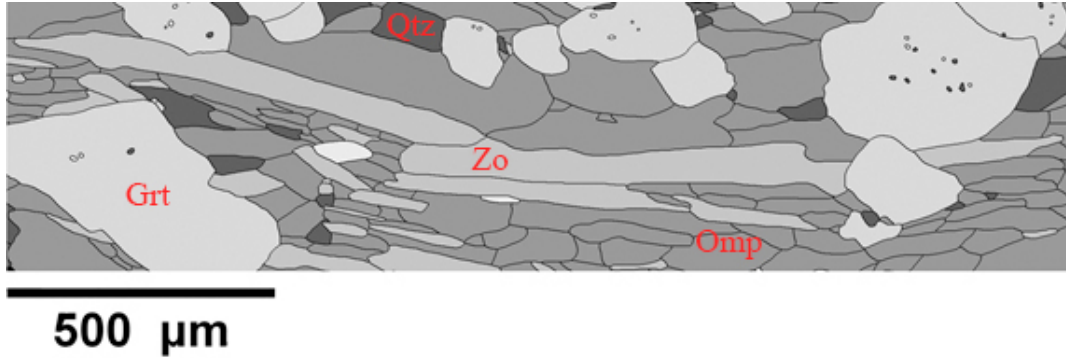


Fig. 4.4.23: elongated zoisite grains parallel to lineation (\leftrightarrow).

Zoisite pole figures from M7-L (see Fig. 4.4.24) show a $\{100\}$ (shortest axis) perpendicular to lineation and parallel to foliation, $\{001\}$ planes form a weak maximum near the plane of foliation perpendicular to lineation and $\{010\}$ planes, the long axis of the zoisite, align strongly parallel to lineation. The zoisite content in M1-L is much less and the pole figures are more diffuse, but the same CPO trend as M7-L is visible (see Fig. 4.4.25).

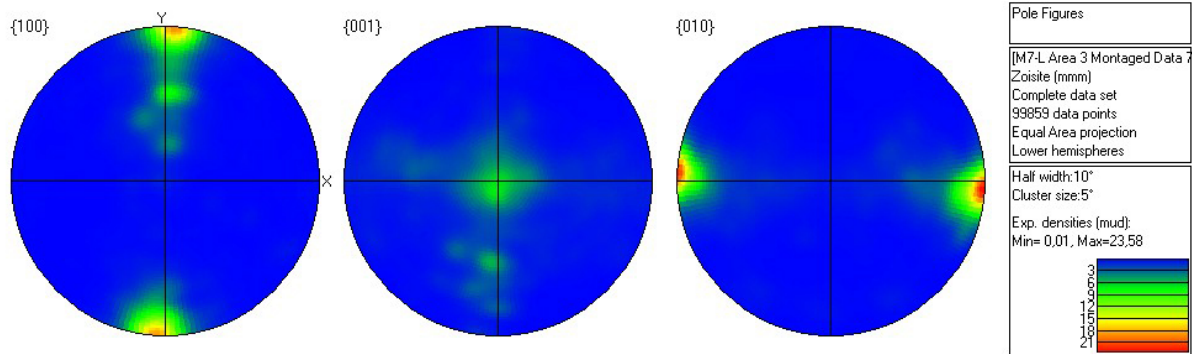


Fig. 4.4.24: zoisite pole figure from M7-L (large map), X=lineation, for ~ 2200 grains.

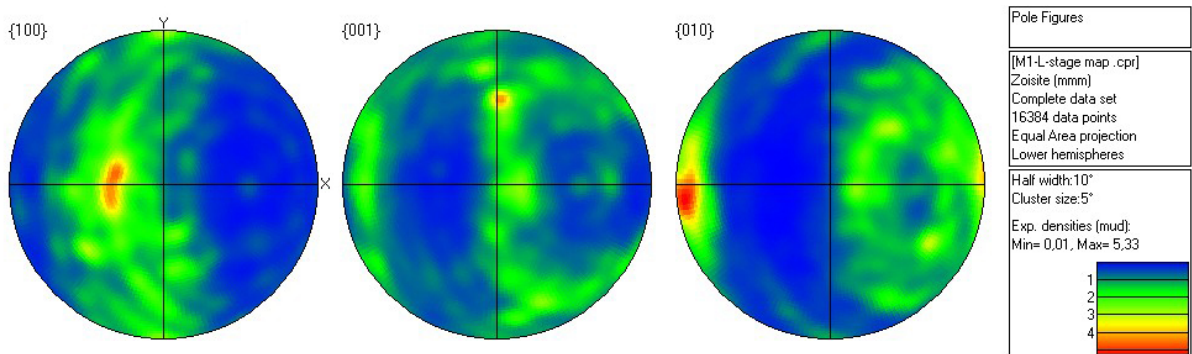


Fig. 4.4.25: zoisite pole figures from M1-L large map, X=lineation, for ~ 250 grains.

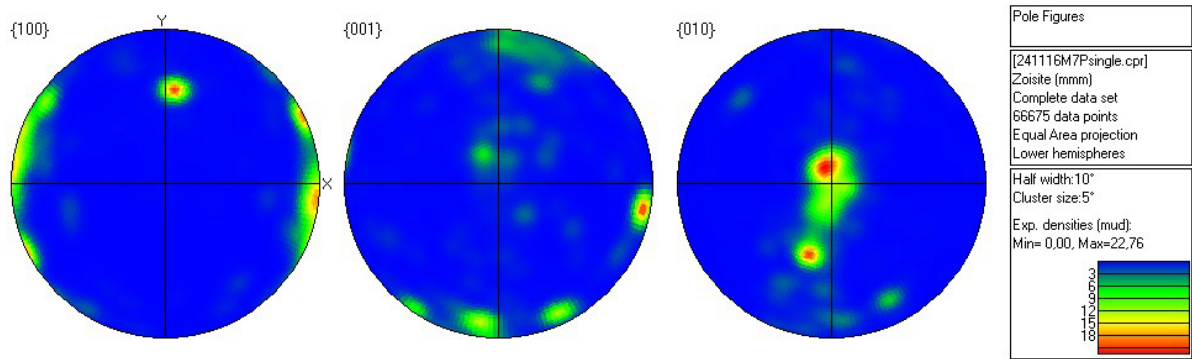


Fig. 4.4.26: zoisite pole figures from M7-P, X=lineation, for ~ 100 grains.

Perpendicular to lineation, zoisite pole figures show a weak alignment of {100} planes parallel to lineation, and a maximum of {010} planes perpendicular to the lineation near the plane of the foliation. The {001} planes show no clear CPO (see Fig. 4.4.26).

SURFOR (Fig. 4.4.27) and PAROR (Fig. 4.4.28) analysis for zoisite from M1-L, M1-P, M7-L and M7-P as for the omphacite and garnet. Both M1 and M7 samples show similar results, even though the volume fraction of zoisite is lower in M1 than M7.

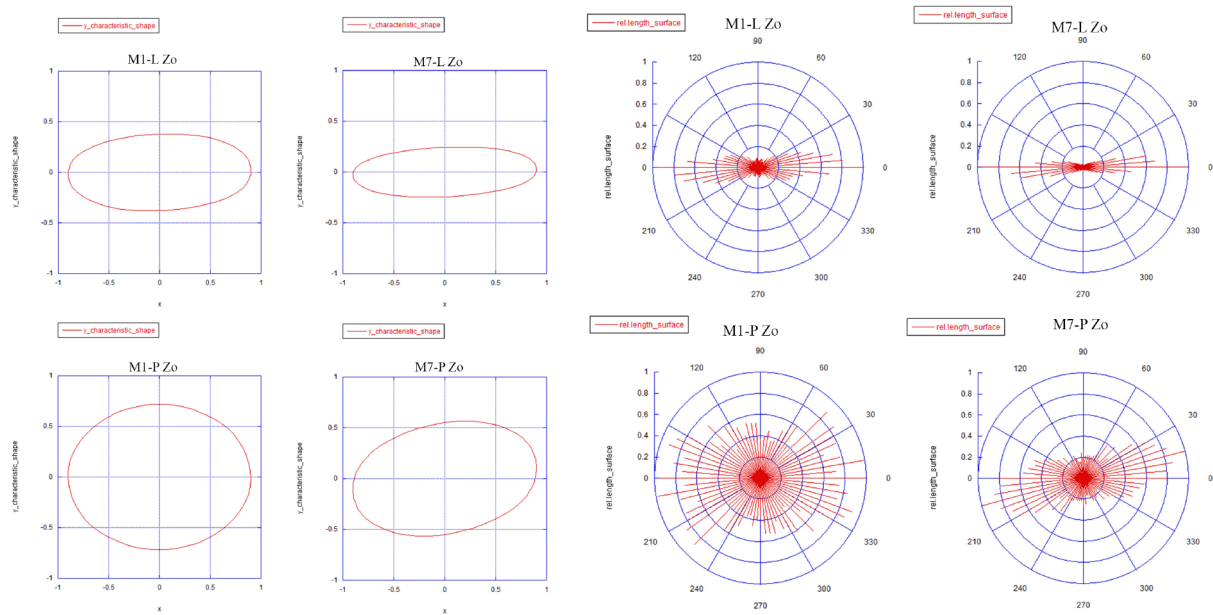


Fig. 4.4.27: SURFOR analysis of zoisite from M1-L (86 grains), M7-L (630 grains), M1-P (54 grains) and M7-P (165 grains). To the left characteristic shape of the particles and to the right rose diagram of the surface ODF.

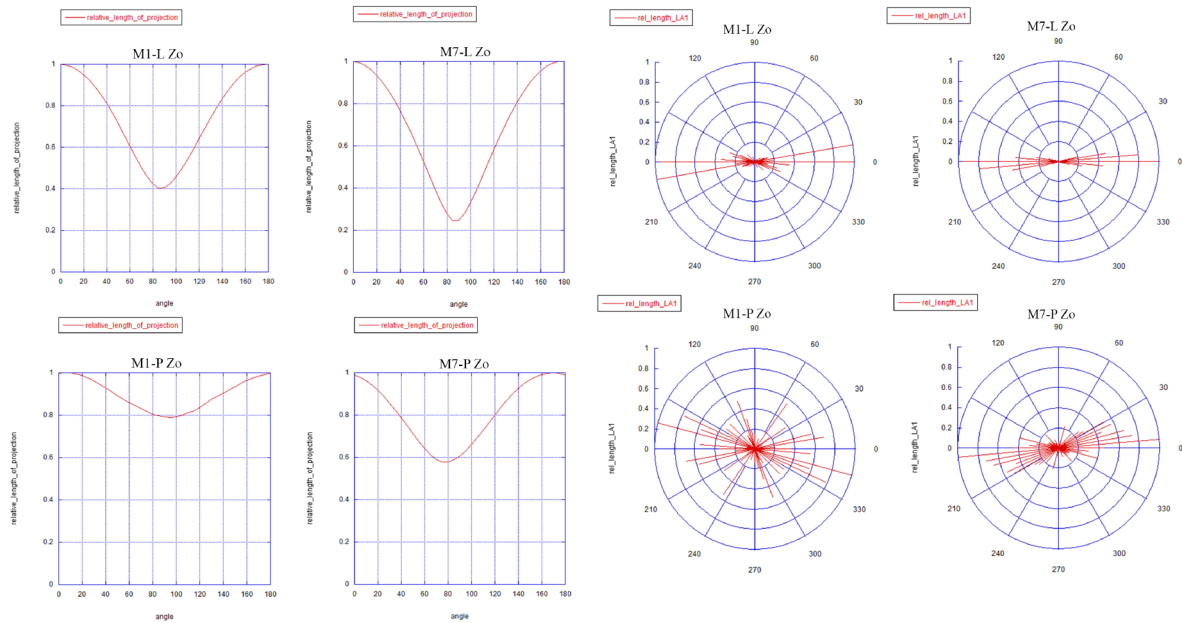


Fig. 4.4.28: PAROR analysis of zoisite particles (same input file as SURFOR analysis). To the left projection curve for relative length and to the right rose diagrams of the longest axis of the particles.

The zoisite particles are strongly elongated in the lineation direction in M1-L and M7-L, as seen in the rose diagrams, and have a strong SPO nearly parallel to lineation. Axial ratio for the zoisite particles for PAROR analysis are:

0.402 for M1-L

0.242 for M7-L

0.789 for M1-P

0.577 for M1-P

For the SURFOR analysis the axial ratio is:

0.422 for M1-L

0.271 for M7-L

0.799 for M1-P

0.597 for M7-P

Due to the tabular shape, the zoisite particles show a weak elongation also perpendicular to lineation in M1-P and M7-P.

4.4.4 Hornblende

Hornblende mostly occurs as larger grains overgrowing the fabric, with a random orientation while replacing the omphacite (see Fig. 4.4.29). Hornblende also occurs in retrograde rims in the kelyphites observed around some garnet grains (see Fig. 4.4.16).

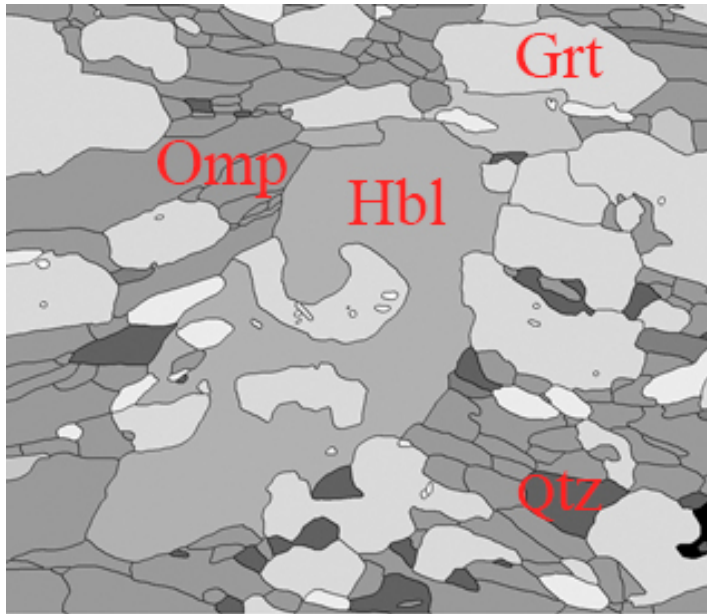


Fig. 4.4.29: large hornblende grain (in the middle) replacing omphacite and overgrowing the fabric with a random orientation compared to lineation (\leftrightarrow) from M1-L.

Hornblende pole figures show a weak $\{001\}$ alignment parallel to lineation, and most probably a weak $\{010\}$ planes alignment perpendicular to lineation and parallel to foliation in M7-L (Fig. 4.4.30) and M1-L (Fig. 4.4.31). The CPO fabric in the hornblende show similar patterns as for omphacite pole figures.

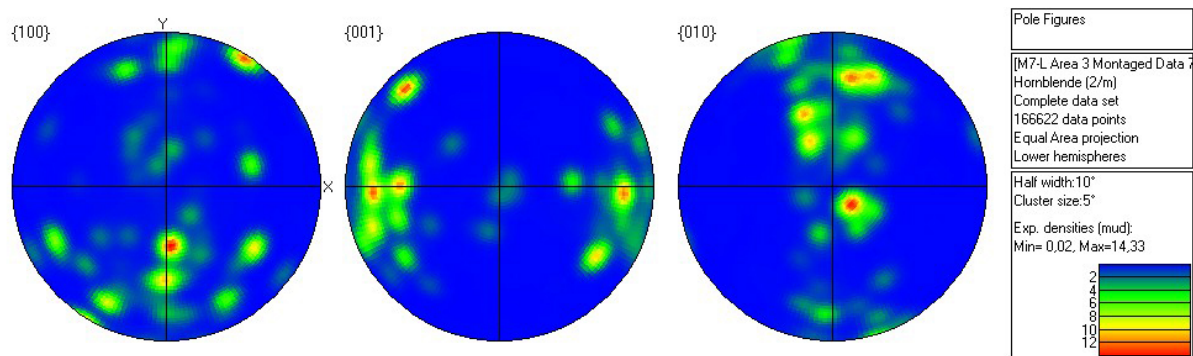


Fig. 4.4.30: hornblende pole figures from M7-L (large map), X=lineation, for ~ 80 grains.

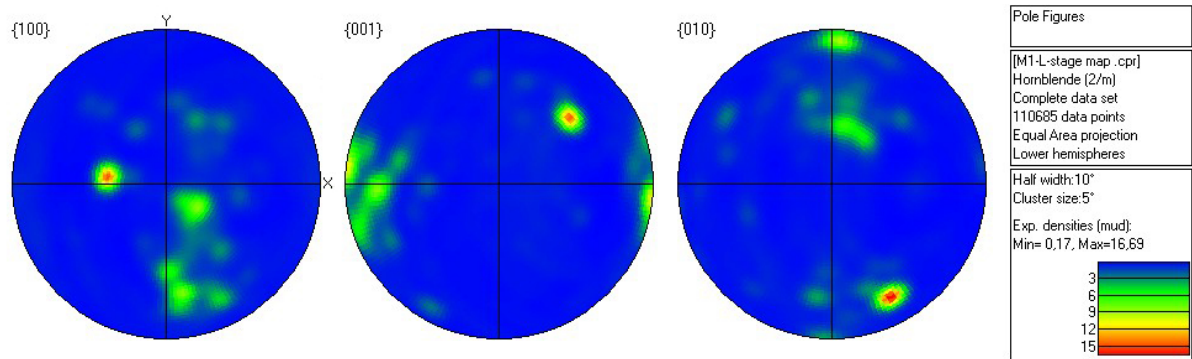


Fig. 4.4.31: hornblende pole figures for M1-L, X=lineation for ~ 50 grains.

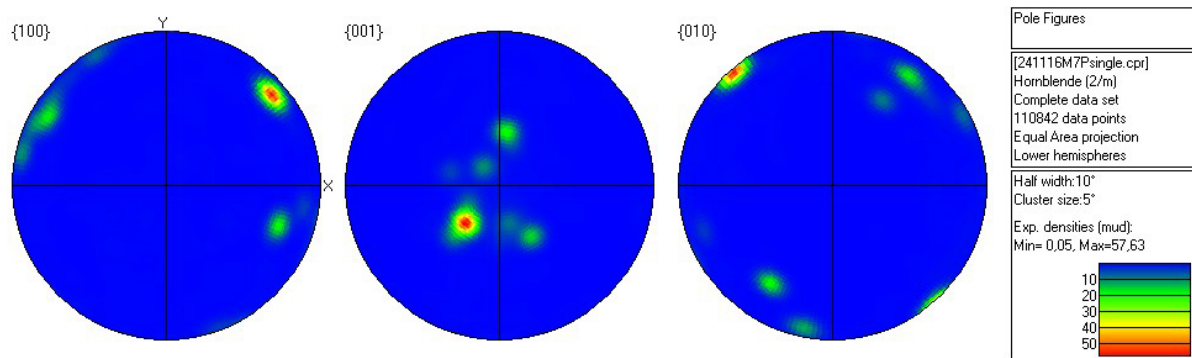


Fig. 4.4.32: hornblende pole figures for M7-P, X=lineation, for ~ 10 grains.

EBSD image for M7-P contains fewer grains and data points than M7-L but there are still similarities in the orientations of the planes compared to the omphacite pole figures for M7-P. Especially for $\{001\}$ planes that forms a weak maximum near the plane of the foliation, as expected perpendicular to the lineation (see Fig. 4.4.32).

4.4.5 Quartz

Quartz mostly occurs in pressure shadows of garnets. The quartz around the garnets is more concentrated on the side of the crystal that is parallel to the lineation direction (see Fig. 4.4.33).

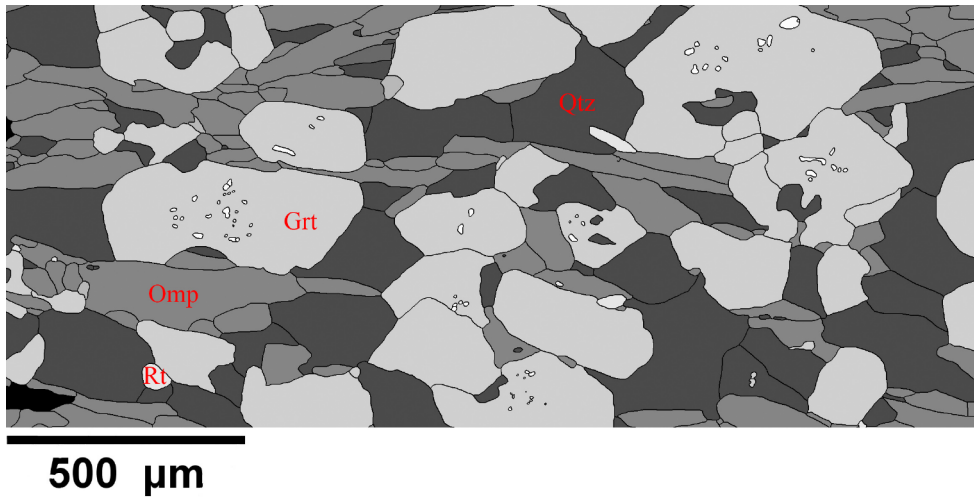


Fig. 4.4.33: quartz in pressure shadow of garnets, parallel to the lineation (\leftrightarrow) from M1-L.

In light microscopy observations, quartz show weak undulose extinction, but no other signs of intracrystalline deformation for example lobate grain boundaries or sub grains.

Quartz pole figures show a low mud and a no obvious CPO for any crystallographic planes or directions. In M7-L (Fig. 4.4.34) and M1-L (Fig. 4.4.35) a weak maximum perpendicular to lineation near the plane of foliation may be present for $\{0001\}$ plane.

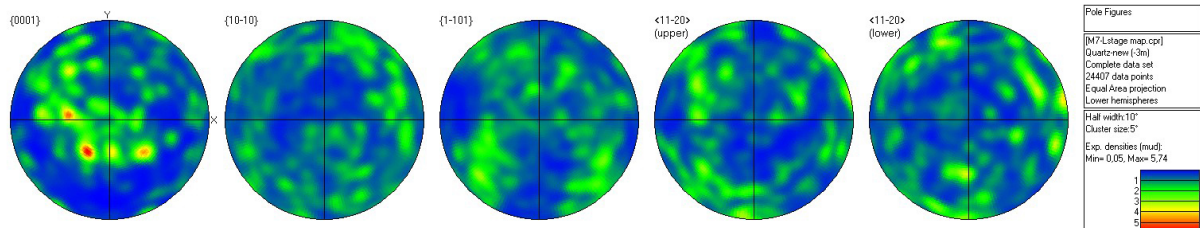


Fig. 4.4.34: quartz pole figure from M7-L (large map), X=lineation, for ~ 1700 grains.

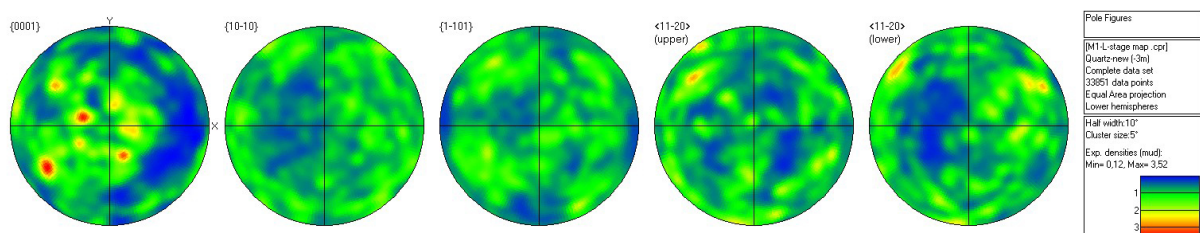


Fig. 4.4.35: quartz pole figures from M1-L (large map), X=lineation, for ~ 1700 grain.

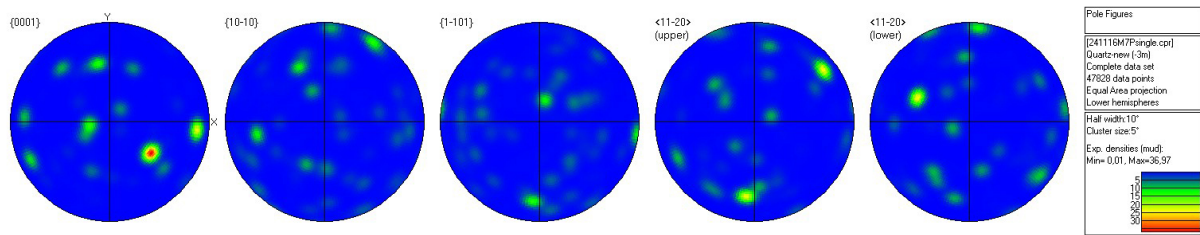


Fig. 4.4.36: quartz pole figures from M7-P, X=lineation, for ~ 50 grains.

4.5 Grain size analysis

The average 2D diameter for mean, mode and median grain size for each phase in M1-L, M1-P, M7-L and M7-P was calculated using statistical data in Kaleidagraph. In the selected samples the mean (see Table 4.5.1) > median (see Table 4.5.2) > mode (see Table 4.5.3), typical for a positive skewed histogram (Heilbronner and Barrett, 2014). As presented earlier in results the amount of grains per sample varies (see Table 4.1.1). Since the mode indicates the most occurring grain size, from binned data and histograms, this was used for an average grain size in the description of thin sections (chapter 4.3).

Table 4.5.1: mean 2D grain size diameter for all phases in all samples.

Phase	M1-L	M1-P	M7-L	M7-P
Hornblende	323,63 μm	464,06 μm	254,95 μm	289,29 μm
Garnet	133,45 μm	224,71 μm	126,53 μm	266,71 μm
Paragonite	74,781 μm	113,52 μm	35,969 μm	Not present
Omphacite	82,688 μm	114,51 μm	81,660 μm	87,817 μm
Quartz	70,783 μm	95,041 μm	42,585 μm	55,989 μm
Rutile	45,671 μm	84,727 μm	39,590 μm	55,339 μm
Zoisite	122,88 μm	102,53 μm	78,305 μm	71,130 μm

Table 4.5.2: median 2D grain size diameter for all phases in all samples.

Phase	M1-L	M1-P	M7-L	M7-P
Hornblende	285,34 μm	402,33 μm	195,12 μm	279,79 μm
Garnet	114,31 μm	178,00 μm	91,385 μm	290,17 μm
Paragonite	56,618 μm	93,631 μm	36,012 μm	Not present
Omphacite	68,622 μm	97,402 μm	72,586 μm	77,182 μm
Quartz	49,084 μm	66,920 μm	27,376 μm	32,582 μm
Rutile	35,708 μm	73,709 μm	29,569 μm	48,362 μm
Zoisite	81,776 μm	87,351 μm	59,401 μm	62,457 μm

Table 4.5.3: modal 2D grain size diameter for all phases in all samples.

Phase	M1-L	M1-P	M7-L	M7-P
Hornblende	180 μm	350 μm	200 μm	200 μm
Garnet	60 μm	125 μm	60 μm	300 μm
Paragonite	35 μm	75 μm	40 μm	Not present
Omphacite	50 μm	100 μm	50 μm	60 μm
Quartz	20 μm	40 μm	15 μm	25 μm
Rutile	15 μm	50 μm	15 μm	30 μm
Zoisite	30 μm	40 μm	45 μm	45 μm

Mean values for the grain size show the largest average grain size followed by the median. The mean is calculated by adding all values for grain size and dividing by number of grains. While the median is the value in the middle of a sorted set of values from smallest to largest. So the mean and median average values will be more effected by a large difference in grain size, than the mode value that presents the most occurring value of grain sizes.

5.0 Discussion

The two samples used for this study, M1 and M7, exhibit some differences in mineral assemblage. Based on the three eclogite types in terms of mineral assemblage (Schmädicke et al., 1995; Klapova et al., 1998), the Meluzina eclogite is similar to a type-1 eclogite, while M7 from the Na Skalách is more similar to type-2 or an intermediate between the two, based on the higher zoisite content. Disregarding the slight difference in mineral assemblage the two samples are structurally similar with a strong lineation fabric.

5.1 Metamorphic history and zonation

The metamorphic history of the Czech part of the Erzgebirge eclogites is exposed in the chemical zonation of the omphacite and garnet as well as the occurrence of minerals and structures that are a product of retrogression. Garnets in this study exhibit a zonation with a change from a more almandine composition to pyrope from core to rim, typical for a prograde zonation (Konrad-Schmolke et al., 2006). In the outermost thin rim a chemical change to a more almandine composition was observed. This indicates a change back to lower P-T conditions confirmed by chemical change indicating retrograde metamorphism. Around some garnet grains retrograde rims or kelyphites composed of amphibole and plagioclase were observed. Amphibole and plagioclase are normally not stable in an eclogite facies mineral assemblage and also indicate retrogression of the stable mineral assemblage during a pressure and temperature decrease, and possibly hydration of the eclogite (Massonne, 2012). The outermost thin rim with a more almandine composition in the garnets are most probably the start of the decreasing pressure and temperature related to the exhumation of the eclogites. The kelyphite rims composed of plagioclase and amphibole are a continuation of the retrograde reactions during decreasing P-T conditions most probably related to the continuing exhumation.

Omphacite exhibits a chemical zonation from a more diopside compositional core to a more jadeite composition in the rim. Omphacite is a solid solution between diopside and jadeite, where jadeite is the high pressure equivalent. Decrease in Mg and Ca (diopside endmember) found towards the rim and increase in Na and Al (jadeite endmember) indicates a pressure increase and a prograde zonation from core to rim in omphacite. Around omphacite grains a fine grained (1-5 μm wide) symplectite rim was observed. EDS analysis confirmed that the symplectite was composed of diopside and plagioclase. It indicates a pressure decrease and

breakdown of the stable eclogite facies mineral omphacite by replacement of the solid solution lower pressure equivalent in omphacite, diopside, and plagioclase (Vogel, 1967; Engels, 1972). The diopside and plagioclase symplectites indicate a pressure decrease, most likely during the onset of exhumation of the eclogites, and the rocks leave the stable P-T conditions needed for stable eclogite facies minerals.

Larger hornblende grains overgrowing the fabric were observed in the eclogites. Replacement of omphacite by hornblende is a known process during retrogression and exhumation in eclogites (Engels, 1972; Zhang et al., 2003). During retrogression and hydration of the eclogites omphacite is no longer stable, and hornblende grows as symplectites or replaces entire grains.

In both garnet and omphacite, the subduction, peak P-T conditions and exhumation history are preserved in the chemical zonation of the minerals. From prograde metamorphism during subduction until peak P-T conditions was reached, and change to lower P-T conditions during exhumation exposed as retrogression of the stable eclogite facies mineral assemblage.

The metamorphic history of the Czech part of the Erzgebirge eclogites have been studied by e.g. Klapova et al. (1998), Schulmann et al. (2009) and Collett et al. (2017) that all proposed a prograde chemical zonation in the garnets, and retrograde metamorphism exposed as symplectite and kelyphite formation, as well as amphibole replacing the omphacite.

Peak metamorphic conditions has been determined to be 600-650 °C and 25-26 kbar for the Meluzina eclogites by Klapova et al. (1998) and 615 °C and 26 kbar for the Erzgebirge eclogites by Collett et al. (2017). By using the information about peak metamorphic conditions, the prograde to retrograde zonation observed in garnet and omphacite, as well as formation of hornblende grains and retrograde symplectite rims a simple illustration of a P-T diagram is shown in Fig. 5.1.1.

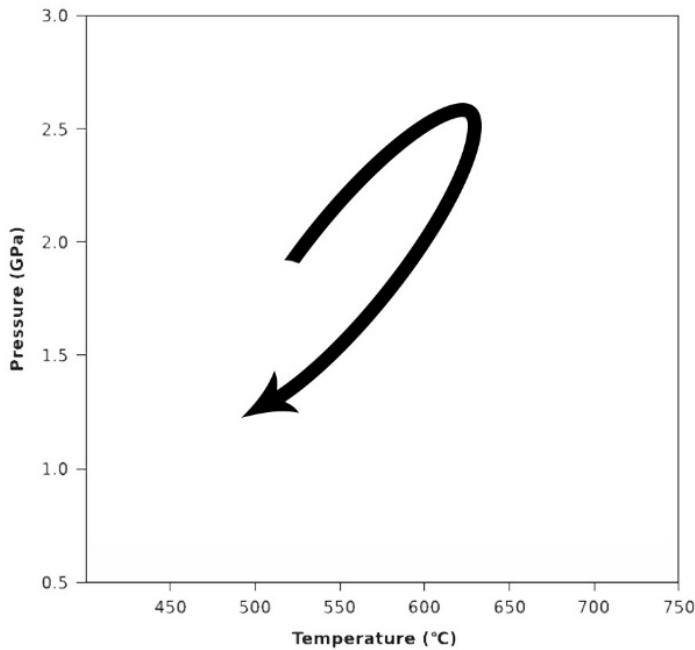


Fig. 5.1.1: illustration of a P-T diagram for the prograde-retrograde path of the eclogites. This is just a sketch and no values for P-T conditions are valid except for estimated peak metamorphic conditions (Klapova et al., 1998; Collett et al., 2017).

5.2 Deformation structures and zonation pattern

The chemical zonation in the omphacite and the garnet exhibit an asymmetric shape, where the prograde rim of the zonation in the particles are wider in the lineation direction. The fact that the prograde rim is wider in the elongation direction of the grains indicates that the fabric developed during prograde metamorphism and peak metamorphic conditions. Hence, the omphacite and garnet grew in the elongation direction of the rock during subduction. The lineation is the strongest feature in the eclogites, but a weak foliation of compositional layering with alternating garnet rich layers is present.

The most obvious feature in the eclogites are the elongated omphacites, zoisites and garnets, which form a strong lineation in the foliation plane of the eclogites. EBSD analysis and construction of pole figures for the different phases show that the omphacite and zoisite have a strong CPO with their long axis parallel to the lineation direction. Omphacite [001] direction have a strong maximum alignment parallel to lineation and [010] direction perpendicular to lineation. This omphacite CPO corresponds to a typical L-type fabric in omphacite (Helmstaedt et al., 1972). While the garnet does not exhibit any clear CPO and a low mud, the observed maximums in the [100] plane pole figures may indicate a weak CPO. Mainprice et al. (2004) compared numerical simulations and EBSD data for garnet CPO in different strain regimes. By

comparing the pole figures from this study to the numerical simulations there may be some similarities in the pole figures for pure shear (see Fig. 5.2.1), but the overall garnet CPO in this study is weak and cannot explain the elongation of the garnets.

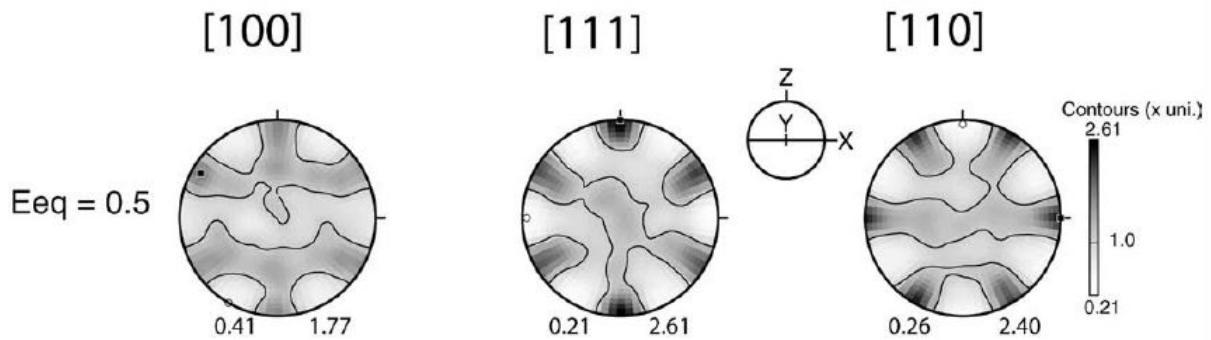


Fig. 5.2.1: Garnet pole figures from Mainprice et al. (2004). Z=compressional axis and X=extension axis. Lower hemisphere plots. Minimum and maximum mud is presented.

Fig.4.4.22 presents CPO pole figures for a single garnet in rims and core. The pole figures for the rim and core are identical. This clearly shows that the CPO is completely independent from chemical zonation.

Hornblende occurs as larger grains that overgrow the fabric, with a random orientation compared to the lineation. The amount of hornblende grains is much less than the amount of omphacite grains, so this may weaken the result of the EBSD data. However hornblende pole figures show similar CPO as the omphacite, with [001] direction showing a weak alignment parallel to the lineation and [010] direction forming a weak girdle perpendicular to lineation. Since the fabric in the eclogites most likely developed during subduction, and peak eclogite metamorphism at P-T conditions where hornblende is not part of the stable mineral assemblage, homotactic growth of the hornblende on expense of omphacite is likely to explain the similar crystallographic orientation of the hornblende (Rehman et al., 2016). Symplectites surrounding the omphacite and some garnet grains also show a fabric parallel to the lineation direction. The symplectites are composed of diopside, plagioclase and/or amphibole. Since the symplectites, which are a product of retrogression during exhumation, show elongation parallel to the elongation direction during prograde metamorphism, the elongation direction is expected to be the same throughout the entire metamorphic path and deformation history of the eclogites.

Shape and particle orientation analysis show that omphacite, garnet and zoisite are elongated and show a strong SPO in the lineation direction of the rock. Perpendicular to lineation

omphacite and garnet show a more rounded shape and a more random SPO fabric. This indicates that in a 3D presentation of the particles garnet and omphacite are dominantly elongated in the lineation direction of the eclogite. Perpendicular to the lineation zoisite shows a weak elongation and SPO perpendicular to lineation (see Fig. 4.4.26). The reason for this might be that the tabular grain shape of zoisite will show some elongation also perpendicular to its longest axis in the [010] direction.

Quartz is most often seen in connection with garnet, and has crystallized on the sides of the garnet particle that are parallel to the elongation direction. Quartz forms elongated aggregates of grains, with straight grain boundaries. There are no observed CPO of the quartz grains, and no signs of recrystallization and intracrystalline deformation, except for weak undulose extinction observed in the light microscope.

5.3 Deformation mechanisms and fabric development

If the dominant mechanism for fabric development in eclogites is grain boundary diffusion or dislocation creep is discussed by several studies. The asymmetric prograde zonation of the omphacite and garnet in the eclogites from the Czech part of the Erzgebirge indicate that grain boundary diffusion or pressure solution was the dominant deformation mechanism in these rocks. Omphacite exhibits a CPO with [001] direction strongly aligned parallel to the lineation, while garnet shows no clear CPO. The weak CPO in the garnets indicate that dislocation creep mechanism most likely did not cause the elongation and deformation of the garnet grains. Since both the omphacite and garnet have correlating prograde asymmetric zonation wider in the lineation direction, and an SPO parallel to lineation, this may indicate that the mechanism for the formation of the asymmetric zonation and elongation of the grains was the same for omphacite and garnet.

The C-axis of the omphacite is parallel to the elongation direction of the eclogite, and most likely normal to the highest stress. If the omphacite crystals were rotated so the C-axis already was somewhat parallel, grain boundary diffusion can be a possible mechanism for the fabric and CPO development of omphacite (Bons and den Brok, 2000). Deformation during subduction will cause dissolution of material on the sides of the grain normal to the highest stress and precipitation and growth in the elongation direction of the particles. Mauler et al.

(2001) presented that in omphacite the precipitation rate parallel to the C-axis is more efficient than for any other crystallographic directions. This is the case in the omphacite in these studied eclogites, with a wider prograde rim parallel to the lineation direction and to the C-axis of the omphacite. It indicates anisotropic growth and orientation dependent grain boundary diffusion creep to most likely be the dominant mechanism for the elongation of the omphacite, CPO and fabric development.

This is illustrated in Fig.5.3.1 with prograde mineral growth in omphacite parallel to the C-axis and dissolution perpendicular to the C-axis. The pole figure illustrates the same CPO observed in the omphacites in this study with [001] direction parallel to lineation and [010] direction perpendicular to lineation.

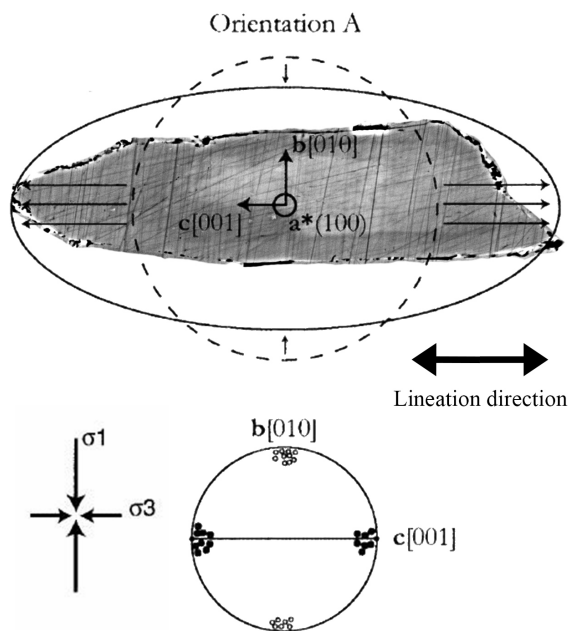


Fig. 5.3.1: illustration modified from Mauler et al. (2001) showing the asymmetric chemical zonation and prograde growth of omphacite parallel to the C-axis, normal to the highest stress and in the lineation direction. As well as preferred growth of the omphacite in the [001] direction, and dissolution in the [010] direction. Omphacite grain is oriented parallel to lineation (\leftrightarrow).

Garnet mostly acts as rigid particles in rocks, so elongation by pure flattening is not likely. Strain partitioning normally accommodate the strain in eclogites in mechanically weaker minerals, e.g. omphacite, and garnet particles are normally not deformed (Mainprice et al., 2004; Rehman et al., 2016). It was not observed any strong CPO in garnets in these eclogites, so deformation by dislocation creep is also ruled out to be the mechanism for the elongation of garnet grains. The asymmetric zonation wider in the lineation direction, indicates that grain

boundary diffusion by dissolution on high stress areas and precipitation on low stress areas of the grain is the most likely mechanism for the elongation of garnet. Fig.4.4.22 shows identical CPO data from different areas in the garnet crystal (core and rim) and clearly shows that the CPO is completely independent from the chemical zonation and therefore from the elongation of garnet grains. If recrystallization processes by dislocation creep was an accommodating mechanism for elongation of garnet we would expect signs of change in the CPO in the garnet from core to rim e.g. as subgrains during crystal growth. Therefore the chemical zonation is independent from the microstructures and elongation most probably is a product of grain boundary diffusion processes and anisotropic crystal growth during prograde metamorphism.

Stünitz (1993) proposed that zoisite grains acts as rigid particles during deformation and do not show any signs of intra crystal plastic deformation by dislocation creep. If this is the case also for the zoisite particles in these eclogites, the strong CPO and elongation of zoisite parallel to lineation can be a result of rotation and grain boundary diffusion as in omphacite and garnet. Collett et al. (2017) suggested that zoisite is a product of hydration and/or cooling during early exhumation. If the elongation direction has been the same during the retrograde path of the eclogites this may be the case, but the strong CPO and SPO parallel to the omphacite and garnet in the lineation direction may point to rotation and grain boundary diffusion during subduction as a mechanism for elongation of zoisite in the lineation direction. However there is no asymmetric zonation in zoisite to confirm that the elongation occurred during prograde metamorphism.

The results of this study indicate that the strong lineation fabric mostly produced by elongation of omphacite, garnet and zoisite in the Czech Erzgebirge eclogites dominantly is a result of anisotropic grain growth by grain boundary diffusion and not crystal plastic deformation by dislocation creep. As well as the main mechanisms for CPO development in omphacite by orientation dependent grain growth in the C-axis direction of the omphacites.

Quartz is dominantly found in pressure shadows of garnet in aggregates parallel to the lineation direction, and more quartz and garnet rich layers occur as Keppler et al. (2016) observed. One explanation for the garnet and quartz association might be that quartz has a larger stability field than e.g. omphacite. Quartz will then crystallize in areas with lower stress than omphacite in the pressure shadows of garnet. As discussed for diffusion processes, material will precipitate at areas with lower stress parallel to the elongation direction. The pressure shadows of garnet

will be parallel to the elongation direction, where quartz is found in these eclogites. So another possibility is that quartz formed by a grain boundary diffusion process, where excess SiO_2 from garnet was dissolved at areas with high stress and transferred by diffusion to areas of lower stress. In addition the formation of quartz aggregates in pressure shadows also are a result of dissolution and precipitation by grain boundary diffusion creep. The absent CPO and recrystallization structures, as well as straight grain boundaries indicates that quartz has not been deformed by intracrystalline processes, or that post-tectonic deformation by GBAR and grain growth have effected quartz as Mauler et al. (2001) proposed. The fact that quartz is placed in pressure shadows of the rigid garnet particles can also be the reason for the lack of deformation structures in quartz.

Symplectites surrounding the omphacite grains are another structure facilitating grain boundary diffusion. The rims surrounding omphacite are somewhat wider in the lineation direction, as well as the fibrous, kelyphite rims around garnet is oriented in the lineation direction. The formation of the symplectites require diffusion along the grain boundaries to break down omphacite and/or garnet and to precipitate the new minerals. Since the symplectites and the fibrous rims are elongated parallel to the prograde lineation, the elongation direction has to be the same during exhumation. The same processes for dissolution at sites on the grain exposed to the highest stress and precipitation at low stress areas during grain boundary diffusion, can explain the wider symplectite rims parallel to the lineation direction.

The L-type fabric of omphacites in the Czech eclogites from the Erzgebirge are based on the model from Helmstaedt et al. (1972), formed in a constrictional regime ($\epsilon_1 > \epsilon_2 = \epsilon_3$). This model is based on the type of strain regime during deformation and recrystallization to be the main process for CPO development in omphacite. In the eclogites in this study the fabric seems to be formed by dominantly grain boundary diffusion processes, and that the fabric is a result of pure grain growth, and not directly connected to a constrictional regime and recrystallization. So to connect the L-type fabric in these eclogites to a constrictional regime and recrystallization formed by dislocation creep processes can in this respect be misleading. Pure or simple shear can also form L-type fabric if the lineation is dominantly formed by crystal growth in a preferred orientation.

Dislocation creep is a known formation process of CPO in minerals, and may have interfered in the formation of the strong CPO in omphacite and zoisite. However the weak CPO in garnet,

the correlation in chemical zonation patterns in omphacite and garnet, the precipitation of quartz in pressure shadows of garnet and symplectite formation, all point to grain boundary diffusion as a dominant mechanism for the fabric development and omphacite CPO.

Dynamic recrystallization of minerals is a mechanism accommodated by dislocation creep in the crystal lattice. No recrystallized grains or signs of BLG, SGR or GBM are observed in the eclogites. Deformation twinning and kinking are also signs of intracrystalline deformation, and where not observed in any studied particles.

6.0 Conclusions

Mafic eclogites samples from the northeastern part of the Czech Republic of the Saxothuringian domain in the central Erzgebirge were studied in this thesis. Samples M1 and M7 exhibit the same strong lineation fabric with elongated omphacite, garnet and zoisite in the lineation direction of the eclogites. This study was done to find the main deformation mechanism for fabric and CPO development in eclogite facies minerals. From the results of this thesis and comparison to previous work, these are the conclusions of this thesis:

1. The chemical changes in the zonation in omphacite and garnet indicate elongation of the particle and fabric development during prograde metamorphism. Retrograde rims as symplectites, kelyphites and a thin outer almandine rich rim in garnet indicate pressure decrease probably at the start of exhumation of the eclogites. The eclogites show the prograde – retrograde path of subduction, peak metamorphism and exhumation.
2. Asymmetric zonation patterns in omphacite and garnet indicate that grain boundary diffusion creep is an important mechanism for prograde growth of omphacite and garnet stronger in the lineation direction, as well as the fabric development in the eclogite. The [001] direction, the longest axis of the omphacite particles, is parallel to the lineation and have a strong CPO. By rotation and orientation dependent growth in the [001] and lineation direction, grain boundary diffusion is a possible main mechanism for CPO development in the omphacite.
3. If the elongation of minerals and formation of fabric are a product of grain growth by grain boundary diffusion, connecting L-type or S-type fabric to a constrictional or flattening regime can be misleading. If orientation dependent growth during grain boundary diffusion is the main mechanisms for CPO development in the omphacite, the CPO can develop in different strain regimes, and is not connected to recrystallization by dislocation creep processes.
4. Quartz is always associated with garnet and has most likely crystallized in pressure shadows of garnet parallel to the lineation direction, either in unfavorable areas for HP minerals e.g. omphacite to crystallize, or as a result of excess SiO₂ in the system and dissolution by grain boundary diffusion in the elongation direction of the eclogite.

7.0 References

- BASCOU, J., BARRUOL, G., VAUCHEZ, A., MAINPRICE, D. & EGYDIO-SILVA, M. 2001. EBSD-measured lattice-preferred orientations and seismic properties of eclogites. *Tectonophysics*, 342, 61-80.
- BONS, P. D. & DEN BROK, B. 2000. Crystallographic preferred orientation development by dissolution–precipitation creep. *Journal of Structural Geology*, 22, 1713-1722.
- CHRISTIAN, J. W. & MAHAJAN, S. 1995. Deformation twinning. *Progress in materials science*, 39, 1-157.
- COLLETT, S., ŠTÍPSKÁ, P., KUSBACH, V., SCHULMANN, K. & MARCINIAK, G. 2017. Dynamics of Saxothuringian subduction channel/wedge constrained by phase-equilibria modelling and micro-fabric analysis. *Journal of Metamorphic Geology*, 35, 253-280.
- ENGELS, J. P. 1972. The catazonal poly-metamorphic rocks of Cabo Ortegal (NW Spain). *A structural and petrofabric study. Leidse Geol Meded*, 48, 83-133.
- GERALD, J., ETHERIDGE, M. & VERNON, R. 1983. Dynamic recrystallization in a naturally deformed albite. *Texture, Stress, and Microstructure*, 5, 219-237.
- GODARD, G. & VAN ROERMUND, H. L. M. 1995. Deformation-induced clinopyroxene fabrics from eclogites. *Journal of Structural Geology*, 17, 1425-1443.
- GUILLOPE, M. & POIRIER, J. 1979. Dynamic recrystallization during creep of single - crystalline halite: An experimental study. *Journal of Geophysical Research: Solid Earth*, 84, 5557-5567.
- HEILBRONNER, R. & BARRETT, S. 2014. *Image Analysis in Earth Sciences: Microstructures and Textures of Earth Materials*, Berlin, Heidelberg, Springer Berlin Heidelberg: Berlin, Heidelberg.
- HELMSTAEDT, H., ANDERSON, O. L. & GAVASCI, A. T. 1972. Petrofabric studies of eclogite, spinel-Websterite, and spinel-lherzolite Xenoliths from kimberlite-bearing breccia pipes in southeastern Utah and northeastern Arizona. *Journal of Geophysical Research*, 77, 4350-4365.
- HIRTH, G. & TULLIS, J. 1992. Dislocation creep regimes in quartz aggregates. *Journal of Structural Geology*, 14, 145-159.
- HOTH, K., LORENZ, W. & BERGER, H. 1983. Die Lithostratigraphie des Proterozoikums im Erzgebirge. *Z Angew Geol*, 29, 413-418.

- HURYCH, V. & BRUECKNER, H. K. 1995. Eclogites from the Meluzina and Medenec localities of the Krušné hory Mountains, western part of the Bohemian Massif, Czech republic. *Journal of the Czech Geological Society*, 40/3.
- JEŘÁBEK, P., KONOPÁSEK, J. & ŽÁČKOVÁ, E. 2016. Two-stage exhumation of subducted Saxothuringian continental crust records underplating in the subduction channel and collisional forced folding (Krkonoše-Jizera Mts., Bohemian Massif). *Journal of Structural Geology*, 89, 214-229.
- JOANNY, V., VAN ROERMUND, H. & LARDEAUX, J. M. 1991. The clinopyroxene/plagioclase symplectite in retrograde eclogites: A potential geothermobarometer. *Geologische Rundschau*, 80, 303-320.
- KEPPLER, R., STIPP, M., BEHRMANN, J. H., ULLEMEYER, K. & HEIDELBACH, F. 2016. Deformation inside a paleosubduction channel – Insights from microstructures and crystallographic preferred orientations of eclogites and metasediments from the Tauern Window, Austria. *Journal of Structural Geology*, 82, 60-79.
- KLAPOVA, H., KONOPASEK, J. & SCHULMANN, K. 1998. Eclogites from the Czech part of the Erzgebirge: Multi-stage metamorphic and structural evolution. *Journal of the Geological Society*, 155, 567-583.
- KNIPE, R. 1989. Deformation mechanisms—recognition from natural tectonites. *Journal of Structural Geology*, 11, 127-146.
- KONOPÁSEK, J. & SCHULMANN, K. 2005. Contrasting Early Carboniferous field geotherms: evidence for accretion of a thickened orogenic root and subducted Saxothuringian crust (Central European Variscides). *Journal of the Geological Society*, 162, 463-470.
- KONRAD-SCHMOLKE, M., BABIST, J., HANDY, M. R. & O'BRIEN, P. J. 2006. The Physico-Chemical Properties of a Subducted Slab from Garnet Zonation Patterns (Sesia Zone, Western Alps). *Journal of Petrology*, 47, 2123-2148.
- LORENZ, W. 1979. Lithostratigraphie, Lithologie und Lithofazies metamorpher Komplexe. *Z. geol. Wiss*, 7, 405-418.
- LORENZ, W. & HOTH, K. 1967. Räumliche Gesetzmäßigkeiten der Skarnverbreitung im Erzgebirge. *Geologie*, 16, 1007-1030.
- LORENZ, W. & HOTH, K. 1990. Lithostratigraphie im Erzgebirge-Konzeption, Entwicklung, Probleme und Perspektiven. *Abh. Sächs. Museum Min. u. Geol*, 37, 7-35.
- MAINPRICE, D., BASCOU, J., CORDIER, P. & TOMMASI, A. 2004. Crystal preferred orientations of garnet: comparison between numerical simulations and electron back-

- scattered diffraction (EBSD) measurements in naturally deformed eclogites. *Journal of Structural Geology*, 26, 2089-2102.
- MASSONNE, H.-J. 2012. Formation of amphibole and clinozoisite–epidote in eclogite owing to fluid infiltration during exhumation in a subduction channel. *Journal of Petrology*, 53, 1969-1998.
- MAULER, A., GODARD, G. & KUNZE, K. 2001. Crystallographic fabrics of omphacite, rutile and quartz in Vendée eclogites (Armorican Massif, France). Consequences for deformation mechanisms and regimes. *Tectonophysics*, 342, 81-112.
- PANOZZO, R. H. 1983. Two-dimensional analysis of shape-fabric using projections of digitized lines in a plane. *Tectonophysics*, 95, 279-294.
- PASSCHIER, C. W. & TROUW, R. A. 1998. Deformation Mechanisms. *Microtectonics*. Springer.
- REHMAN, H. U., MAINPRICE, D., BAROU, F., YAMAMOTO, H. & OKAMOTO, K. 2016. EBSD-measured crystal preferred orientation of eclogites from the Sanbagawa metamorphic belt, central Shikoku, SW Japan. *European Journal of Mineralogy*.
- ROLLETT, A., HUMPHREYS, F., ROHRER, G. S. & HATHERLY, M. 2004. *Recrystallization and related annealing phenomena*, Elsevier.
- SCHMÄDICKE, E., MEZGER, K., COSCA, M. & OKRUSCH, M. 1995. Variscan Sm - Nd and Ar - Ar ages of eclogite facies rocks from the Erzgebirge, Bohemian Massif. *Journal of Metamorphic Geology*, 13, 537-552.
- SCHULMANN, K., KONOPÁSEK, J., JANOUŠEK, V., LEXA, O., LARDEAUX, J.-M., EDEL, J.-B., ŠTÍPSKÁ, P. & ULRICH, S. 2009. An Andean type Palaeozoic convergence in the Bohemian Massif. *Comptes Rendus Geoscience*, 341, 266-286.
- SCHULMANN, K., LEXA, O., JANOUŠEK, V., LARDEAUX, J. M. & EDEL, J. B. 2014. Anatomy of a diffuse cryptic suture zone: An example from the Bohemian Massif, European Variscides. *Geology*, 42, 275-278.
- SCHWARTZ, A. J., KUMAR, M., ADAMS, B. L. & FIELD, D. P. 2009. *Electron backscatter diffraction in materials science*, Springer.
- SIIVOLA, J. & SCHMID, R. 2007. List of mineral abbreviations. Cambridge University Press: New York.
- ŠTÍPSKÁ, P. & POWELL, R. 2005. Constraining the P–T path of a MORB - type eclogite using pseudosections, garnet zoning and garnet - clinopyroxene thermometry: an example from the Bohemian Massif. *Journal of Metamorphic Geology*, 23, 725-743.

- STOREY, C. D. & PRIOR, D. J. 2005. Plastic Deformation and Recrystallization of Garnet: A Mechanism to Facilitate Diffusion Creep. *Journal of Petrology*, 46, 2593-2613.
- STÜNITZ, H. 1993. Transition from fracturing to viscous flow in a naturally deformed metagabbro. *Defects and processes in the solid state: geoscience applications: the Mc-Laren volume (Developments in Petrology, Vol. 4)*. Amsterdam, Elsevier Science, 121-150.
- VOGEL, D. E. 1967. Petrology of an eclogite-and pyrigarnite-bearing polymetamorphic rock complex at Cabo Ortegal, NW Spain. *Leidse Geologische Mededelingen*, 40, 121-213.
- WHEELER, J. 1992. Importance of pressure solution and coble creep in the deformation of polymineralic rocks. *Journal of Geophysical Research: Solid Earth (1978–2012)*, 97, 4579-4586.
- WINTSCH, R. & YI, K. 2002. Dissolution and replacement creep: a significant deformation mechanism in mid-crustal rocks. *Journal of Structural Geology*, 24, 1179-1193.
- WONG, T.-F. & BIEGEL, R. 1985. Effects of pressure on the micromechanics of faulting in San Marcos gabbro. *Journal of structural geology*, 7, 737-749.
- ZHANG, J., GREEN II, H. W. & BOZHILOV, K. N. 2006. Rheology of omphacite at high temperature and pressure and significance of its lattice preferred orientations. *Earth and Planetary Science Letters*, 246, 432-443.
- ZHANG, R. Y., LIU, J. G., ZHENG, Y. F. & FU, B. 2003. Transition of UHP eclogites to gneissic rocks of low-amphibolite facies during exhumation: evidence from the Dabie terrane, central China. *Lithos*, 70, 269-291.

8.0 Appendix

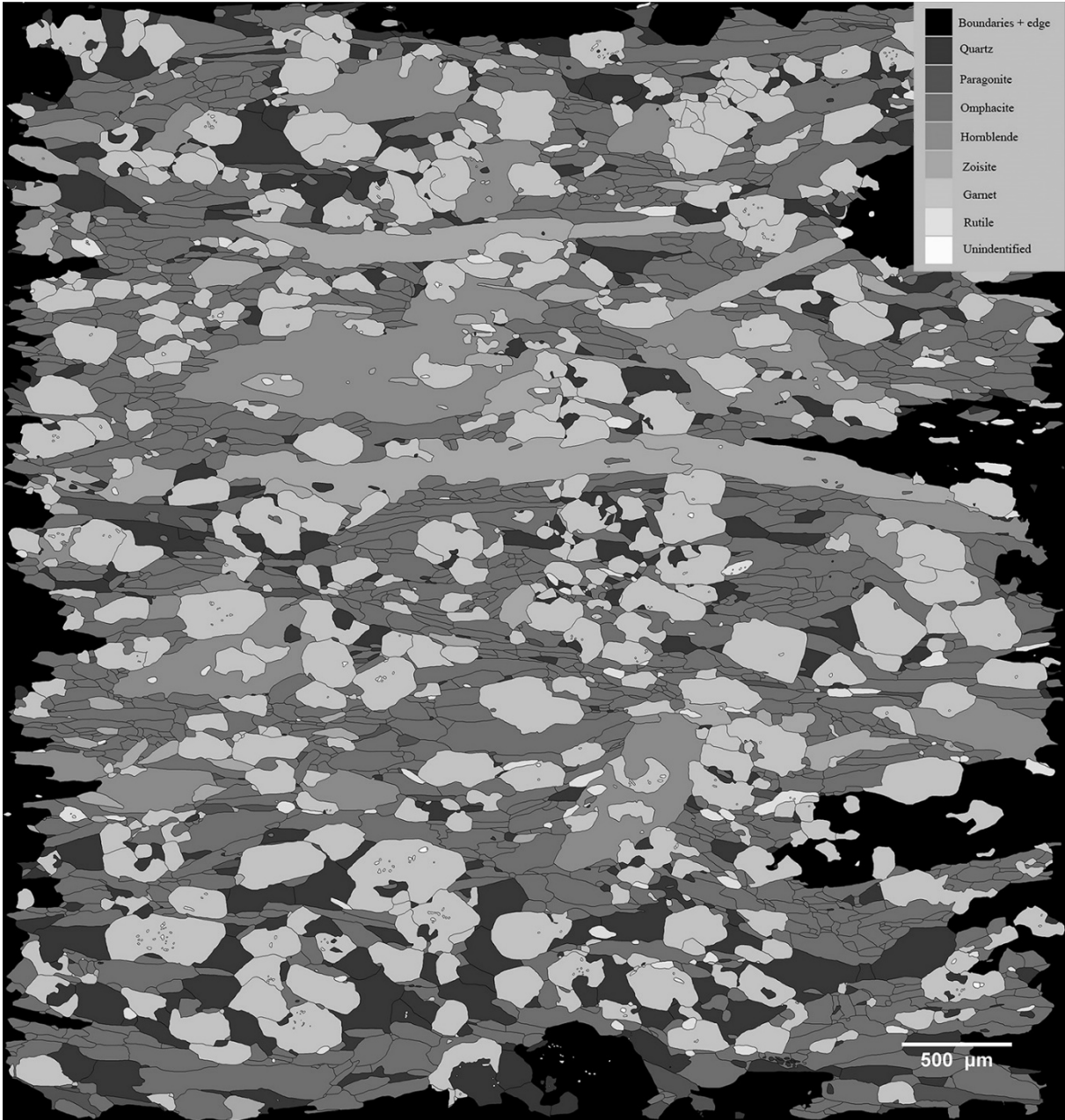


Fig. 8.1: grain boundary and phase map for M1-L. Gray scale of different phases are presented in the legend, parallel to lineation (↔).

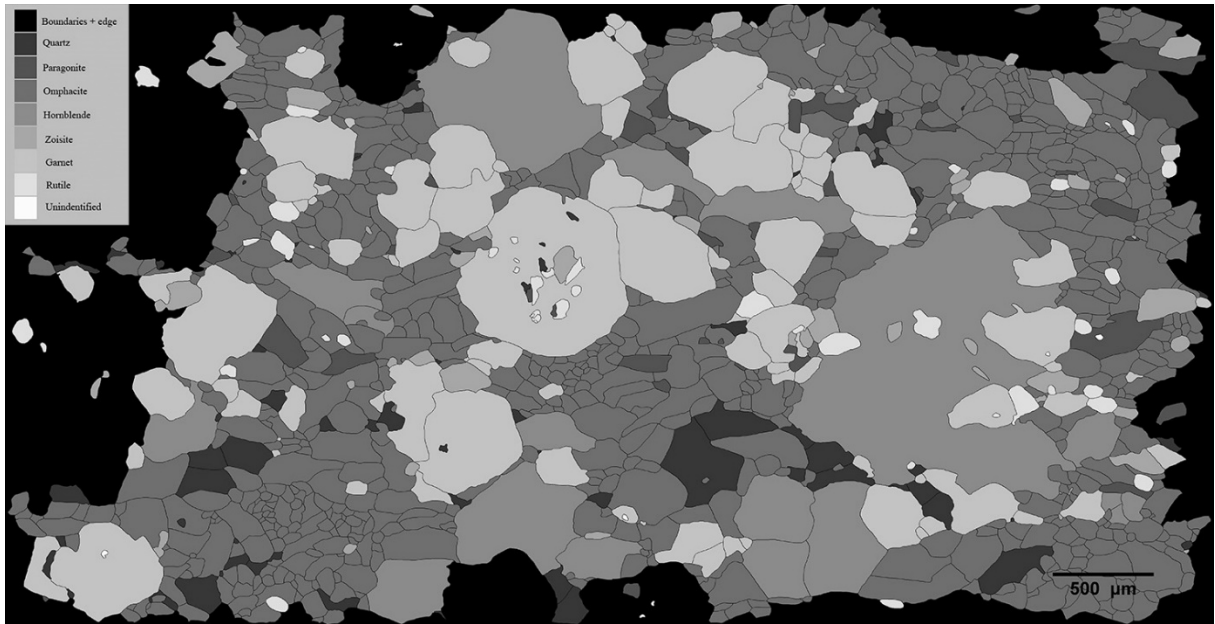


Fig. 8.2: grain boundary and phase map for M1-P, perpendicular to lineation.

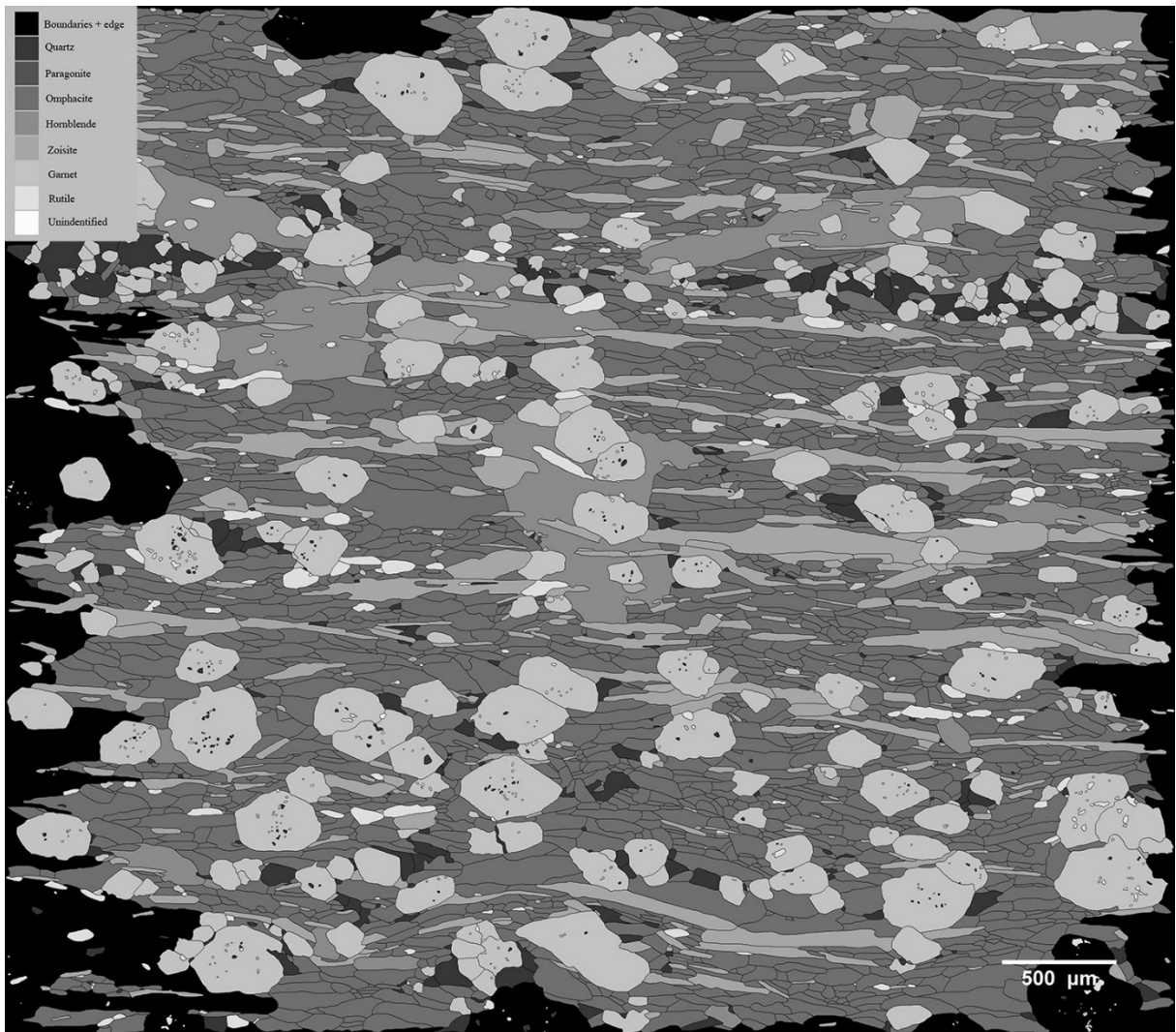


Fig. 8.3: grain boundary and phase map for M7-L, parallel to lineation (↔).

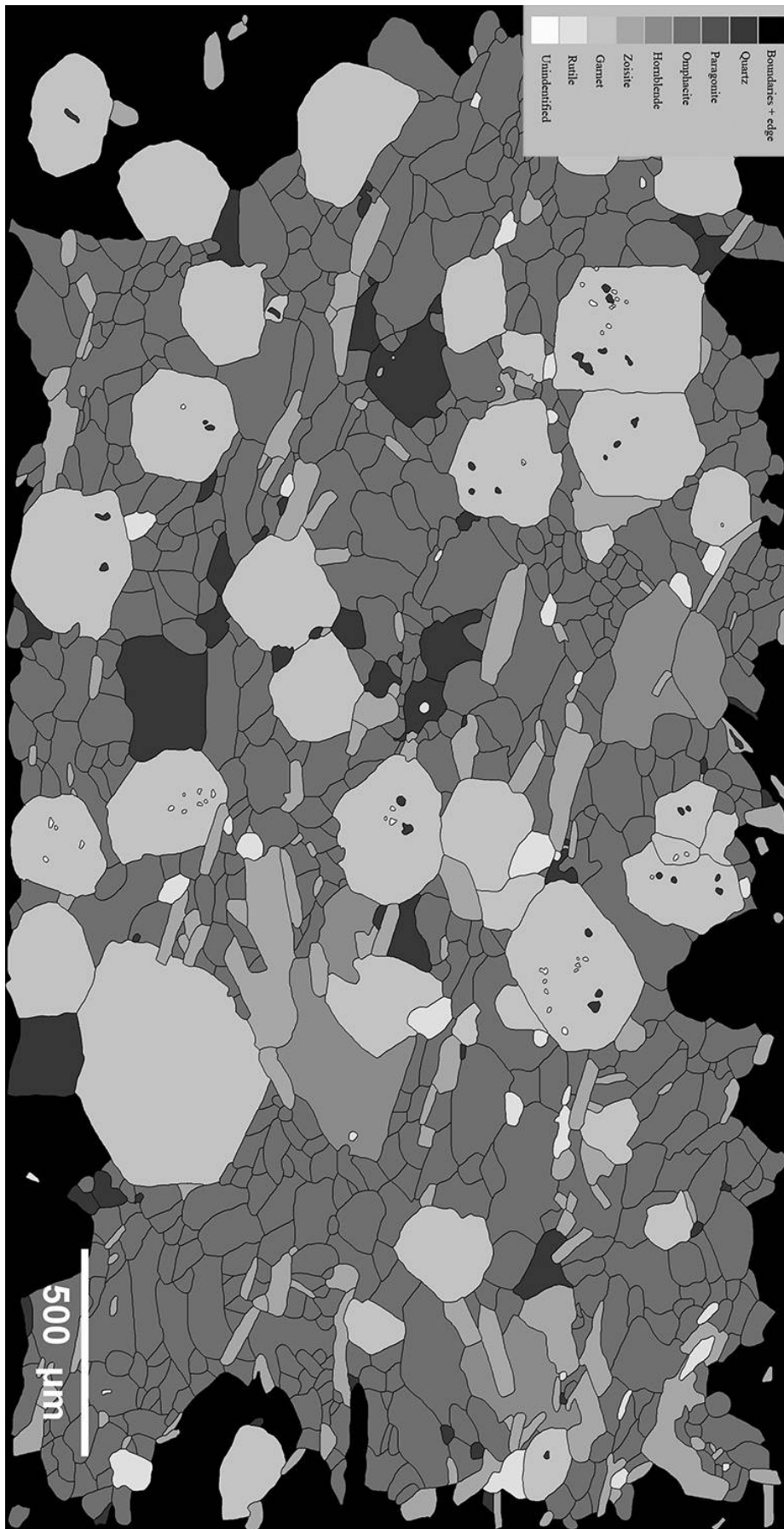


Fig.8.4: grain boundary and phase map for M7-P, perpendicular to lineation.

